University of Alberta
Department of Civil &
Environmental Engineering

Fatigue Strength of Coped Steel Beams

by

Michael C.H. Yam

and

J.J. Roger Cheng

June, 1988

Fatigue Strength of Coped Steel Beams

by

Michael C. H. Yam

and

J. J. Roger Cheng

Department of Civil Engineering
University of Alberta
Edmonton, Alberta

June, 1988

ABSTRACT

Coped beams are often used in steel construction to provide enough clearance for the supports when the framing beams are at the same elevation as the main girder or when flanges of the intersecting beams are held to the same elevation for architectural purposes. Coped beams subjected to cyclic loading are susceptible to fatigue damage due to the stress concentration produced by the geometric discontinuities at the cope. In order to investigate the fatigue behavior of coped beams, nine full scale specimens were tested; stress range and cope radius were the two test parameters. The stress concentration produced by different cope radii and the effect of cope fabrication procedures were also examined in the testing program. It was found that the stress concentration effect produced by the cope geometry was very localized and, as expected, increased with decreasing cope radius. The fatigue life of the specimens decreased with either increasing nominal stress range or decreasing cope radius. The finite element method was employed to investigate the stress concentration produced by the cope geometry. This analysis results showed good agreement with the test results. Linear elastic fracture mechanics was used to analyse the fatigue strength of the test specimens. Reasonable agreement was obtained between the analytical results and the test results. Test results were also compared with the existing S-N curves in the Canadian design standard CAN-3-S16.1-M84 (1984). A preliminary design guideline was proposed based on the available test data and the analytical study. Recommendations for future research are also proposed.

ACKNOWLEDGEMENTS

Table of Contents

List of Tables

List of Figures

1. INTRODUCTION

1.1 General

Fatigue of metals may be defined as the formation of a crack or cracks resulting from cyclic loads that are too low to cause failure under a single load application. The mechanism of fatigue crack growth can be described as the alternate blunting and resharpening of the crack at the crack tip under cyclic loadings (Broek 1986). The major factors governing fatigue strength of metals are the applied stress range, the number of stress cycles, and the type of structural details. The size and variability of pre-existing flaw is also a significant factor.

Nowadays, the design of structural members subjected to fatigue loading basically follows the stress range versus stress cycle (S-N) curve approach which considers stress range, geometric detail, and number of stress cycles as the basic parameters. Structural details are classified into different categories in the S-N diagram (CAN3-S16.1-M84). This classification system, in fact, categorizes the structural details according to the severity of the local stress gradient caused by the geometric discontinuities of the detail (Albrecht and Yamada 1977). It also implicitly includes the variability of initial discontinuity inherent in the different types of detail into the S-N curves.

1.2 Statement of Problem

In steel construction, beam flanges must often be coped in order to provide enough clearance for the supports when the framing beams are at the same elevation as the main girders or when flanges of the intersecting beams are held to the same elevation for architectural purposes, as shown

1

Figure 1.1. Removing the flange of the beam not only reduces the cross-sectional bending resistance by as much as 90%, but also introduces a high stress concentration in the web at the cope corner due to the geometric discontinuities (Cheng and Yura 1986).

The flame cut procedure is usually employed in fabricating coped beams. This fabrication procedure produces metallurgical changes such as the formation of a martensite layer at the cut edge (Goldberg 1973). The martensite layer, which is produced by heat and cooling rate of the flame cut, is susceptible to microcracking because of its hard and brittle nature. Hence, initial micro-flaws are believed to exist in the martensite layer. Flame cutting also introduces high tensile residual stresses at the cut edge due to the differential temperature during the cooling process. The magnitude of these residual stresses can be as high as the yield strength of the material (Fisher 1977), hence fatigue cracking can also be developed under cyclic compressive stress (Gurney 1979). The roughness at the cope edge produced by flame cutting is also believed to have an influence on the fatigue strength of coped beams.

1.3 Case Studies

1.3.1 General

Fatigue failures of coped beams have been reported both in Japan and North America. In Japan, about 30 railroad bridges on the high-speed line developed cracks at the coped stringers bolted to the floor beams (Nishimura 1978). Similar fatigue failures of coped stringers in bridges have also been reported in Canada and the United States (Fisher and Yuceoglu 1981). These failures are usually due to the tensile stresses produced by the continuity of coped stringers across the floor beam.

Although there is not sufficient information to evaluate most of these failure cases, two failure cases will be discussed in the following sections.

1.3.2 Fatigue Cracking of Coped Stringers in Bridge 51.5 Windermere Subdivision

In November 1975 a number of fatigue cracks were found at the coped stringers in the Bridge 51.5 Windermere Subdivision of the Canadian Pacific Railroad (Kalousek and Bethune 1976) as shown in Figure 1.2. It was estimated that 1.3 million stress cycles caused by the train traffic were applied to the coped stringers from 1970 to 1975.

The bridge was instrumented and strain measurements with strain gauges were taken in various locations and in particular the area of crack initation. It was found that the ratio of the maximum local stress in the region of the cope to the nominal stress evaluated by simple bending theory ranged from 2.5 to 3.1.

A failure analysis of this structure was performed by Fisher (1984) using Linear Elastic Fracture Mechanics (LEFM). Based on Miner's Law he estimated that the effective stress range at the strain gauge location for the 1.3 million stress cycles was 124 MPa. He then approximated the stress intensity factor, K, for this detail as:

$$K = \left[\frac{0.923 + 0.199 \left(1 - \sin \frac{\pi a}{2b} \right)^4}{\cos \frac{\pi a}{2b}} \right] \frac{2b}{\pi a} \tan \left(\frac{\pi a}{2b} \right)^{1/2} \sigma \sqrt{\pi a} \qquad [1.1]$$

where a is the crack length, b is the depth of the coped section, and σ is the nominal stress measured at 10 mm from the cope edge. It should be noted that equation [1.1] represents the stress intensity factor for a single edge cracked plate in bending (Tada, Paris, and Irwin 1973). Using an assumed initial crack size of 0.38 mm, a final crack size of 100 mm, and an effective stress range of 124 MPa, the estimated fatigue life for the detail was 955 000 cycles. A further discussion about the use of LEFM to evaluate the fatigue strength of coped beams will be presented in Chapter 5.

1.3.3 Fluid Catalytic Cracking Unit Structural Failure

In December 1981 four W36x300 main coped beams supporting a catalyst regenerator, located at Lake Charles Refinery, Oklahoma, suffered extensive fatigue cracking in the coped corner (Richards and Mueller 1982). The fatigue failure occurred after 40 years of operation resulting from cyclic loading produced by catalyst movement in the regenerator. A typical failed coped beam is shown in Figure 1.3 schematically. All cracks were initiated at the sharp cope corner in the bottom flange of the beams. The cracks propagated at roughly a 45° angle to the horizontal.

A fracture mechanics analysis of the beams at the cope location was performed by means of the finite element method. The analysis showed that a crack length of 23 mm to 48 mm could initiate the failure of the beam under normal loading.

The failure was attributed to high stresses due to the combination of the severe stress concentration produced by the 90° cope and the poor quality of the flame cut edge.

1.4 Current Design Specifications for Coped Beams Under Fatigue Loading

Although failures of coped beams have been reported, there are no specific guidelines and recommendations in the current CAN-3-S16.1-M84 (1984) and CAN3-S6-M78 (1978) design codes for the design of coped beams under fatigue loading. The AISC specification (1977) does recommend a cope radius of one half inch for all purposes for coped beams.

The British Standard BS 5400:Part10 (1980) classifies cope details into two categories depending upon the roughness of the flame-cut edges. It provides a set of curves to determine the stress concentration factors (SCF) which are used to modify the nominal stress at the cope section as shown in Figure 1.4. These curves are only valid for a plate with a re-entrant corner loaded uniformly in tension as illustrated in Figure 1.4. They do not take into account the stress gradient effect introduced by both the coped section and bending moment which is the usual loading applied to coped beams. Therefore it is believed that these curves may not be applicable to cope details.

Fisher et al. (1970) suggested that a flame-cut edge parallel to the stress is comparable to Category B details in the AASHTO specifications (1983). He also suggested that the stress concentration effect produced by the cope geometry is likely to reduce this detail to Category C (Fisher 1977).

1.5 Objectives

Based on the above discussion, it is clear that coped beams subjected to cyclic loading are susceptible to fatigue failure. Although failure cases have been reported, no research work related to the fatigue strength of

coped beams has been documented. Therefore, a research project was initiated to investigate the behaviour of coped beams subjected to cyclic loading. The objectives of this project are:

a) To investigate the fatigue strength of coped beams experimentally.

b) To determine the stress concentration at the cope due to different cope profiles.

c) To analyze the fatigue strength of coped beams using the fracture mechanics approach and to compare analytical and the experimental results.

d) To investigate the effect of cope fabrication procedures on the fatigue strength of coped beams.

e) To provide design guidelines for the fatigue strength of coped beams.
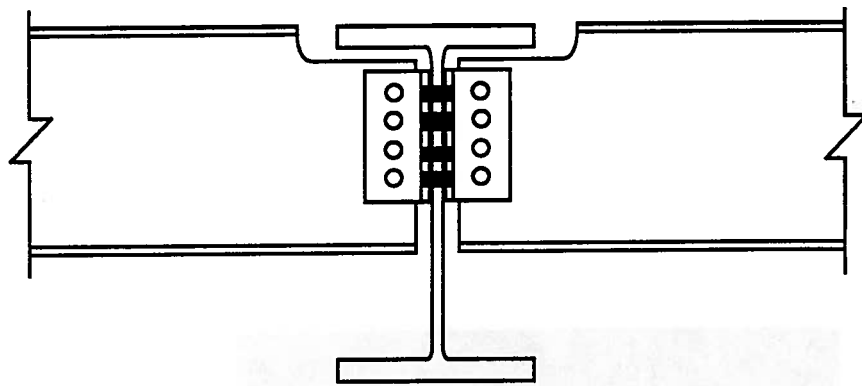
Bolted Clip Angle
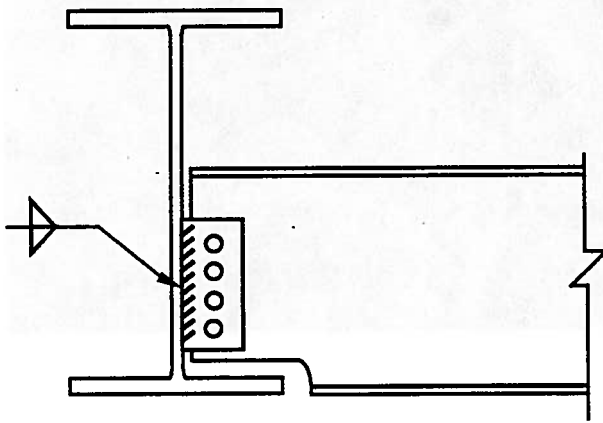
Single Web Plate

Figure 1.1 Types of Coped Beam Connection

Figure 1.2 Crack Observed in the Web near the Coped Area of Bridge 51.1 Windermere Subdivision

Typical Crack
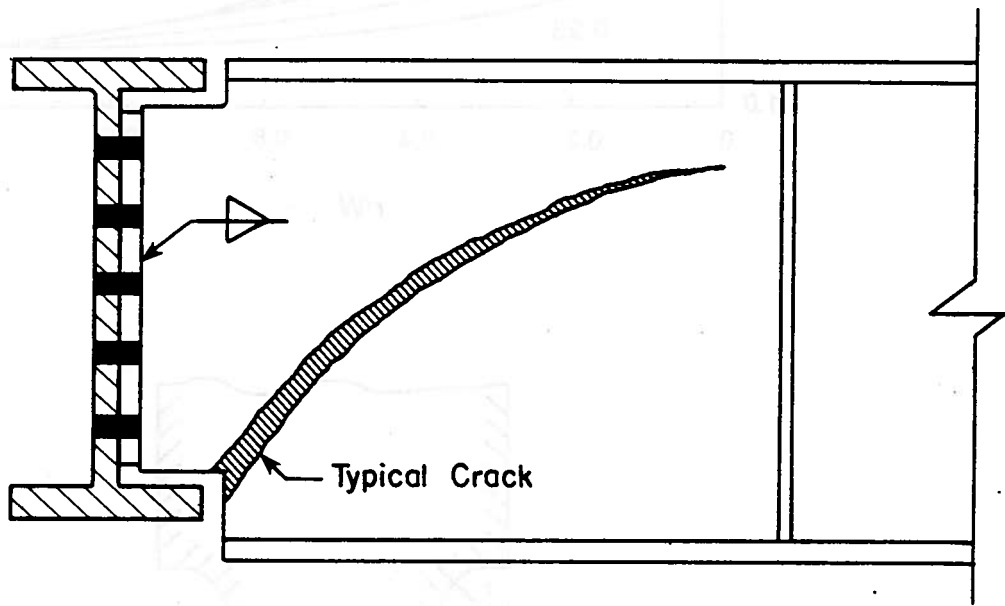
Figure 1.3   Typical Failed Coped Beam for FCCU
Structural Failure
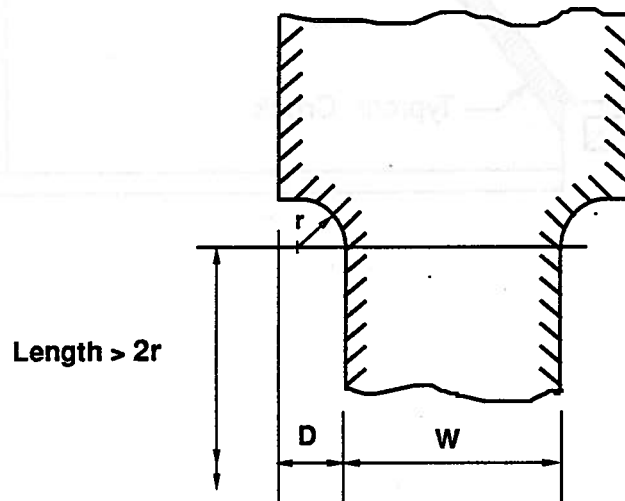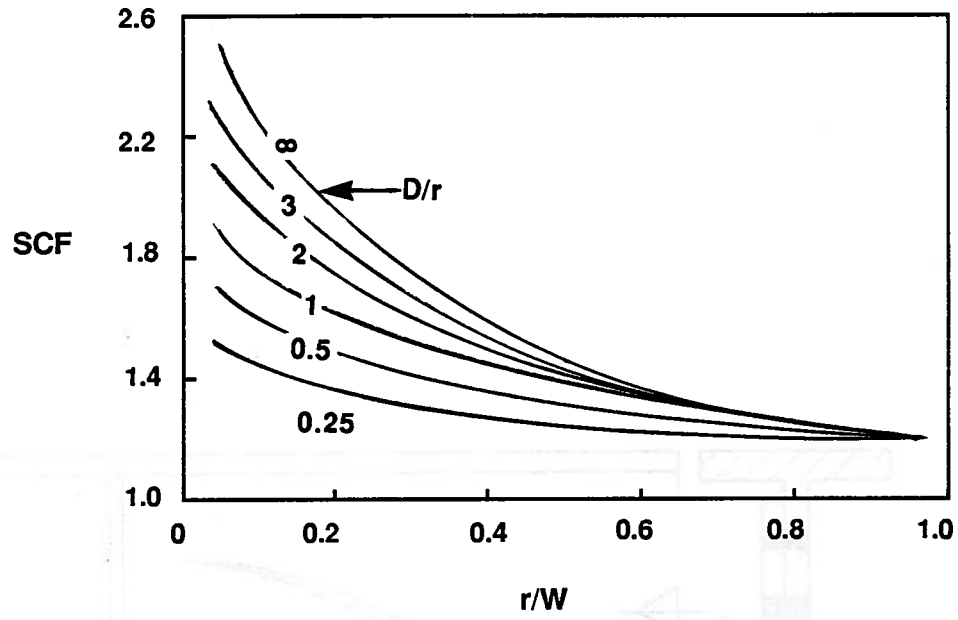
Figure 1.4   Fatigue Stress Concentration Factor for Re-entrant Corners

2. EXPERIMENTAL PROGRAM

2.1 Scope

The main purpose of this experimental program was to examine the fatigue strength of coped beams. Stress concentration effects were also investigated by measuring the stress distribution with electrical strain gauges and rosettes in the vicinity of the cope corner. In order to investigate the effect of roughness of the burned edges and the martensite layer produced by flame cutting on the fatigue strength of coped beams three cope fabrication procedures were used in this test program. These were flame cutting, flame cutting with smooth ground edges, and drilling a hole.

A series of nine full scale specimens were tested in the project with stress range and cope radius considered as the two major test parameters. The cope radius is defined in Figure 2.1. The effect of stress reversal on the fatigue life of coped beams was not investigated in this test program. Other parameters such as cope length and cope depth, defined in Figure 2.1, were kept constant. Only in-plane behaviour was considered in this program and so every test specimen was braced laterally at the load point to prevent out-of-plane movement.

2.2 Specimen Description

Nine specimens were prepared from three W410 x 54 CSA G40.21-M81 300W steel sections. The average measured dimensions of the steel sections are presented in Table 2.1. All test beams were 4876 mm long. Specimen designations and descriptions are presented in Table 2.2. The number in the designation represents the nominal cope radius for the

11

specimen. The last column in this table specifies the cope fabrication procedure for each specimen.

As shown in Table 2.2 the nominal radii investigated in this test program are 0 mm, 10 mm, 20 mm, and 30 mm. The actual radii listed in the third column are measured from the specimens after flame cutting. Specimen CB-0 with a 0 mm cope radius (90 degree cope) was used to establish the worst condition for this kind of detail. Specimens CB-20B and CB-10D were ground smooth after flame-cutting in order to observe the roughness effect on the fatigue life of coped beams. Typical roughness at the cope edge produced by flame cutting is shown in Figure 2.2. By drilling a 10 mm radius hole on specimen CB-10E, followed by flame cutting out the tangents to the hole, an exact 10 mm cope radius was obtained and the roughness at the cope surface was minimized.

The cope length and cope depth of all specimens, defined in Figure 2.1, were 230 mm and 60 mm respectively.

2.3 Test Setup

The test setup is shown schematically in Figure 2.3. All specimens were tested on a 3670 mm span with one point loading at midspan. The test beams were simply supported by roller and rocker systems as shown in Figure 2.4. The rocker allowed free rotation and the rollers permitted horizontal movement of the test beam at the supports. The horizontal stability of the beam was maintained by friction between the loading ram and the test beam. Load transfer from the beam to the support was done through a pair of clip angles bolted at the cope end of the beam. The clip angles were bolted onto the web with two high strength bolts installed by the turn-of-nut method (Figure 2.5). As shown schematically in Figure 2.6

lateral bracing was provided at the load point to prevent out-of-plane movement. The lateral bracing supported the test beam laterally by rollers which allowed the beam to move vertically. A photograph of the lateral bracing is shown in Figure 2.7.

Static and constant amplitude loadings were applied by a Pegasus servo-load simulation system which was supported by hydraulic power. The loading ram, which has a dynamic capacity of 530 kN, was regulated by the Pegasus controller. Load cells were used to record the reactions at the supports during the static tests.

Strain gauges and rosettes were mounted on test specimens at the locations shown in Figure 2.1. Two 2 mm gauge length rosettes were positioned as close to the cope edge as possible in order to measure the stress gradient effect produced by the cope geometry. The distance of the rosettes from the cope edge, d_R, defined in Figure 2.1, is listed in Table 2.2. The rosettes were mounted side by side on the specimen with one of them located at the theoretical point of tangency of the cope radius. Strain gauges were located along a vertical line passing through the middle of the two rosettes, as shown in Figure 2.1. Two strain gauges were positioned at top and bottom flanges of the test beam and 720 mm away from the cope line (Figure 2.1) to monitor the load applied to the test beam.

A data acquisition system was used to collect the data from the static tests. The number of cyclic loading was automatically recorded by the Pegasus system.

2.4 Test Procedure

A static test was carried out on every specimen to determine the elastic stress distribution within the cope region at various load levels.

Since flame cutting produces high tensile residual stresses in the vicinity of the cope edge, premature yielding of the material in this region was expected at an early stage of loading. In order to determine the elastic stress distribution near the cope region, the test beam was loaded to the maximum load level used during the fatigue test and it was then unloaded. This loading and unloading procedure dissipated part of the residual stresses, allowing the material in the cope region to respond elastically within the applied load range upon reloading. Strain gauge readings were then recorded at different load levels through the entire static test.

As shown in Table 2.2, nominal stress ranges of 40 MPa, 50 MPa, and 70 MPa were used in the fatigue tests and the nominal mean stress in all cases was 70 MPa. During the fatigue test the nominal stress range at the cope line was maintained by monitoring the strain range from the strain gauges located at 720 mm from the cope line. This strain range was calculated by simple bending theory based on the nominal stress range at the cope line and was found to agree with the static test readings. The strain range for the fatigue test was established by loading the test beam to the minimum and maximum strain levels and recording the corresponding voltage outputs on an oscilloscope. The fatigue test was then conducted at a loading frequency of 3 to 5 Hz and the dynamic load range on the Pegasus system was adjusted according to the previously recorded voltage outputs on the oscilloscope.

Whitewash was used on the cope region to facilitate the detection of crack initiation by visual inspection. Once the crack has started, the centreline deflection of the test beam increases. In order to detect the crack at an early stage a stroke limit on the loading ram was preset so that

the cyclic loading could be stopped automatically when the centreline deflection exceeded the stroke limit.

Crack growth data were obtained by manually measuring the crack length at convenient intervals after the crack was first detected. The tests were then carried on until net-section failure. Location of crack initiation for every specimen was measured after the test and the fracture surface examined.

2.5 Ancillary Tests

2.5.1 Tension Coupon Tests

Two coupons were cut from the web at each end of the test beams in the longitudinal direction and tested. A 25 mm extensometer was used to measure the strain and the stress-strain curve was directly obtained from the x-y plotter connected to the extensometer. Readings from the digital strain indicator were also taken at convenient time intervals. Elongation at rupture was measured from the failed coupon.

2.5.2 Roughness Measurements

A device was developed to measure the roughness at the coped edge produced by flame cutting. As shown in Figure 2.8, the roughness was detected by a pointer which travelled along the cope surface. The movement of the pointer in both longitudinal and transverse directions was recorded by two linear variable displacement transducers. The longitudinal movement of the pointer was controlled by a variable speed motor.

Table 2.1 Measured Dimensions of Steel Sections

Beam	d (mm)	b (mm)	t (mm)	w (mm)
CB-1	406.0	175.3	10.5	7.87
CB-2	406.3	176.2	10.8	7.92
CB-3	405.3	176.2	10.6	7.69
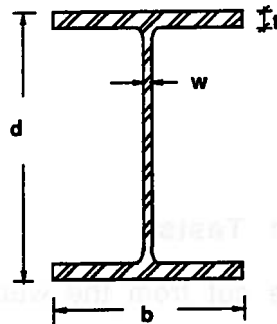
Table 2.2 Specimen Description

Specimen Designation	Nominal Cope Radius (mm)	Actual Cope Radius (mm)	Nominal Stress Range (MPa)	Rosettes Location d_R (mm)	Fabrication Procedure
CB-0	0	0	50	3	F
CB-10A	10	15	50	4	F
CB-20B	20	25	50	5	FG
CB-20A	20	25	50	2	F
CB-30	30	32	50	3	F
CB-10B	10	15	40	4	F
CB-10C	10	15	70	4	F
CB-10D	10	15	70	3	FG
CB-10E	10	10	70	4	D

Note: F = Flame cut edge
FG = Flame cut and
Ground smooth edge
D = Drilled Hole
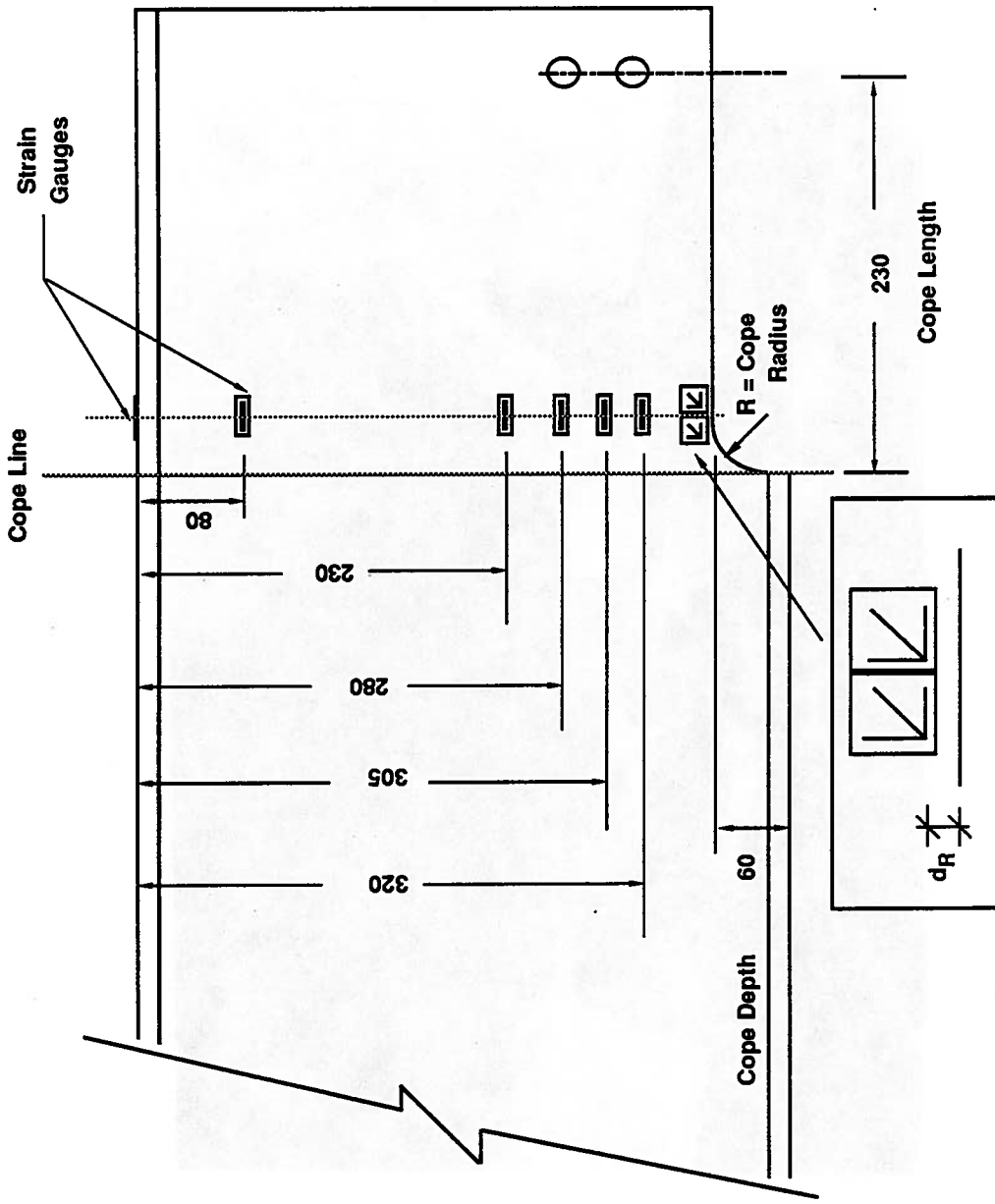
Figure 2.1 Specimen Description
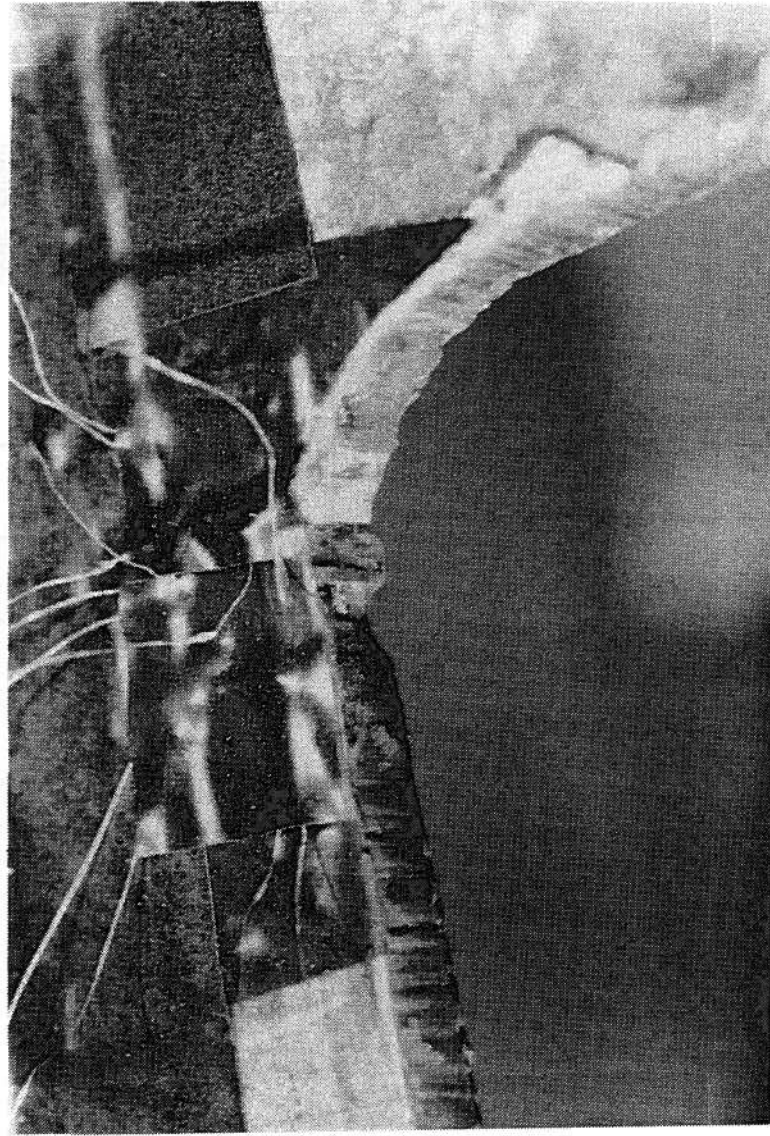
Figure 2.2 Typical Rough Surface Produced by Flame Cutting

Cyclic Load

Test Beam

Roller and Rocker Assembly

1835

1835
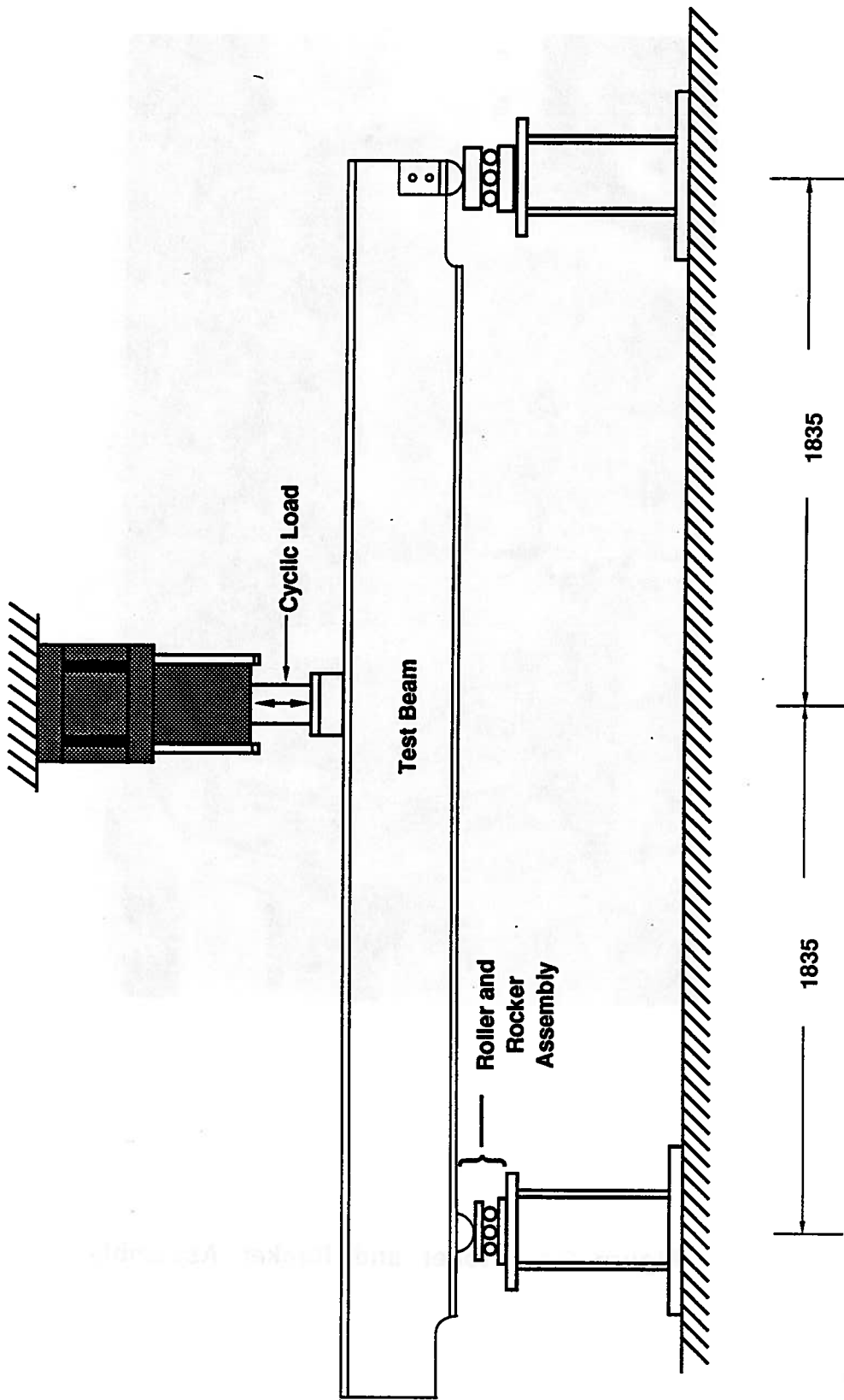
Figure 2.3 Schematic Test Setup
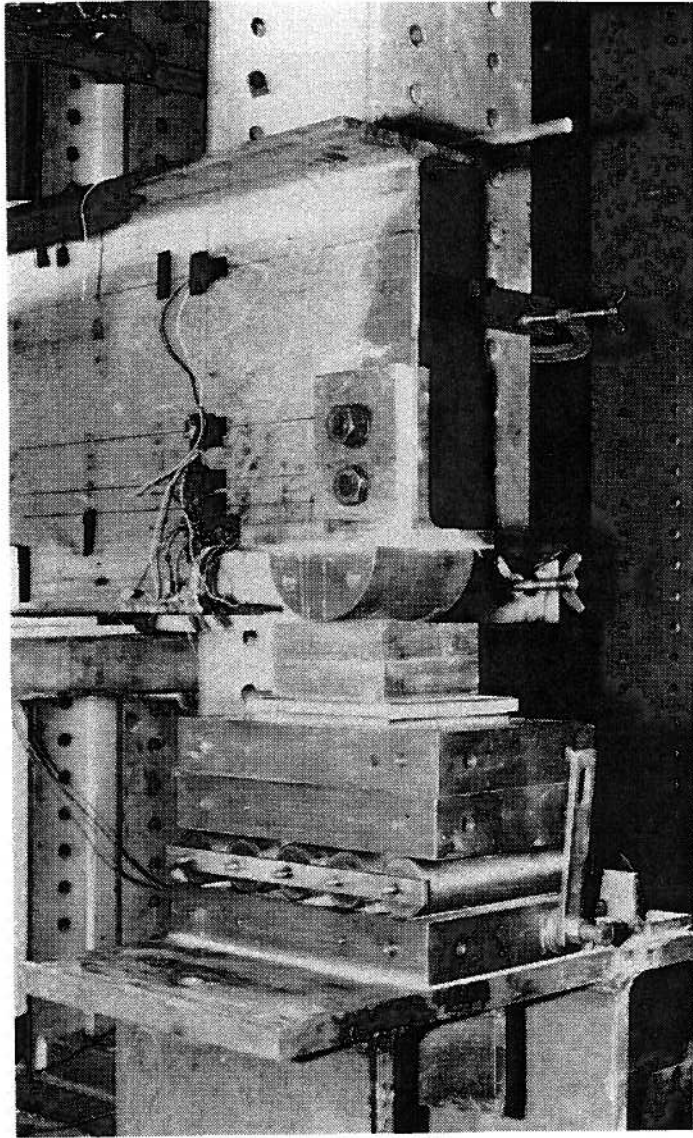
Figure 2.4   Roller and Rocker Assembly
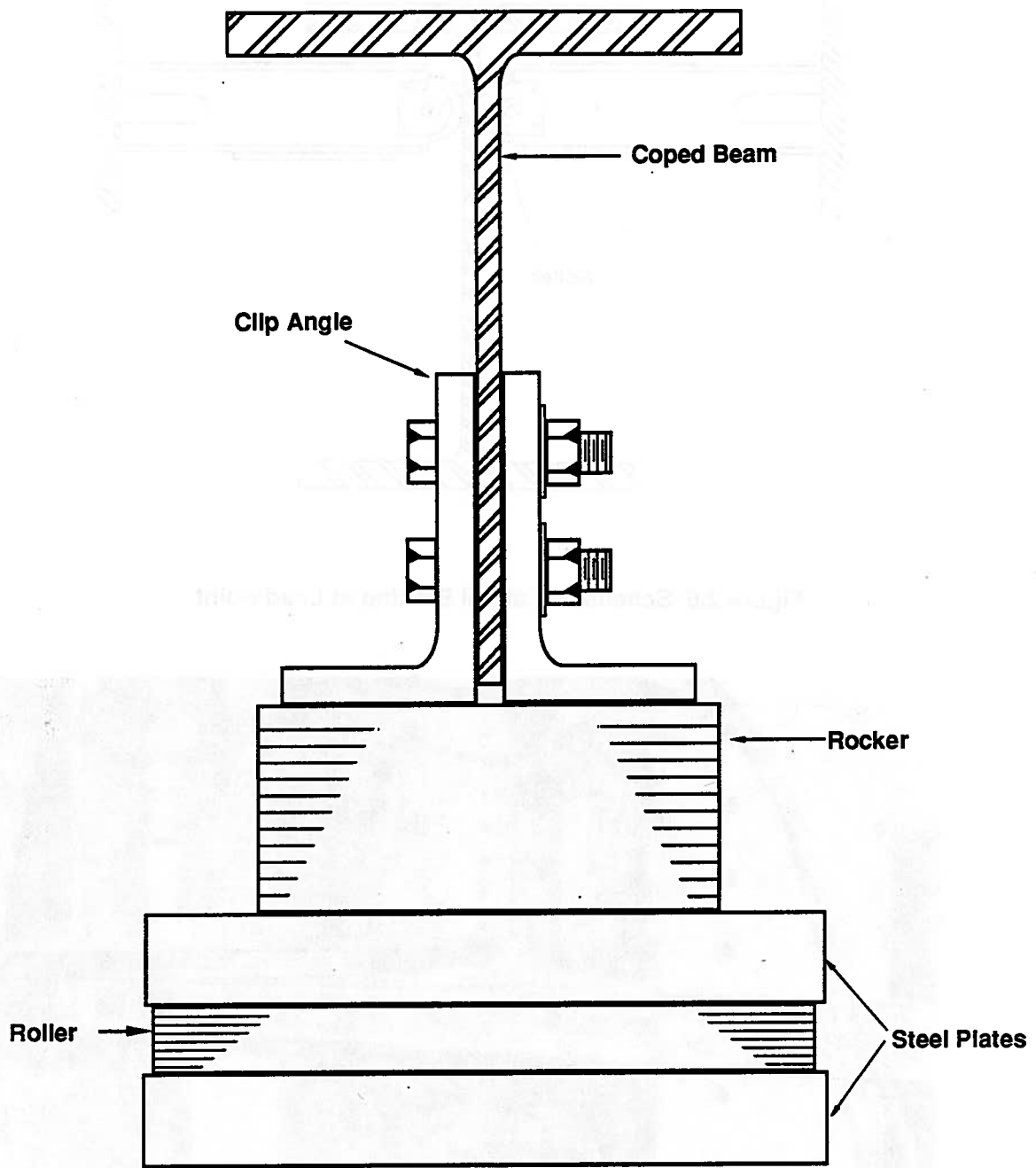
Figure 2.5 Clip Angle Connection at Cope End
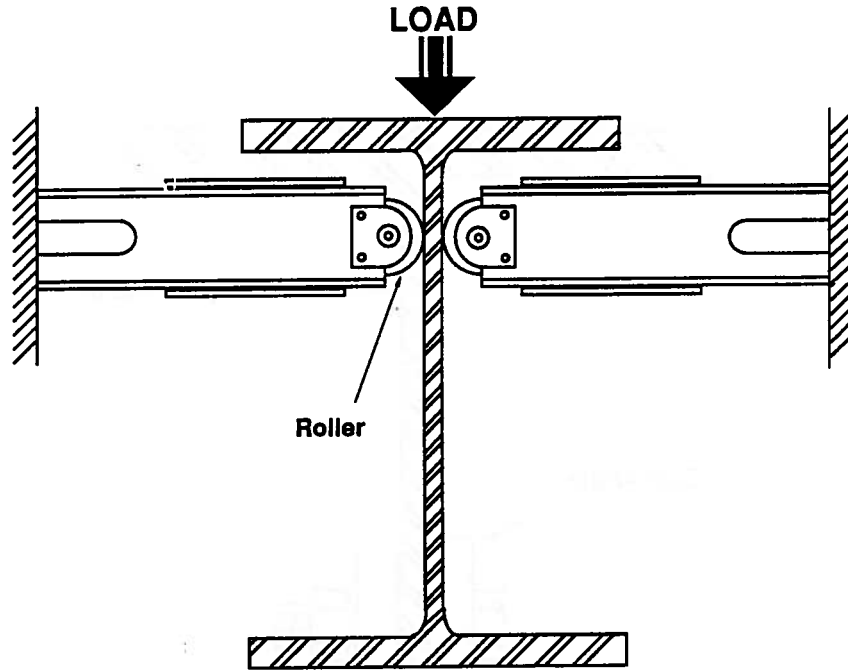
Figure 2.6 Schematic Lateral Bracing at Load Point
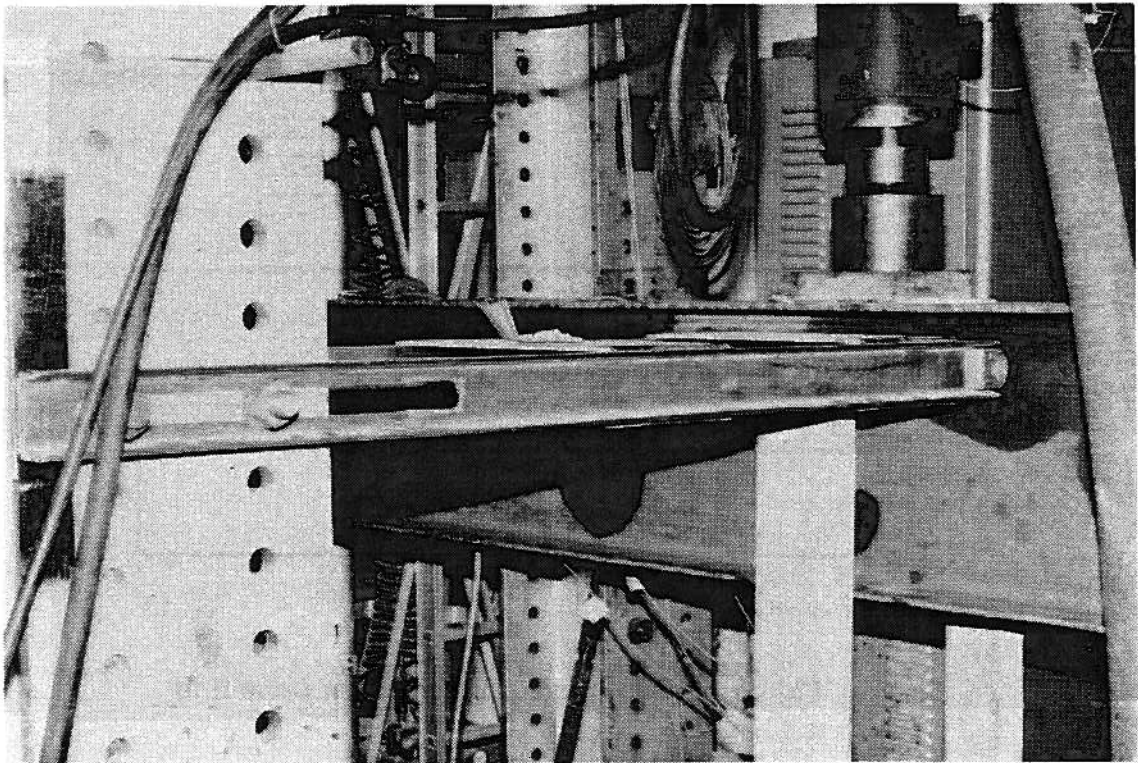
Figure 2.7 Lateral Bracing at Load Point

Variable Speed Motor

Spring

LVDT'S

Pointer
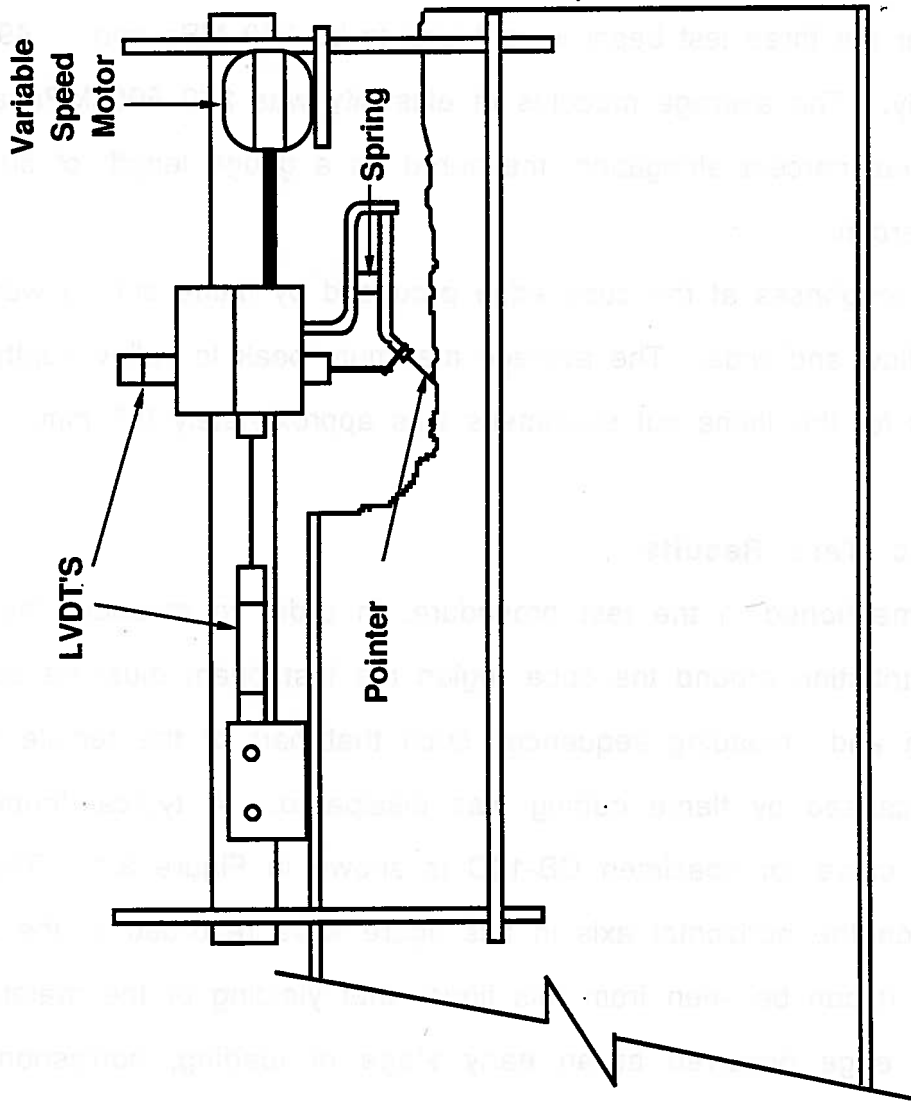
Figure 2.8 Schematic of Roughness Measuring Device

3. EXPERIMENTAL RESULTS AND DISCUSSIONS

3.1 Ancillary Tests Results

The material properties of the tested coupons are presented in Table 3.1 for each test beam. The average static yield strength and ultimate strength for the three test beam were found to be 370 MPa and 493 MPa, respectively. The average modulus of elasticity was 200 500 MPa and the average final percent elongation, measured on a gauge length of 50.8 mm, was 32 percent.

The roughness at the cope edge produced by flame cutting was found to be shallow and wide. The average maximum peak to valley depth of the roughness for the flame cut specimens was approximately 0.7 mm.

3.2 Static Test Results

As mentioned in the test procedure, in order to measure the elastic stress distribution around the cope region the test beam must be subjected to loading and unloading sequences such that part of the tensile residual stresses caused by flame cutting was dissipated. A typical loading and unloading curve for specimen CB-10C is shown in Figure 3.1. The strain readings on the horizontal axis in this figure were recorded at the rosettes location. It can be seen from this figure that yielding of the material near the cope edge occurred at an early stage of loading, corresponding to approximately 15 percent of the yield load. It was found in this study that the tensile residual stresses produced by flame cutting could be as high as 300 MPa. Although stress reversal is not considered in this experimental program, it is believed that coped beams subjected to compressive stress

range will also develop fatigue problems because of the high tensile residual stresses at the cope edge produced by flame cutting.

The measured longitudinal stress distributions, corresponding to an applied load of 100 kN are presented in figures 3.2 to 3.10. The stress distribution predicted by beam theory is also plotted in Figure 3.2. It can be seen from these stress distribution curves that a smaller cope radius has a greater stress concentration effect in the vicinity of the cope edge. For specimen CB-0, a very high stress concentration existed at the cope edge relative to other specimens because this specimen with a right angle cope represented the worst condition in this kind of detail. Since the rosettes were not positioned exactly at the cope edge, the measured bending stresses by the rosettes could not be used to evaluate the stress concentration factors exactly at the cope edge. Nevertheless, the measured stress distribution did illustrate the severity of the stress concentration produced by cope geometry.

3.3 Fatigue Test Results

The fatigue life of each specimen, corresponding to the stage of unstable crack growth, is shown in Table 3.2. For specimen CB-10A, it should be noted that a 1 mm deep notch was found in the cope region where the crack initiated. For other specimens no initial crack or significant notch was detected by visual inspection. The failure of the specimen corresponds to a final crack size of approximately 65 percent of the depth of coped section. The number of cycles required to propagate to a crack size of 30 mm is shown in the last column of this table. The 30 mm crack size was selected as a basis for comparison with the analytical results by linear elastic fracture mechanics (LEFM) presented in chapter 5. This is

because the applicability of LEFM is doubtful for large crack sizes and it is also believed that a 30 mm crack can be easily detected by simple inspection techniques.

It can be seen from this table that stress range and cope radius are the two primary factors that affect the fatigue strength of coped beams. These two factors will be discussed separately in the following sections.

The effect of the cope fabrication procedure on the fatigue strength of coped beams was not fully investigated in this experimental program. Nevertheless, a general discussion of this factor will be presented in the section 3.3.4.

3.3.1 Crack Initiation and Growth

In all specimens, the crack was initiated within the circular curve region of the cope. A typical failed specimen is shown in Figure 3.11. The location of crack initiation site of the failed specimens is presented in Table 3.2. It was found that the crack started at a plane normal to the circular curve and then propagated at an angle approximately $35°$ from the vertical through the web until net section failure as illustrated in Figure 3.11.

A typical failure surface of the failed specimen is shown schematically in Figure 3.12. The fatigue crack started as a tensile mode failure perpendicular to the web surface and this was then followed by a shear mode failure. The occurrence of the shear mode failure is due to the increase in the size of the plastic zone as the fatigue crack propagates; this causes the formation of a plane stress condition (Broek 1986). Beach marks on the fracture surface were observed at the final stage of the crack propagation, as shown in Figure 3.13.

The crack growth-curves for each specimen are presented in figures 3.14 to 3.16. Figure 3.14 shows the crack growth curves for different cope radii with a nominal stress range of 50 MPa. The influence of the nominal stress range on the crack growth rate and fatigue life is illustrated by Figure 3.15. The crack growth curves corresponding to different cope fabrication procedures are shown in Figure 3.16.

3.3.2 Effect of Cope Radius

In Figure 3.14 the slope of the crack growth curves, representing the crack growth rate, was similar because the stress concentration effect produced by the cope geometry only influences the initial stage of crack propagation. Once the crack propagated away from the stress concentration region, the geometric effect of the cope diminished, resulting in similar crack growth rate. The curves in Figure 3.14 also show that with the increase in cope radius, the fatigue life increases. This is because a smaller cope radius has a higher stress concentration effect, thus affecting the initial stage of the crack propagation. This figure also shows that with the increase in nominal cope radius from 10 mm to 30 mm the fatigue life increases by more than three times. Hence it can be seen that cope radius is a dominant factor that affects the fatigue strength of coped beams.

3.3.3 Effect of Stress Range

As expected, Figure 3.15 shows that the fatigue life of coped beams decreases as the nominal stress range increases. It can also be seen from these curves that the rate of crack growth, after the crack has propagated away from the stress concentration region, increases with increasing

nominal stress range. This figure also shows that with the decrease in nominal stress range from 50 MPa to 40 MPa the fatigue life of coped beams is more than doubled.

3.3.4 Effect of Cope Fabrication Procedure

As was presented in Table 3.2, the fatigue lives of specimen CB-20B, which had a ground smooth cope edge, and specimen CB-20A, which had an as-cut edge, were 8.94×10^6 cycles and 1.30×10^6 cycles, respectively. The applied nominal stress range for these two specimens was 50 MPa. Comparison of specimen CB-20B with CB-20A shows that removing the roughness at the flame cut edge by grinding has greatly improved the fatigue life of the beam. However, as shown in Figure 3.16, specimens CB-10C and CB-10D, which were tested at a nominal stress range of 70 MPa, had similar fatigue lives, even though the cope edge of CB-10D was ground smooth and the cope edge of CB-10C was left as cut. One of the reasons for the difference between these two sets of results may be attributed to the fact that specimen CB-20B was ground more deeply than specimen CB-10D. This might have resulted in different thicknesses of the martensite layer at the cope edge in the two cases. Another reason may be the different level of stress range resulting from the different applied nominal stress range and the cope radius effect. According to Gurney (1979), the effect of grinding is more effective in improving the fatigue life at low stress ranges than high stress ranges. This is due to the fact that grinding removes the crack initiating defects. Therefore a crack initiation period, which is longer at low than at high stresses, may be introduced into the fatigue life of the detail. There was no improvement in the fatigue life of the specimen CB-10E, which was produced by hole

drilling method, when comparing with specimen CB-10D. This may be due to the difference between the actual cope radius of the two specimens and the different initial crack mechanisms between the two fabrication procedures.

Table 3.1   Material Properties of Test Beams

Beam	Static Yield Strength (MPa)	Ultimate Strength (MPa)	Modulus of Elasticity (MPa)	Percent Elongation at Rupture
CB-1	375	498	198600	33
CB-2	369	490	200600	32
CB-3	366	490	202300	31

Table 3.2. Fatigue Life of Test Specimens

Specimen Designation	Nominal Stress Range (MPa)	Crack Location F_d (mm)	Cycles to Failure (N)	Cycles to 30 mm Crack (N)	Fabrication Procedure
CB-0	50	At corner	297 000	162 500	F
CB-10A	50	9.98	575 200	405 800	F
CB-20B	50	12.09	8 944 700	8 632 000	FG
CB-20A	50	16.23	1 295 300	1 080 000	F
CB-30	50	24.87	1 657 900	1 390 000	F
CB-10B	40	4.81	1 335 600	928 000	F
CB-10C	70	6.47	437 800	292 500	F
CB-10D	70	7.53	400 900	318 600	FG
CB-10E	70	4.00	269 000	211 500	D

Note : F_d is defined as
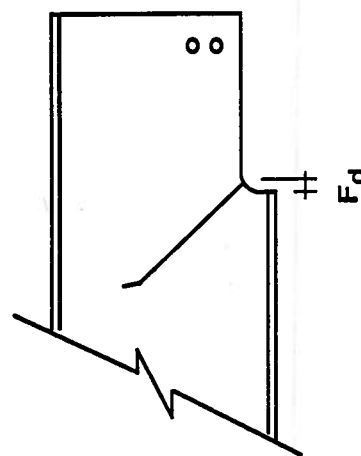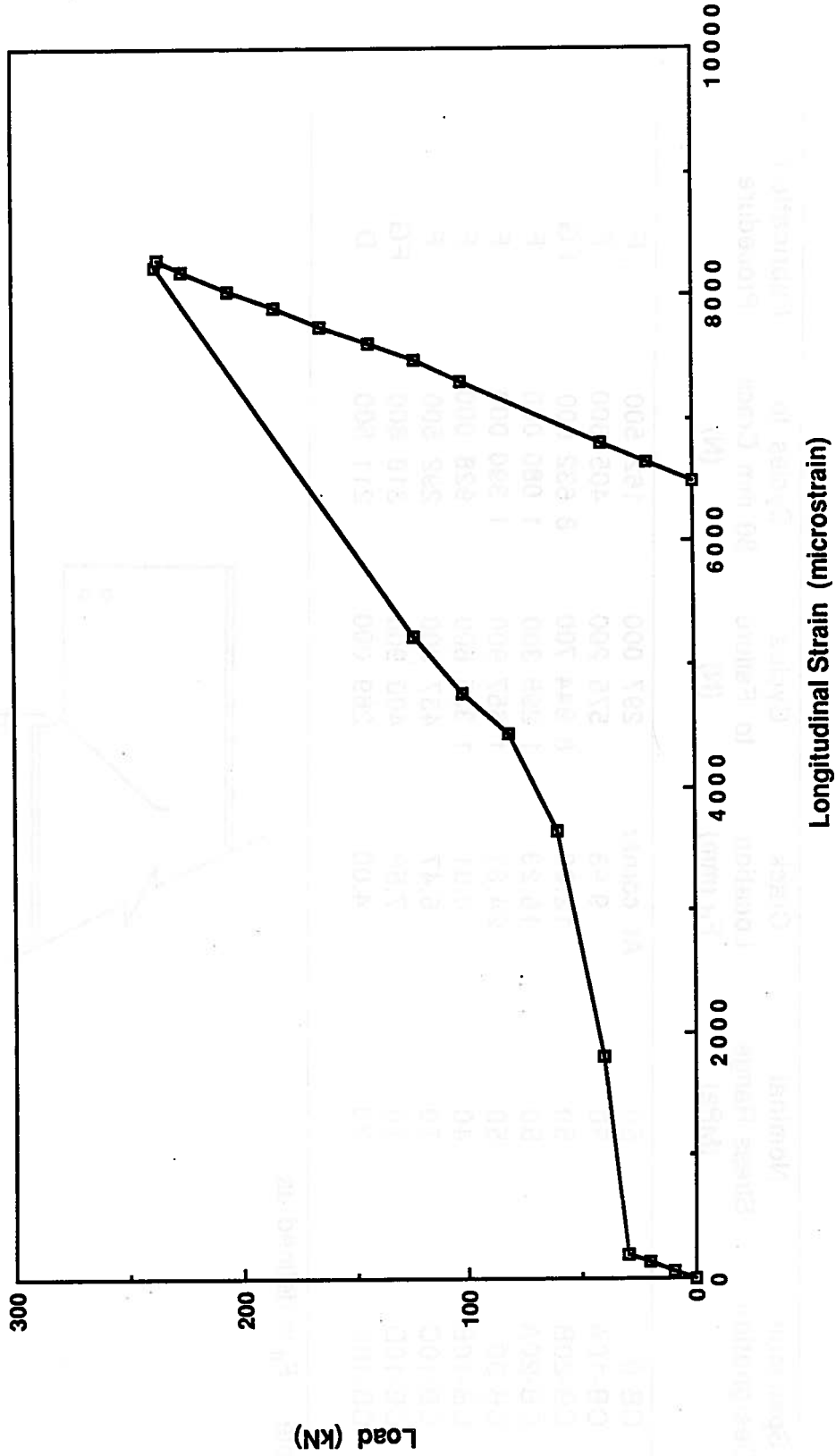
Figure 3.1 Static Test for Specimen CB-10C
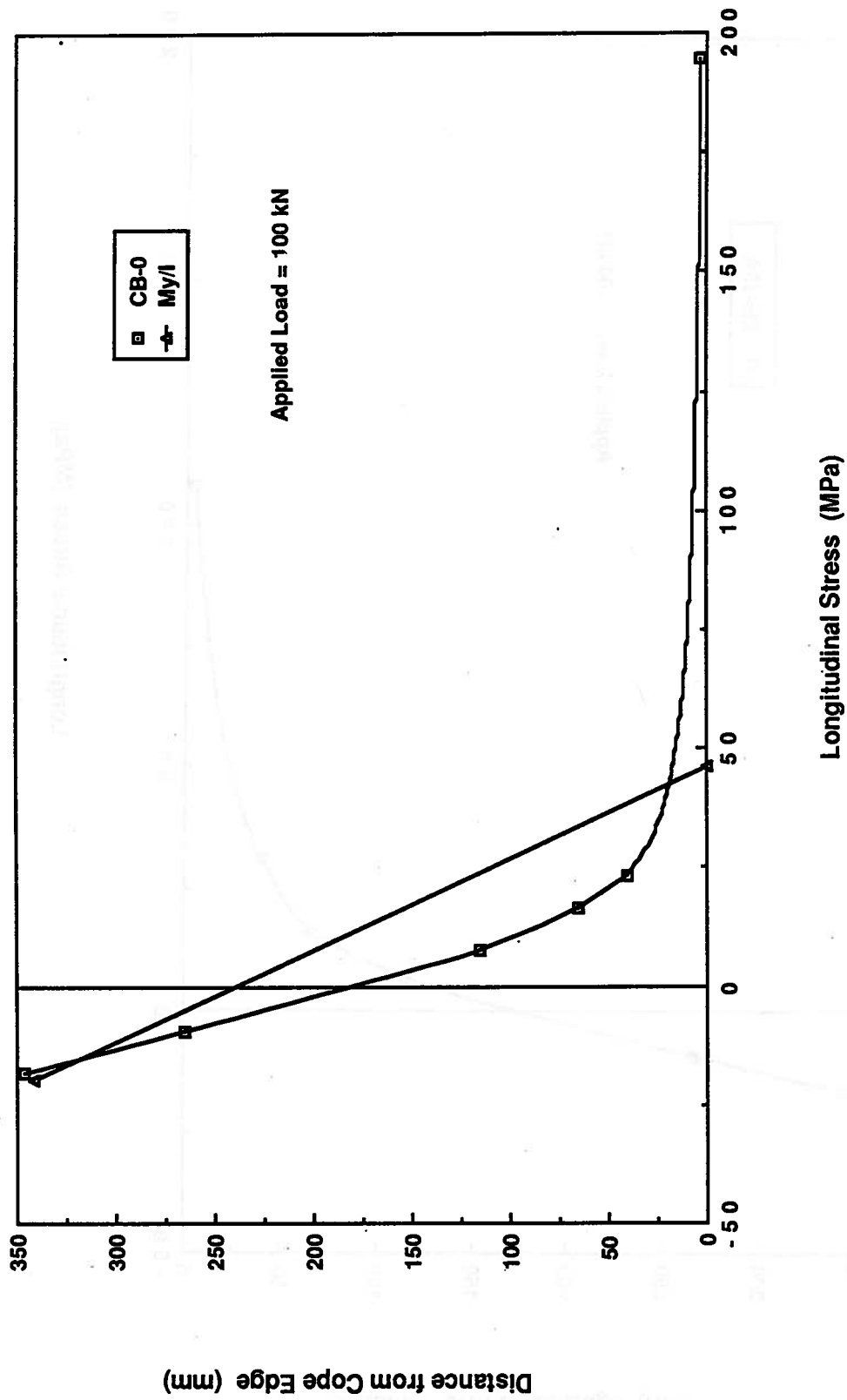
Figure 3.2 Measured Stress Distribution for Specimen CB-0
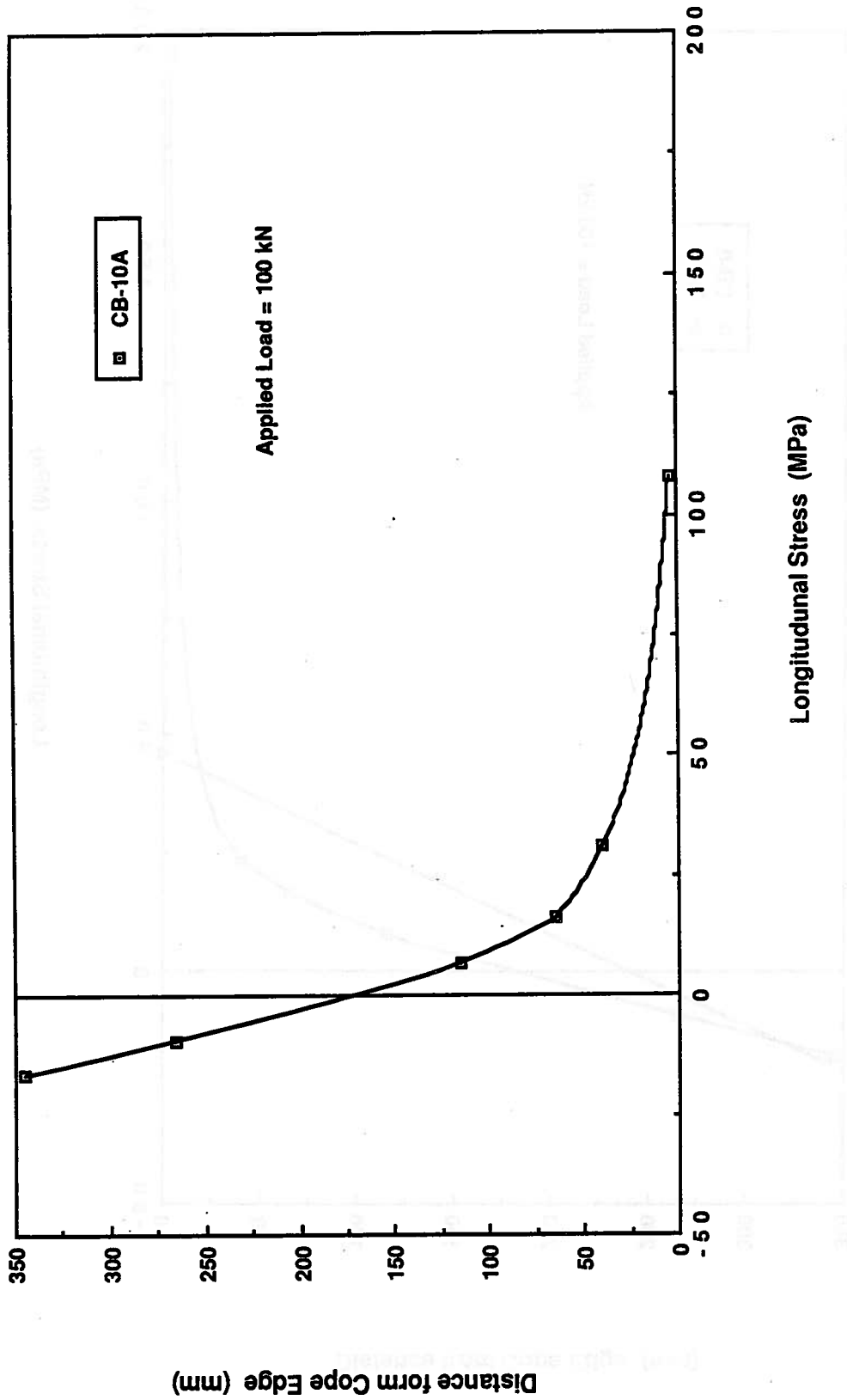
Figure 3.3 Measured Stress Distribution for Specimen CB-10A
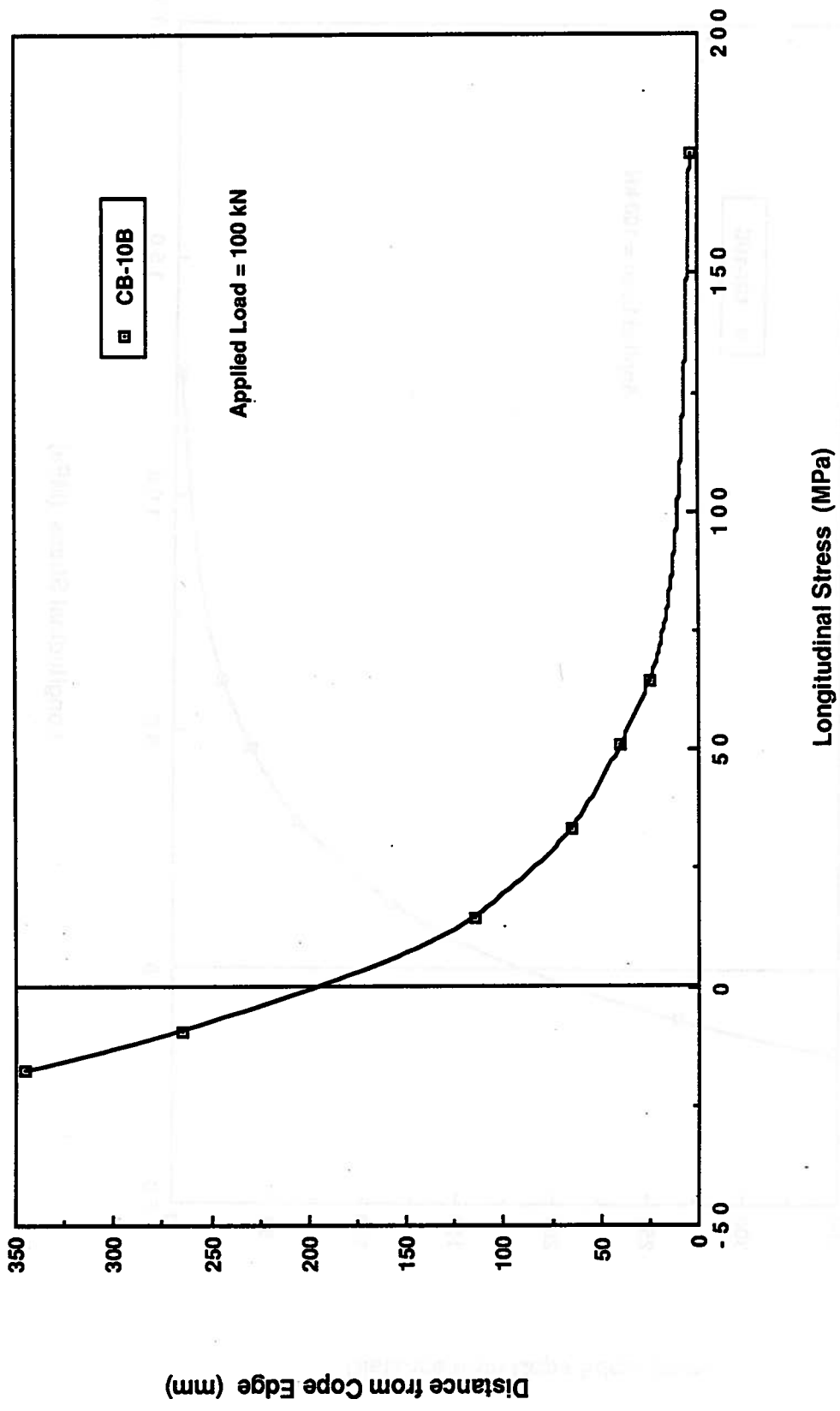
Figure 3.4 Measured Stress Distribution for Specimen CB-10B
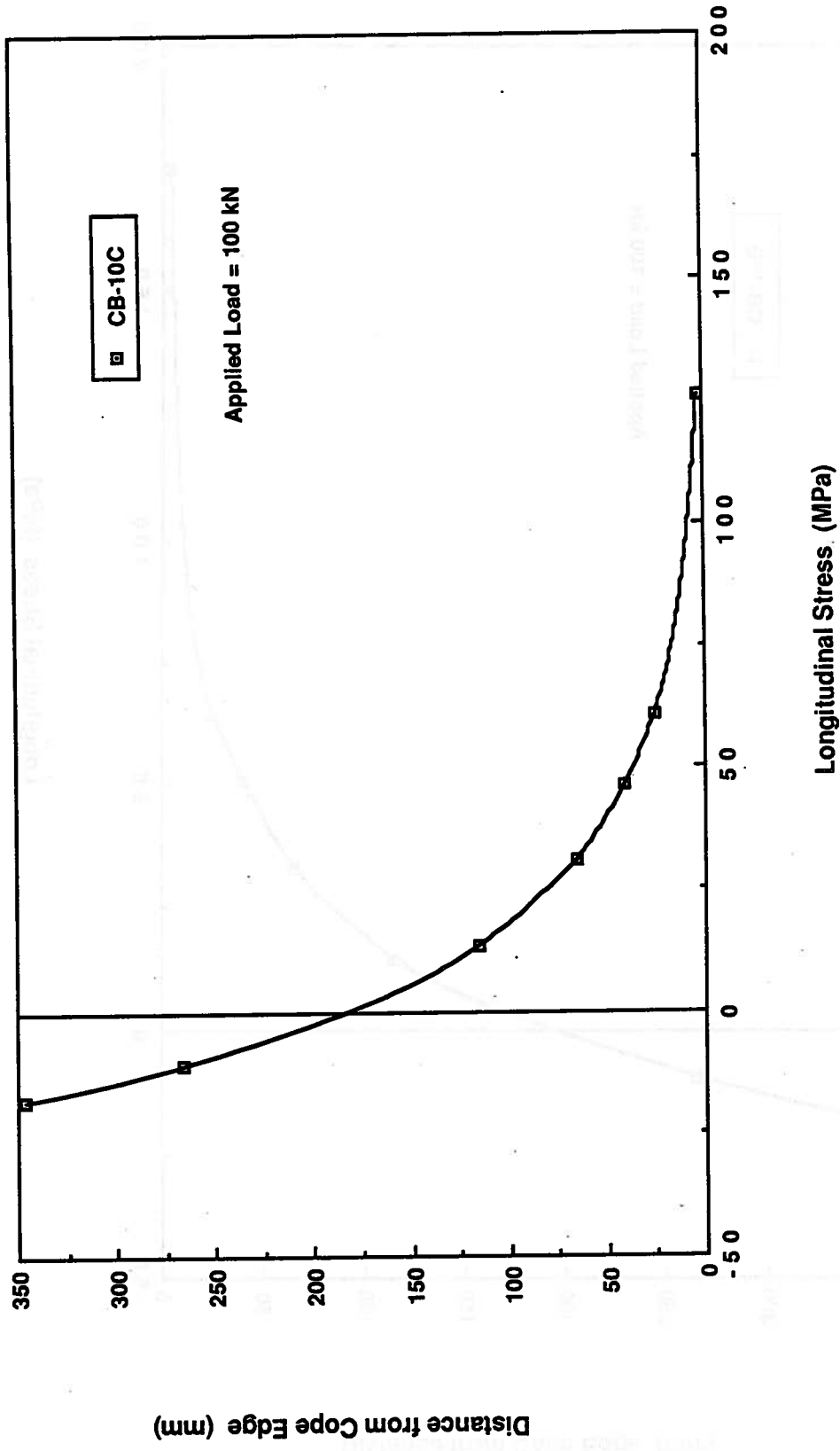
Figure 3.5 · Measured Stress Distribution for Specimen CB-10C
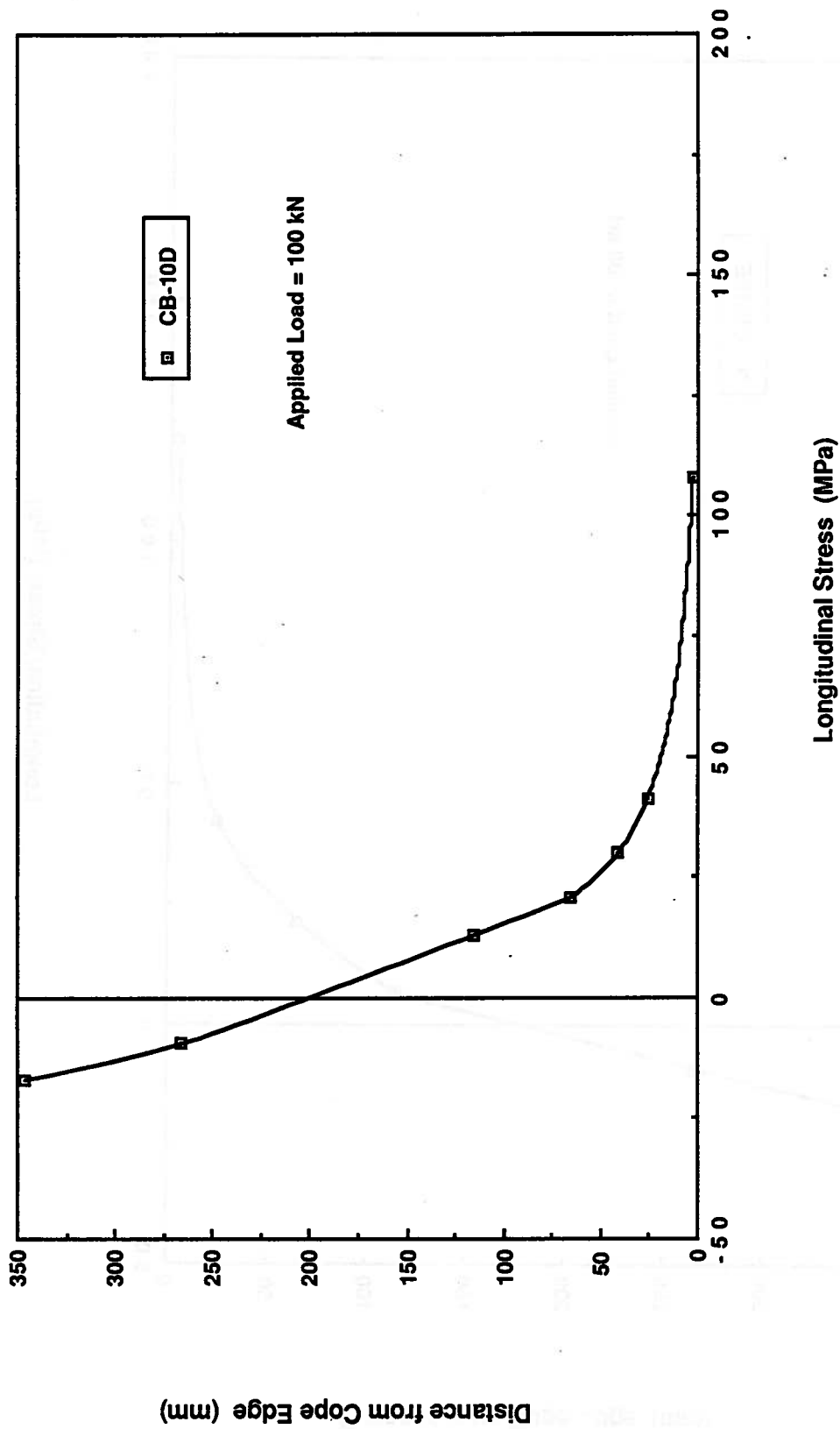
Figure 3.6 Measured Stress Distribution for Specimen CB-10D
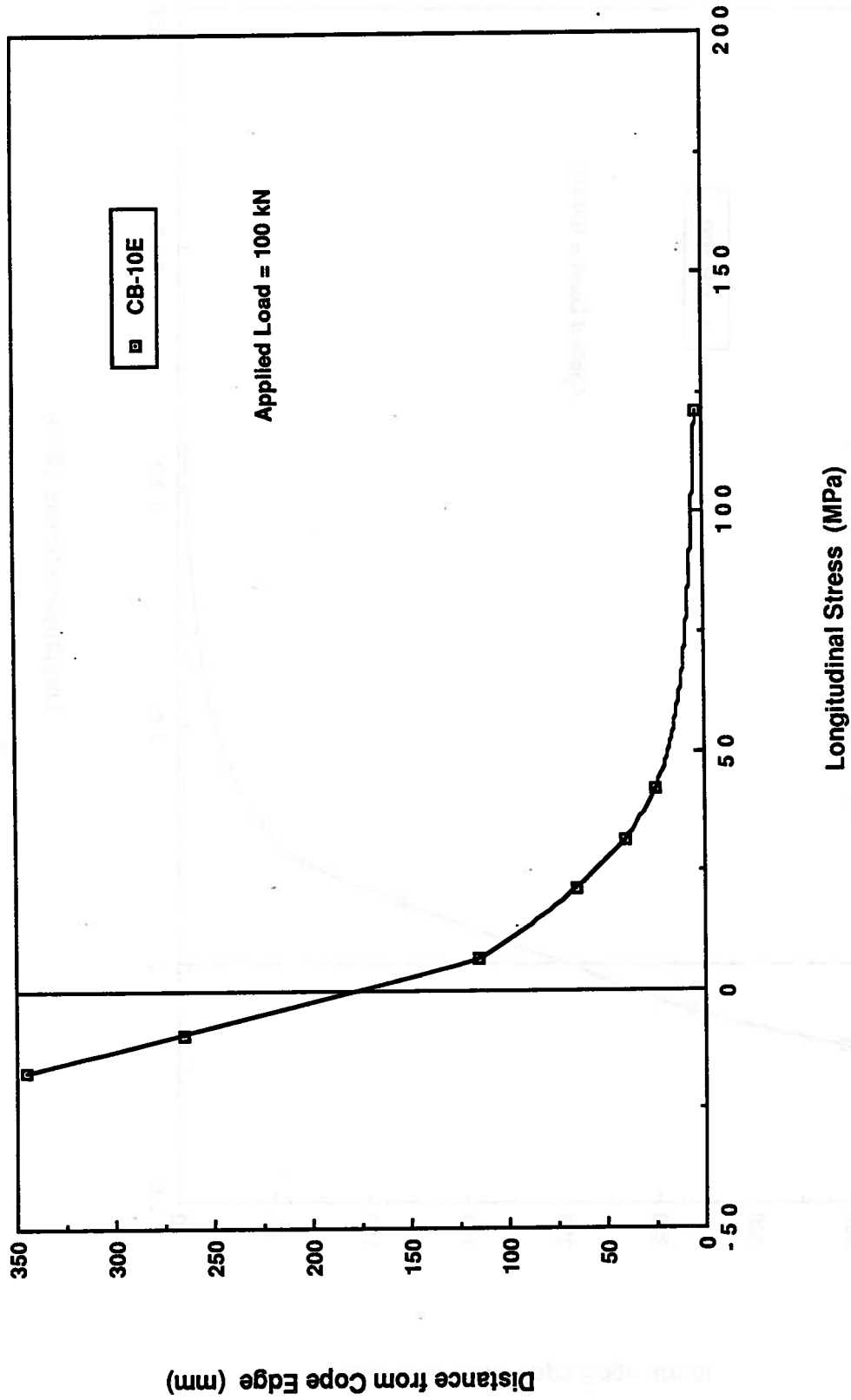
Figure 3.7 Measured Stress Distribution for Specimen CB-10E
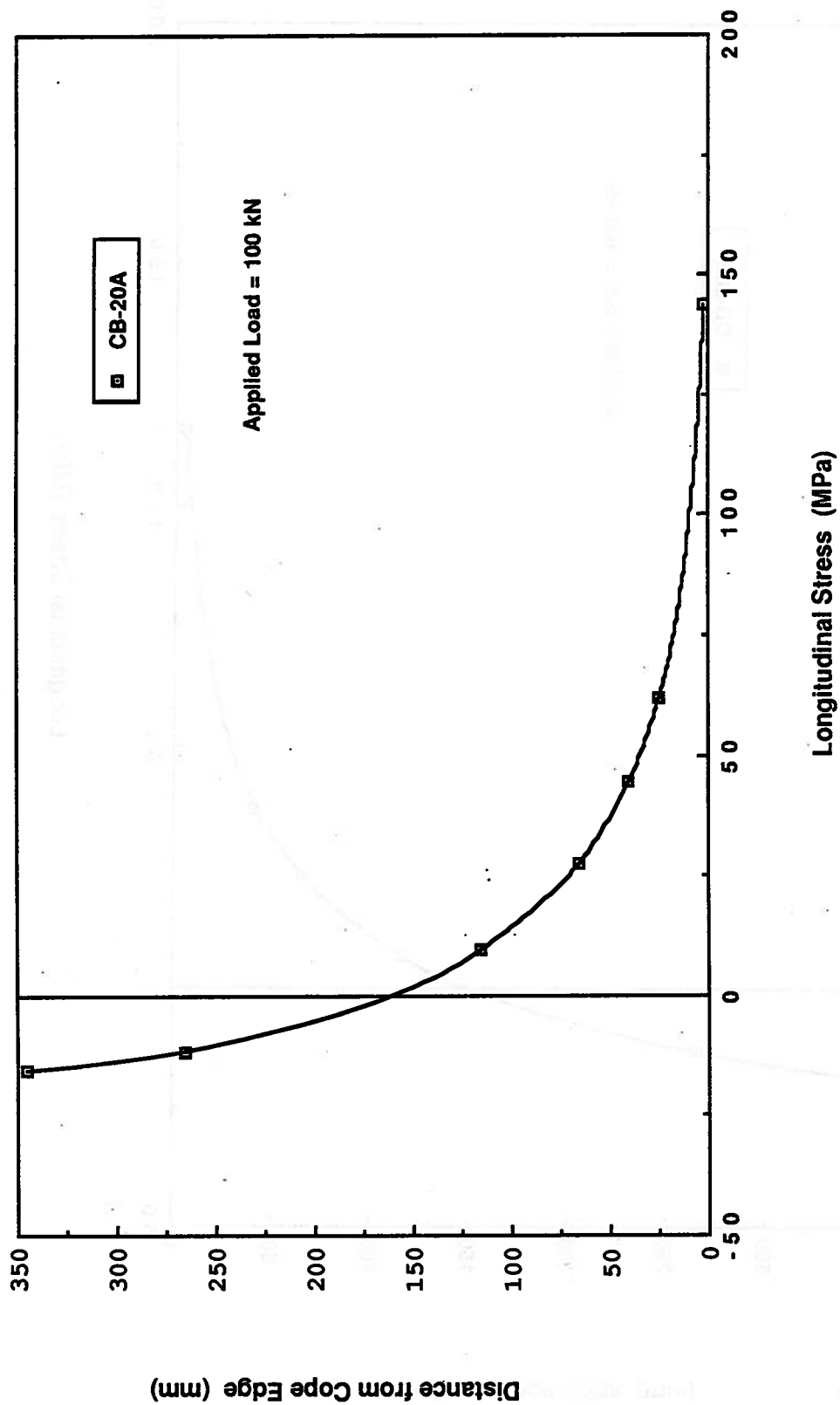
Figure 3.8 Measured Stress Distribution for Specimen CB-20A
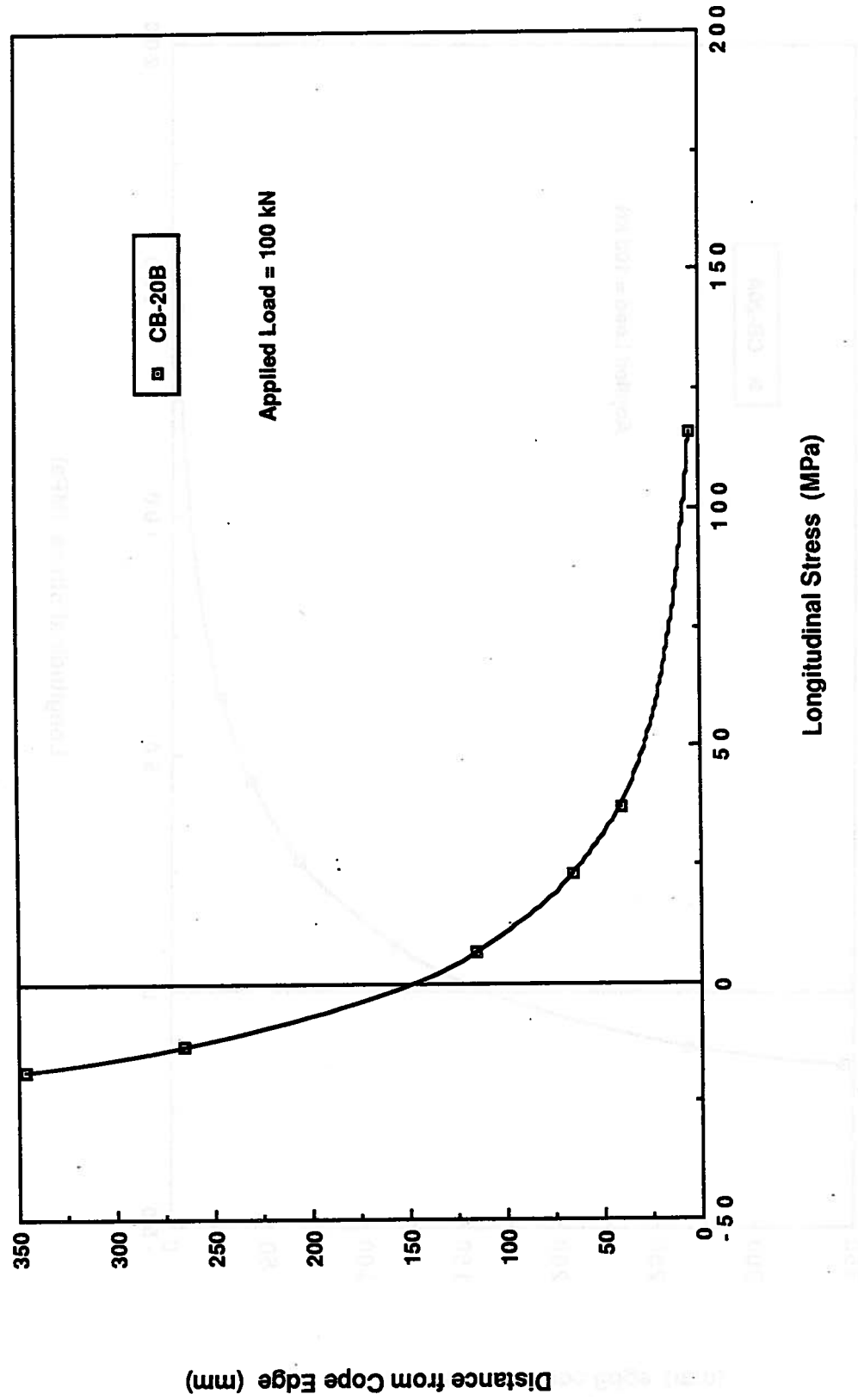
Figure 3.9 Measured Stress Distribution for Specimen CB-20B
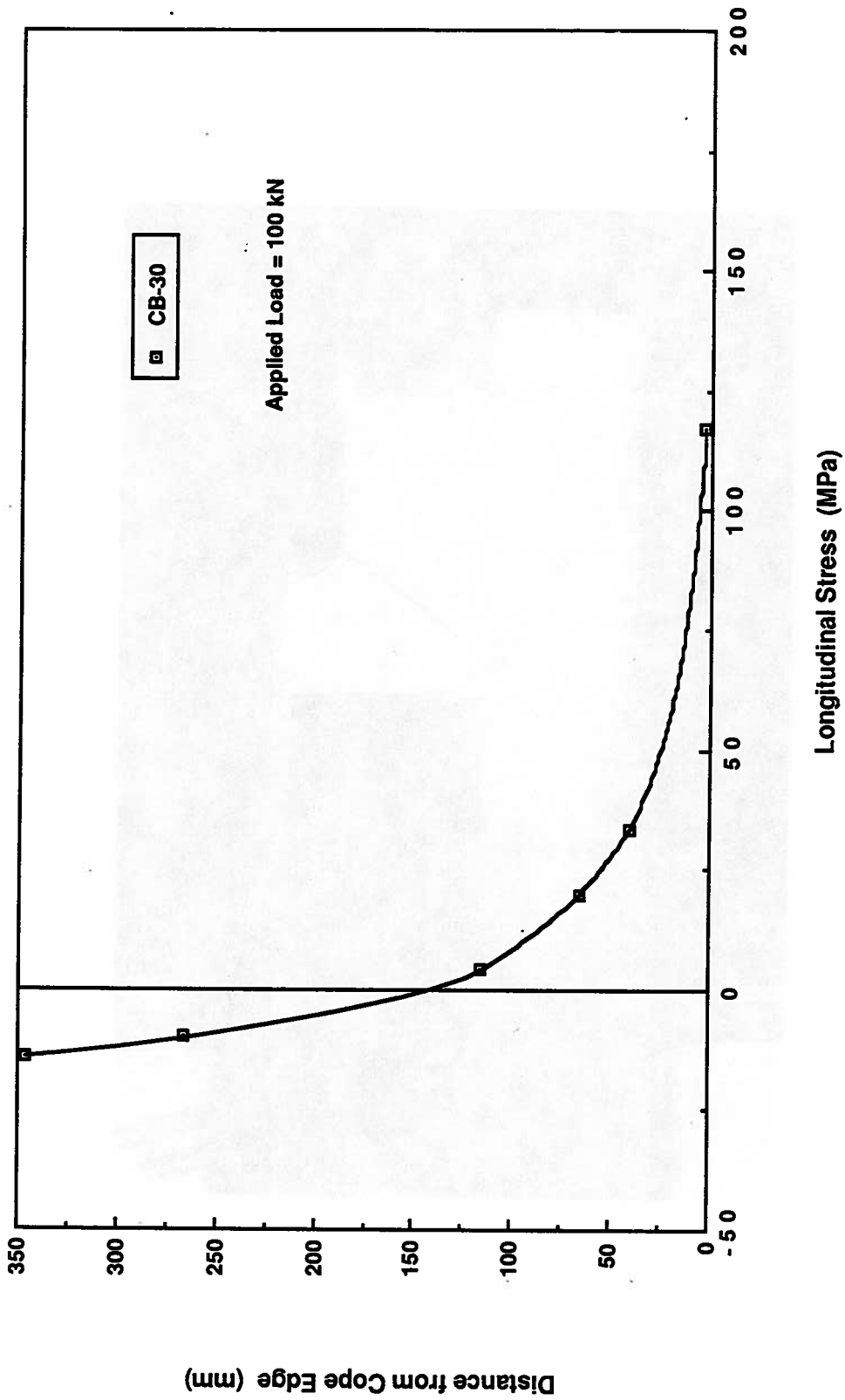
Figure 3.10 Measured Stress Distribution for Specimen CB-30
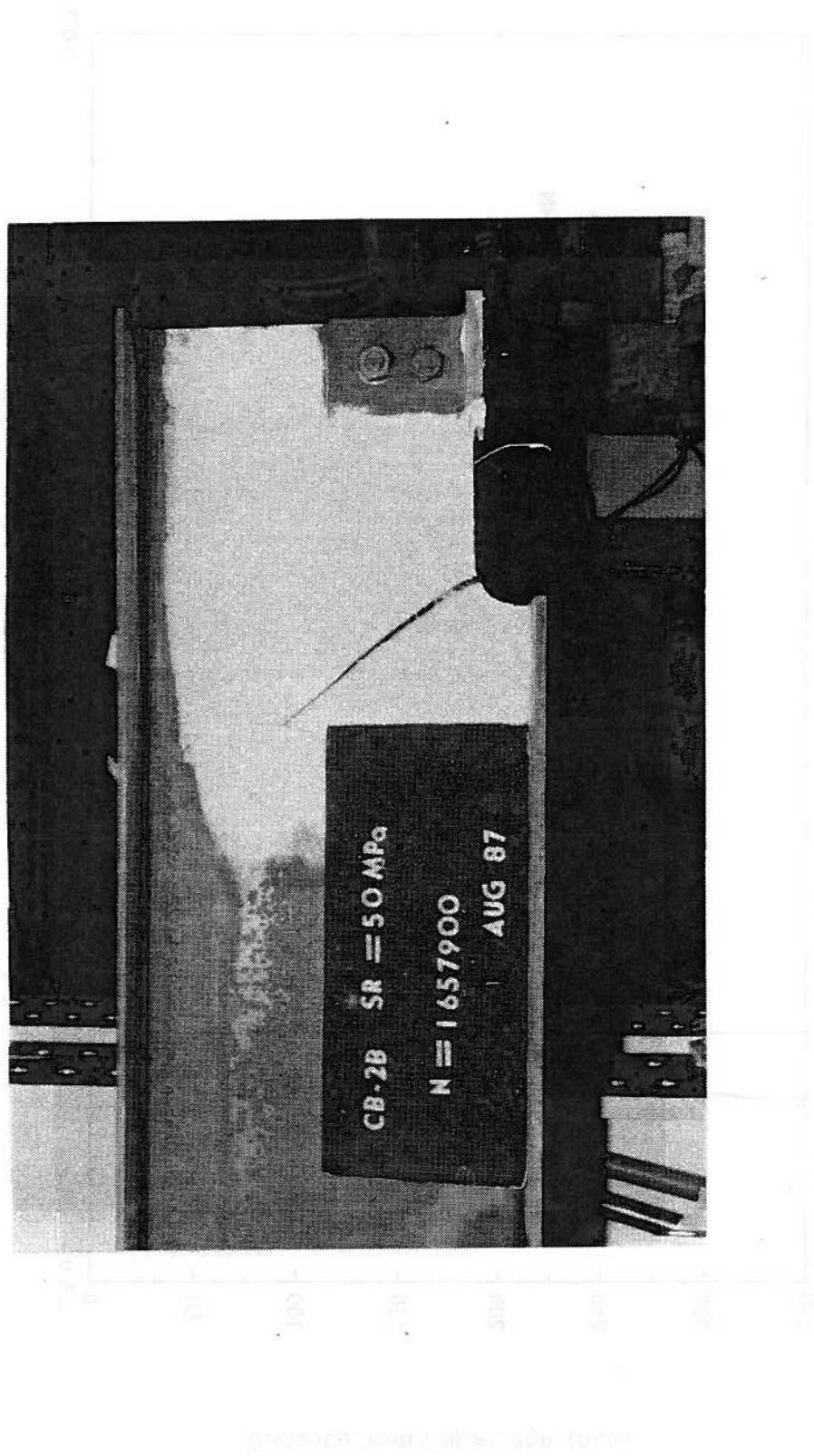
Figure 3.11 Typical Failed Specimen
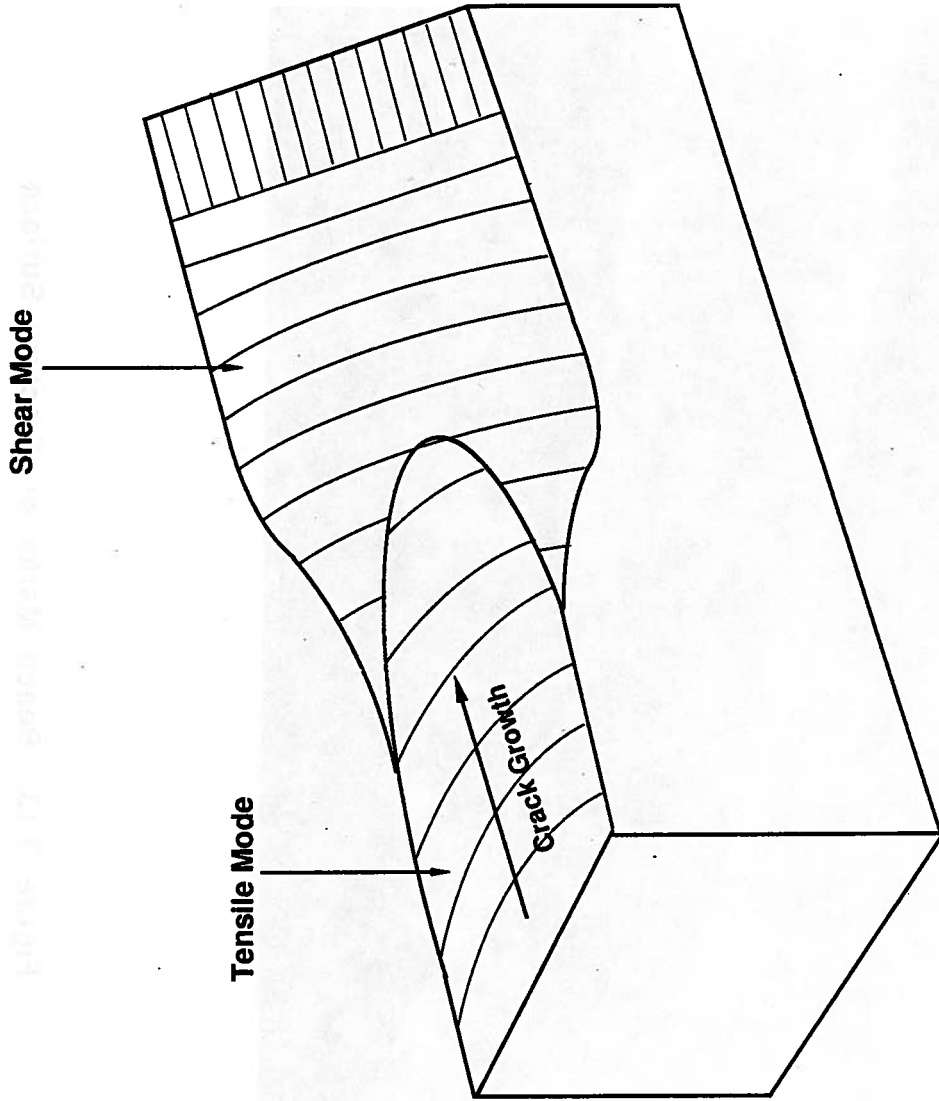
Figure 3.12 Schematic of Typical Failure Surface
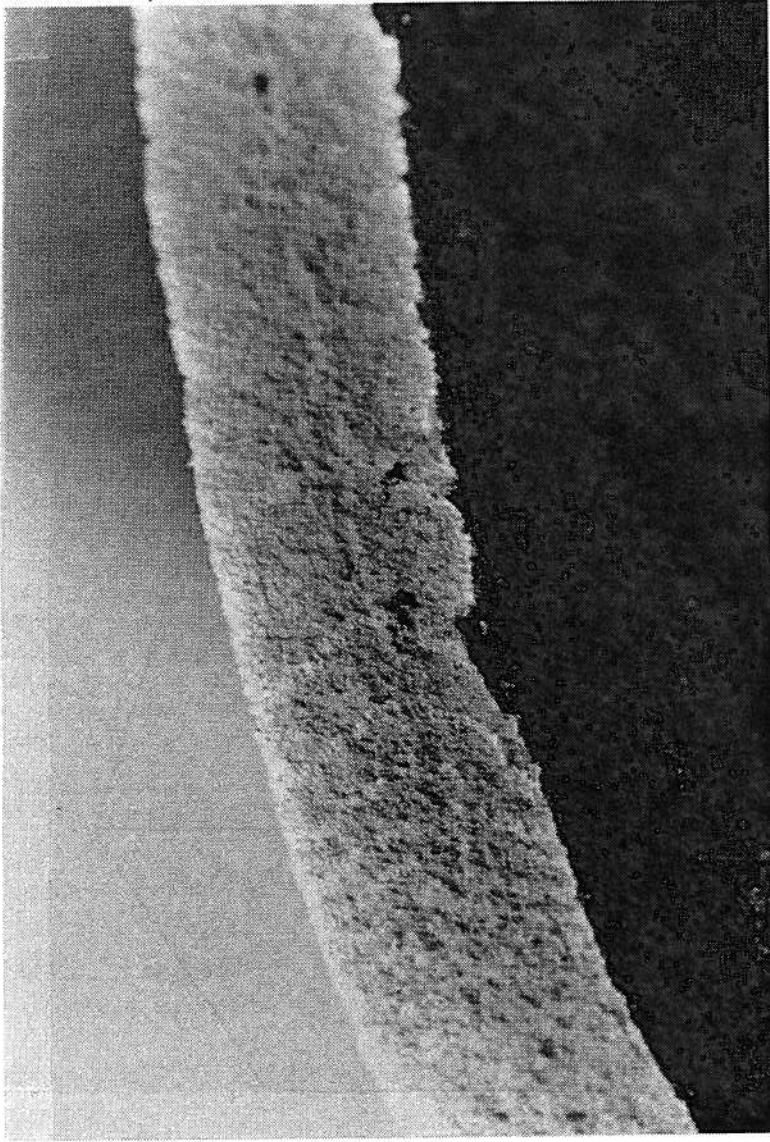
Figure 3.13   Beach Marks on Fracture Surface
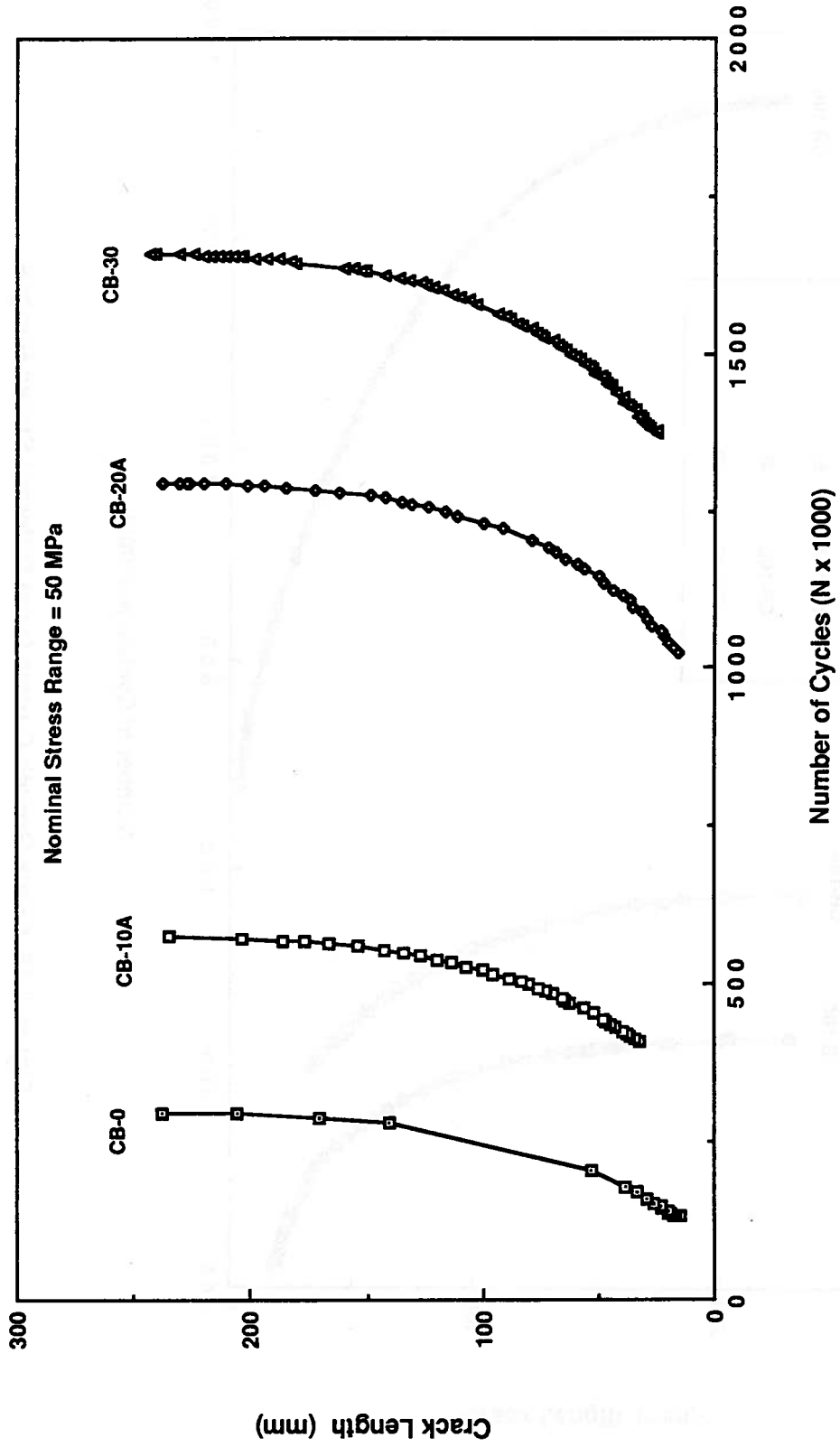
Figure 3.14 Crack Growth Curves for Different Cope Radii
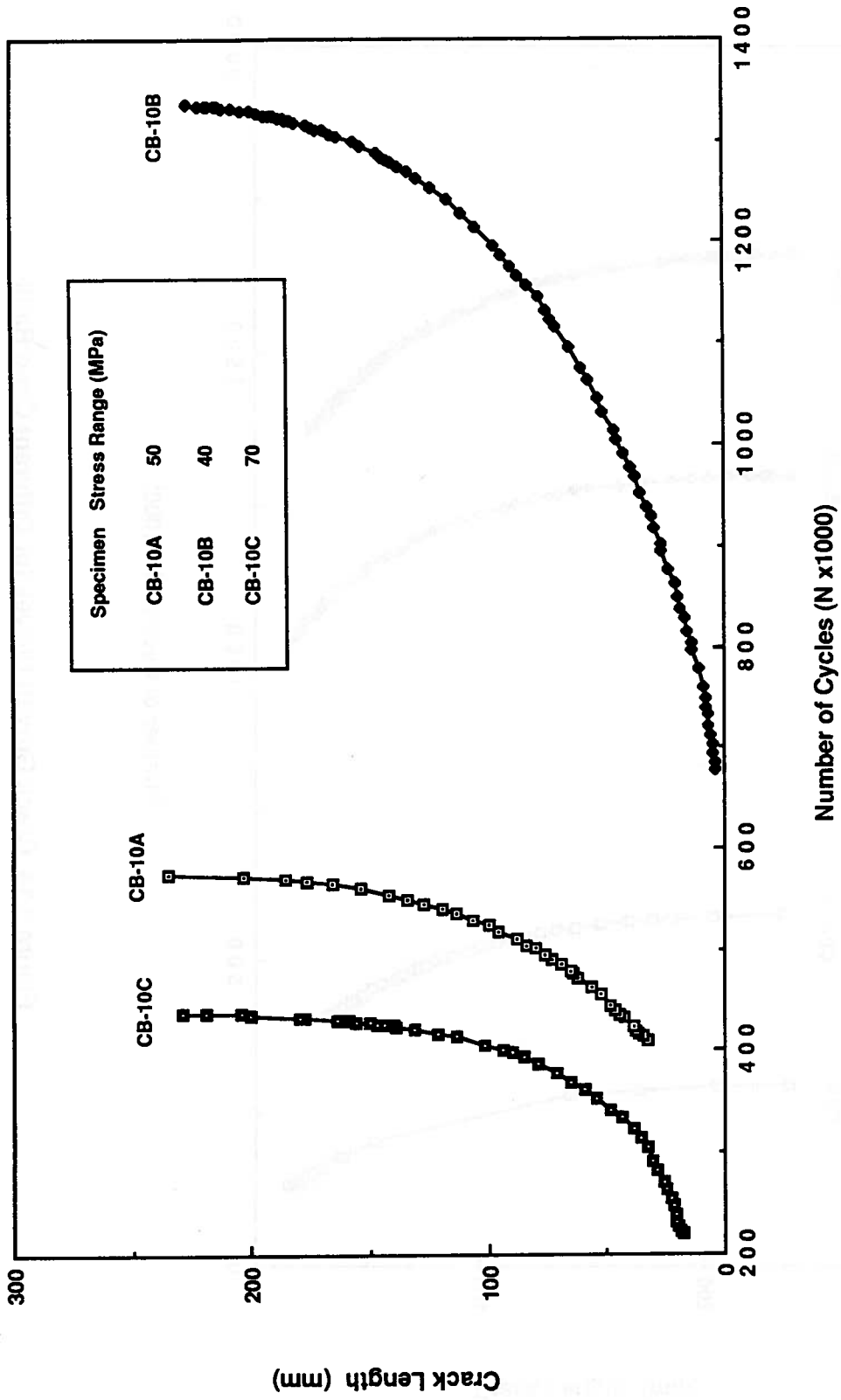
Figure 3.15 Crack Growth Curves for at Different Stress Ranges
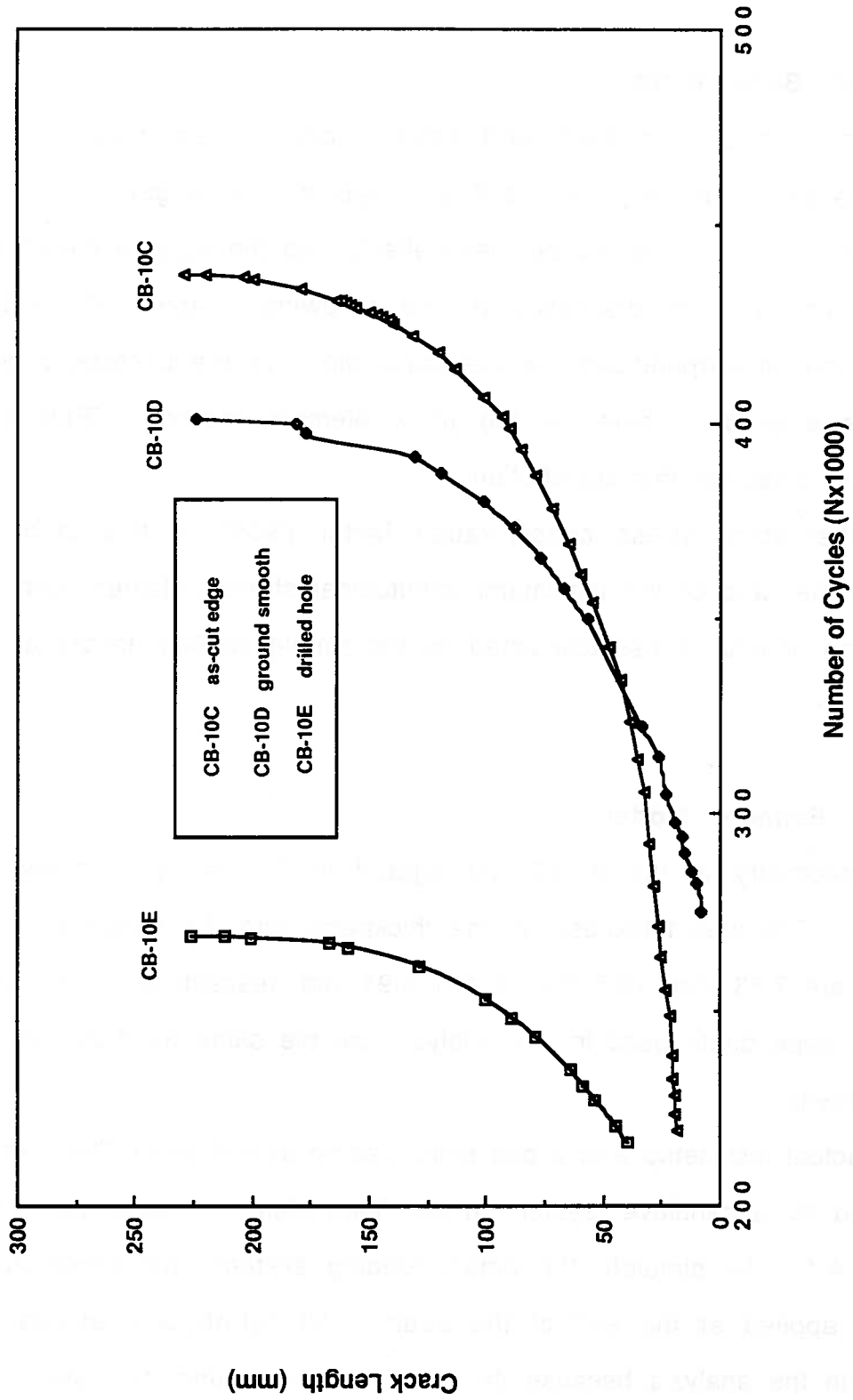
Figure 3.16 Crack Growth Curves for Different Cope Fabrication Procedures

4. STRESS ANALYSIS OF COPE DETAILS BY FINITE ELEMENT METHOD

4.1 General Background

The high stress gradient and severe local stress concentration produced by cope geometry have a direct effect on the fatigue strength of coped beams. In order to include these effects into the fracture mechanics analysis which will be discussed in the following chapter, the actual stress distribution perpendicular to the crack plane in the uncracked body must be evaluated. Therefore the finite element method (FEM) was employed to evaluate this distribution.

The theoretical stress concentration factor (SCF) in this study is defined as the ratio of the maximimum longitudinal stress obtained from the FEM to the nominal stress calculated by the simple bending theory at the cope line.

4.2 Finite Element Model

The geometry of the detail investigated in this study is shown in Figure 4.1. The web thickness, flange thickness, and the flange width of this beam are 7.83 mm, 10.5 mm, and 175.91 mm, respectively. The cope length and cope depth used in this analysis are the same as those for the test specimens.

The actual test setup was a one point loading at midspan. This can be represented by a cantilever system in the finite element model, as shown in Figure 4.1. To simulate the actual loading system, two concentrated loads are applied at the end of the beam. All out-of-plane effects are neglected in the analysis because the test beam was supported laterally at the load point. The cope radius is the only parameter investigated in this

finite element analysis. Five cope radii are considered, namely: 10 mm, 15 mm, 20 mm, 25 mm and 30 mm. The assumption that the cope radius is smooth greatly simplifies the analysis because no stress singularity then exists at the detail.

The finite element program SAPIV (1974) was used to perform the analysis. Rectangular and triangular plane stress elements with two degrees of freedom at each node were selected to model the test beam. An incompatible displacement mode is incorporated in the analysis since the structure is primarily loaded in bending. This incompatible displacement mode, which includes a quadratic displacement function, allows the rectangular plane stress element to behave as a two dimensional beam element. For the triangular plane stress element, incompatible displacement mode is suppressed automatically by the program. The values of Young's modulus and Poisson's ratio used in the analysis are 200 000 MPa and 0.3, respectively.

A general coarse mesh, as shown in Figure 4.2, is used to analyse the cantilever beam. The flanges are modelled by increasing the thickness of the elements at the flange locations. The thickness of those elements is equal to the flange width. Since out-of-plane effects are not investigated in this analysis, modelling of the flange in this manner is believed to be adequate. In order to study the localized effects of the cope radius, the coarse mesh is refined in the cope region. The shaded portion of the coarse mesh in Figure 4.2 is refined to a fine mesh as shown in Figure 4.3. Since the stress concentration is highly localized, it is believed that the stress distribution outside the shaded portion of the coarse mesh should not be affected by the stress concentration in the vicinity of the cope edge. Nodal

displacements at the boundary of the shaded region of the coarse mesh are used as boundary conditions for the fine mesh.

The finite element mesh does contain some error due to the approximation of the circular curve with straight lines between nodal points. The error of approximating the circular curve by chords in terms of percentage is defined as (Zettlemoyer and Fisher 1978) :

$$\% \text{ Error } = 100 \left[1 - \sqrt{1 - \left(\frac{D}{2R}\right)^2} \right] \qquad [4.1]$$

where D and R are defined in Figure 4.4. The maximum error in this analysis, which is found from a cope radius of 10 mm and chord length of 2.5mm, is 0.8% according to equation [4.1]. This small error is believed to have negligible effect on the stress analysis. Furthermore, a chord length of 2.5 mm is also used for the fine mesh in all other cope radii investigated in this study.

The size of the fine element, defined as the length of the fine element in the radial direction shown in Figure 4.3, is determined by successive trials until the maximium longitudinal stress converges. The maximium longitudinal stress is defined as the maximium edge stress in the longitudinal direction from any of the elements. Since the stress concentration increases with decreasing cope radius, the fine mesh used for the 10 mm cope radius is chosen in order to establish the element size for the other cope radii investigated in this study. By varying the element size from 5 mm to 2.5 mm, the difference in maximium longitudinal stress is only 2.6 %. Therefore, convergence is assumed to have been reached at

element size of 5 mm. Hence , an element size of 5 mm is used for all other cope radii in this analysis.

4.3 Analytical Results

Stress contour lines for the cope region are developed using the stress analysis results of the fine mesh for cope radii of 10 mm, 20 mm, and 30 mm, as shown in figures 4.5 to 4.7. The element centroidal stress in the longitudinal direction is used to plot the stress contours. These contour plots illustrate the severity of stress concentration produced by the cope geometry. As shown in the figures the stress concentration becomes more severe as the cope radius is decreased.

The stress distribution from the finite element analysis can be compared with measured stress distributions at the strain gauge locations. These are shown in figures 4.8 to 4.11. As indicated in these figures, reasonable agreement is obtained between the predicted values and the measured values. The stress distribution predicted by beam theory is also plotted in Figure 4.8. It can be seen that the stress concentration effect produced by the cope geometry is concentrated within about 25 mm from the cope edge. Hence, once the crack propagates away from this region the geometric stress concentration effect decreases significantly.

The SCF values obtained from the analysis are plotted against the cope radii as shown in Figure 4.12. As expected, the SCF increases with decreasing cope radius. A logarithmic fit to the solution gives the equation:

$$\log (SCF) = 0.937 - 0.285 \log (R) \qquad [4.2]$$

where R is the cope radius in millmetres.

Although equation [4.2] only considers cope radius as the independent variable, it is believed that other variables such as cope length and cope depth will have a minor effect on the SCF. The location of maximum stress found in this study is roughly at a distance of 0.3R from the point of tangency towards the cope line.

4.4 S-N Curves

The test results tabulated in chapter 3 are plotted in Figure 4.13 along with S-N curves for Categories A and B from the CAN-3-S16.1-M84 (1984) specification. In plotting the data points in the S-N diagram, the theoretical stress range, which is the nominal (experimental) stress range multiplied by the SCF from equation [4.2], is used to illustrate the effect of stress range on the fatigue strength of coped beams.

As mentioned in Chapter 3, the fatigue crack in specimen CB-10A.was initiated at a 1 mm deep notch found in the cope region. Hence, it is believed that the fatigue life for this specimen is lower relative to other specimens as shown in Figure 4.13. Hence, the result for CB-10A was not included in the regression analysis. It should be noted that the fatigue life of the specimen corresponding to a final crack size of 30 mm was used when plotting these data points. The regression line and 95% confident limit for the test data are also shown in the figure. It can be seen from the figure that all test data lie on or above the line for Category B.
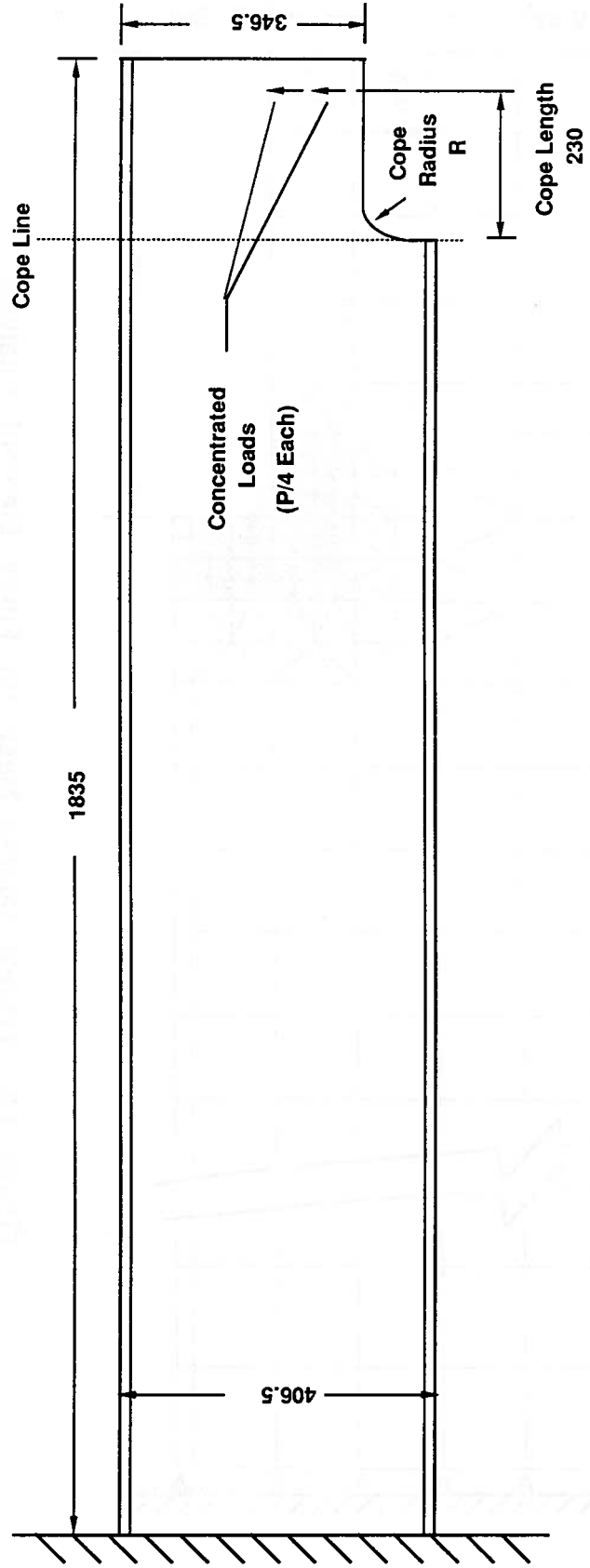
Figure 4.1 Finite Element Model
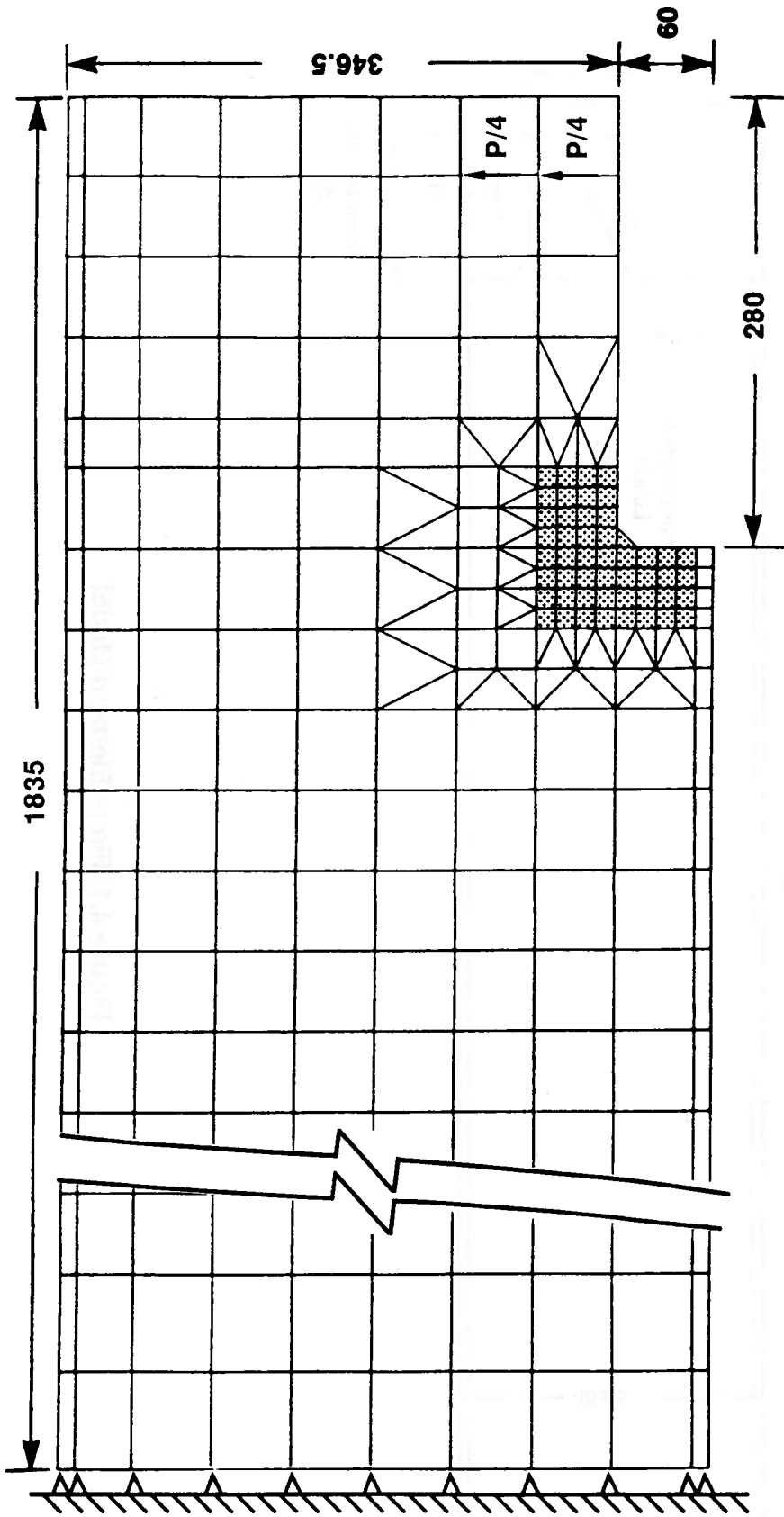
Figure 4.2 Typical Coarse Mesh for Finite Element Analysis
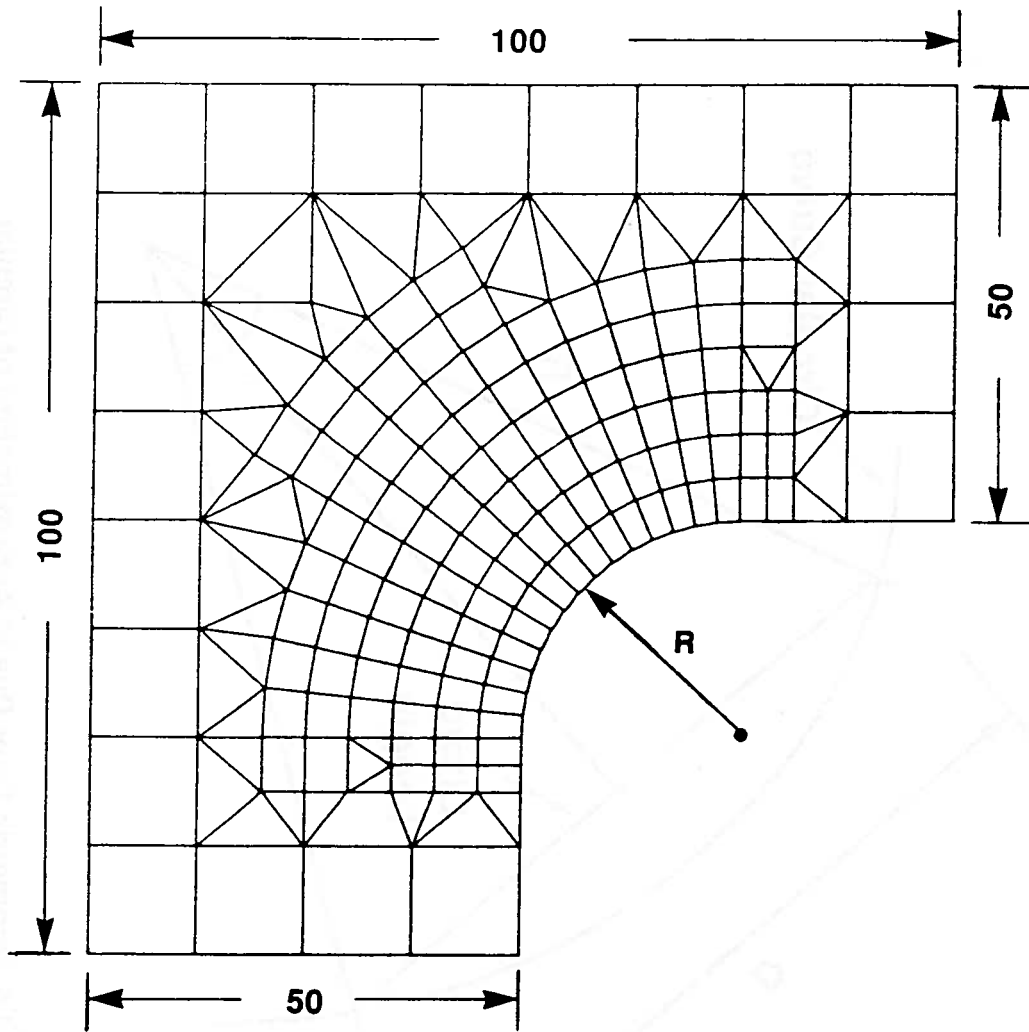
Figure 4.3 Typical Fine Mesh for Finite Element Analysis
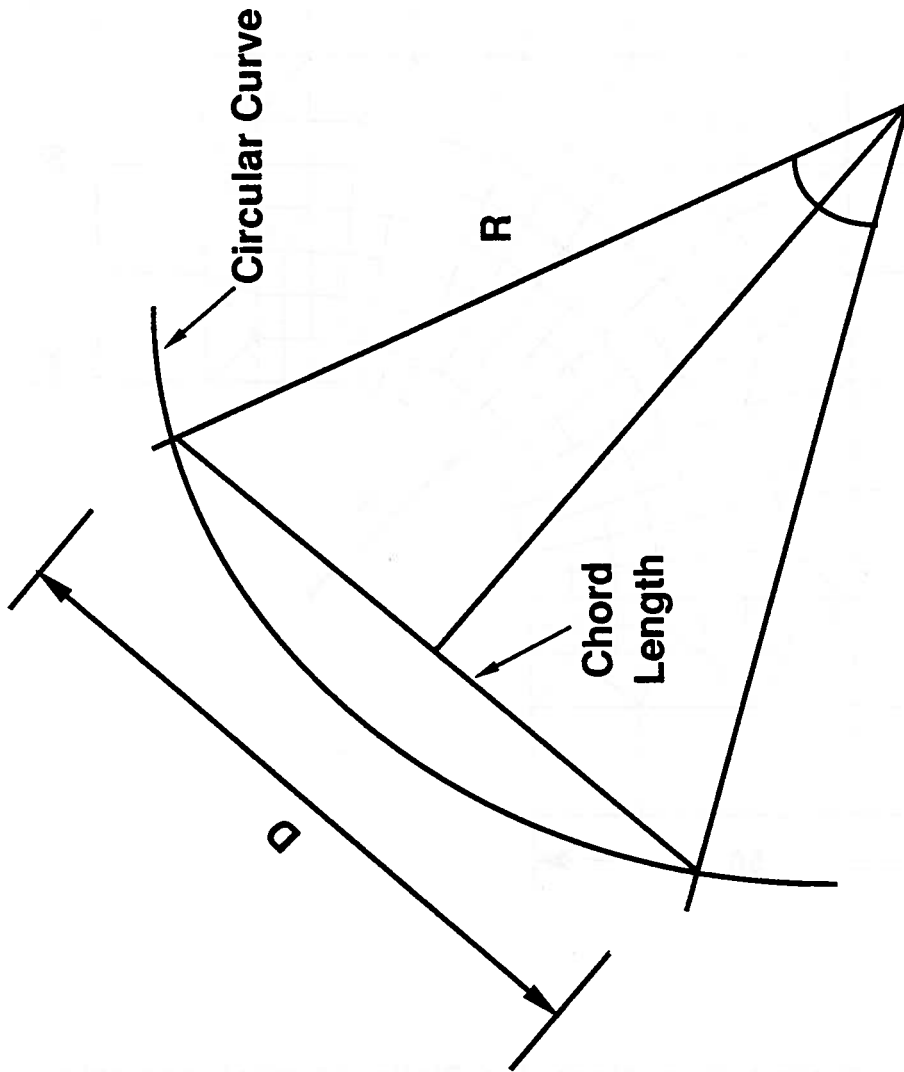
Figure 4.4 Geometric Error Due to Approximation of Circular Curve with Chords
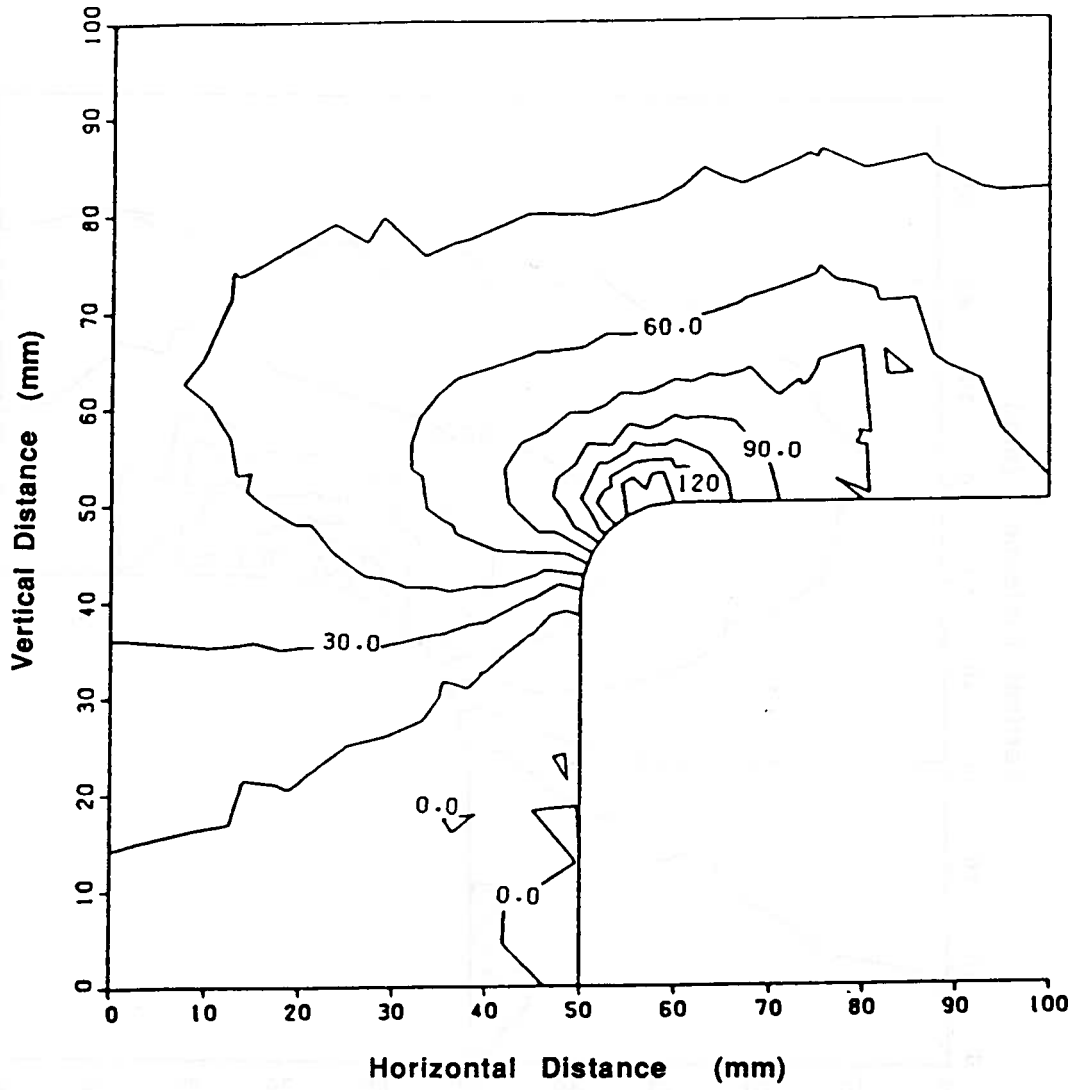
Figure 4.5 Stress Contour for 10 mm Cope Radius
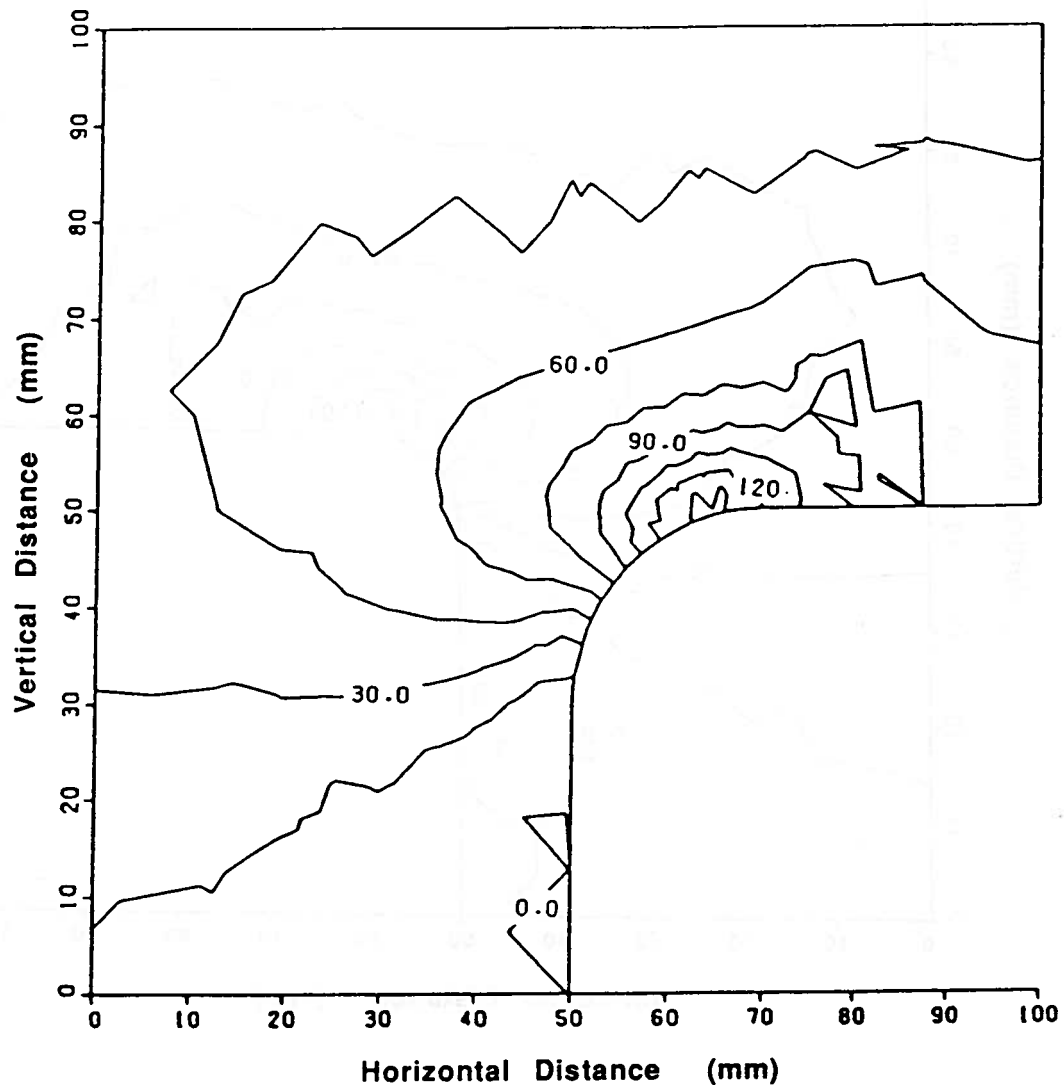
Figure 4.6   Stress Contour for 20 mm Cope Radius
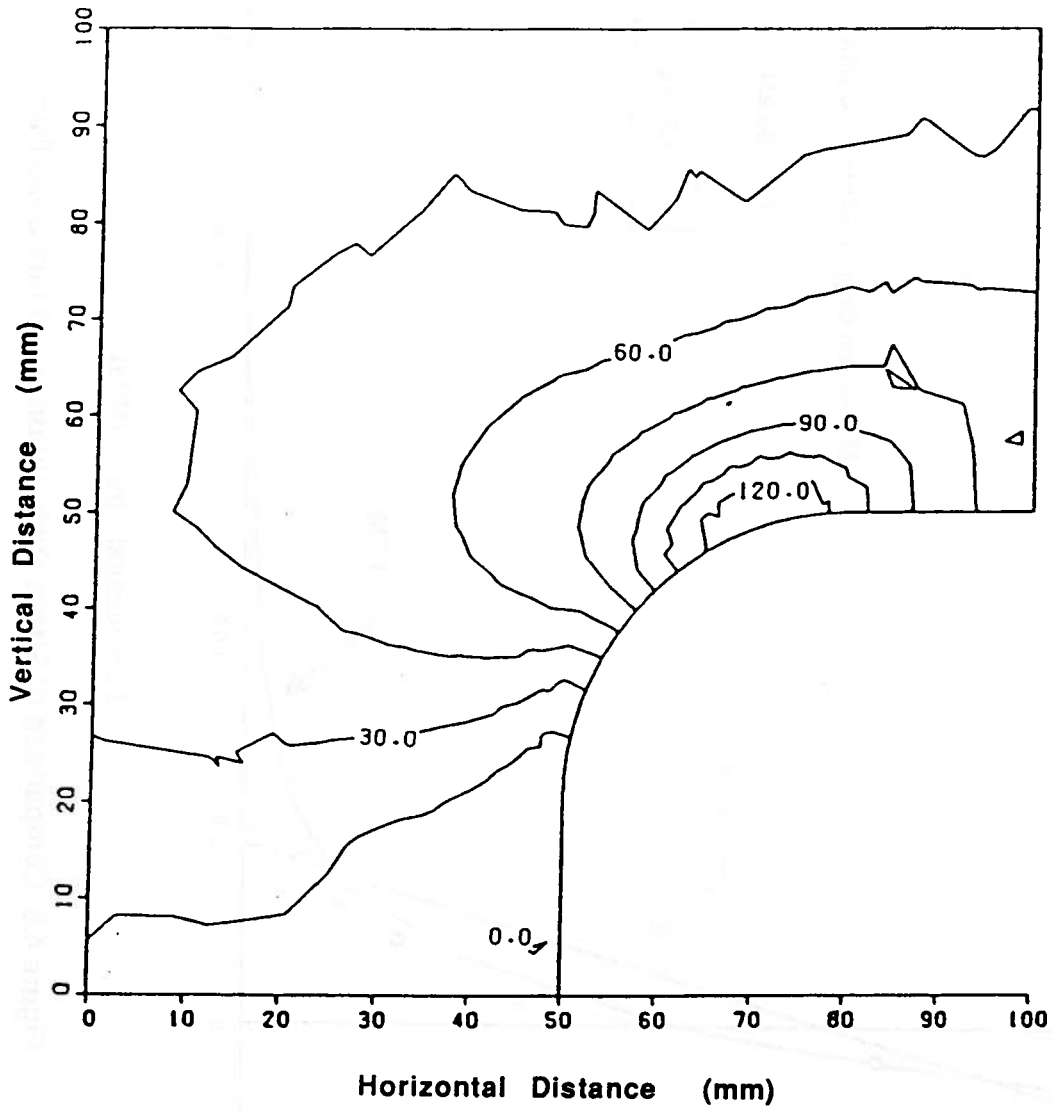
Figure 4.7   Stress Contour for 30 mm Cope Radius
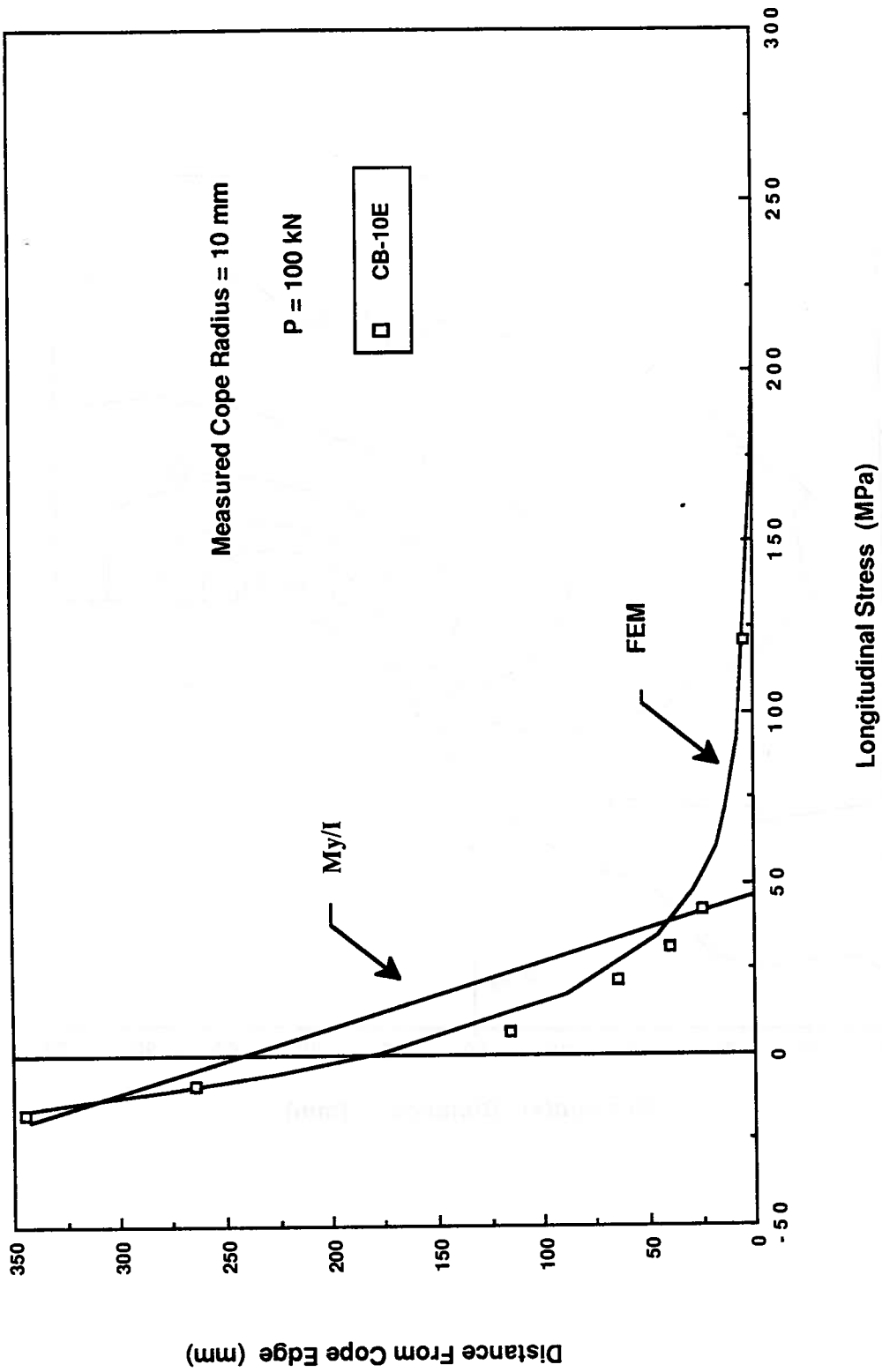
Figure 4.8 Comparison of Stress Distribution for 10 mm Cope Radius
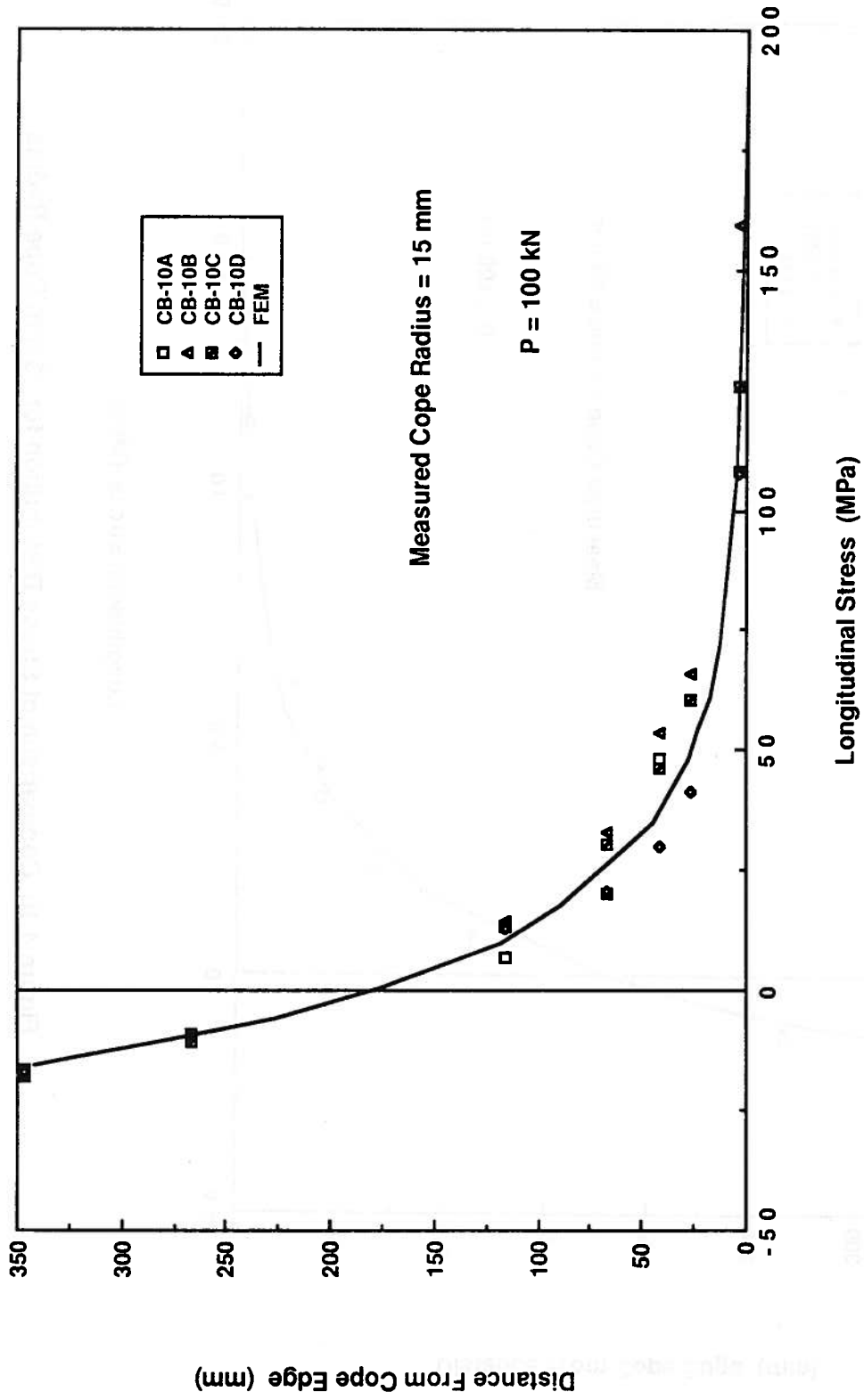
Figure 4.9 Comparison of Stress Distribution for 15 mm Cope Radius
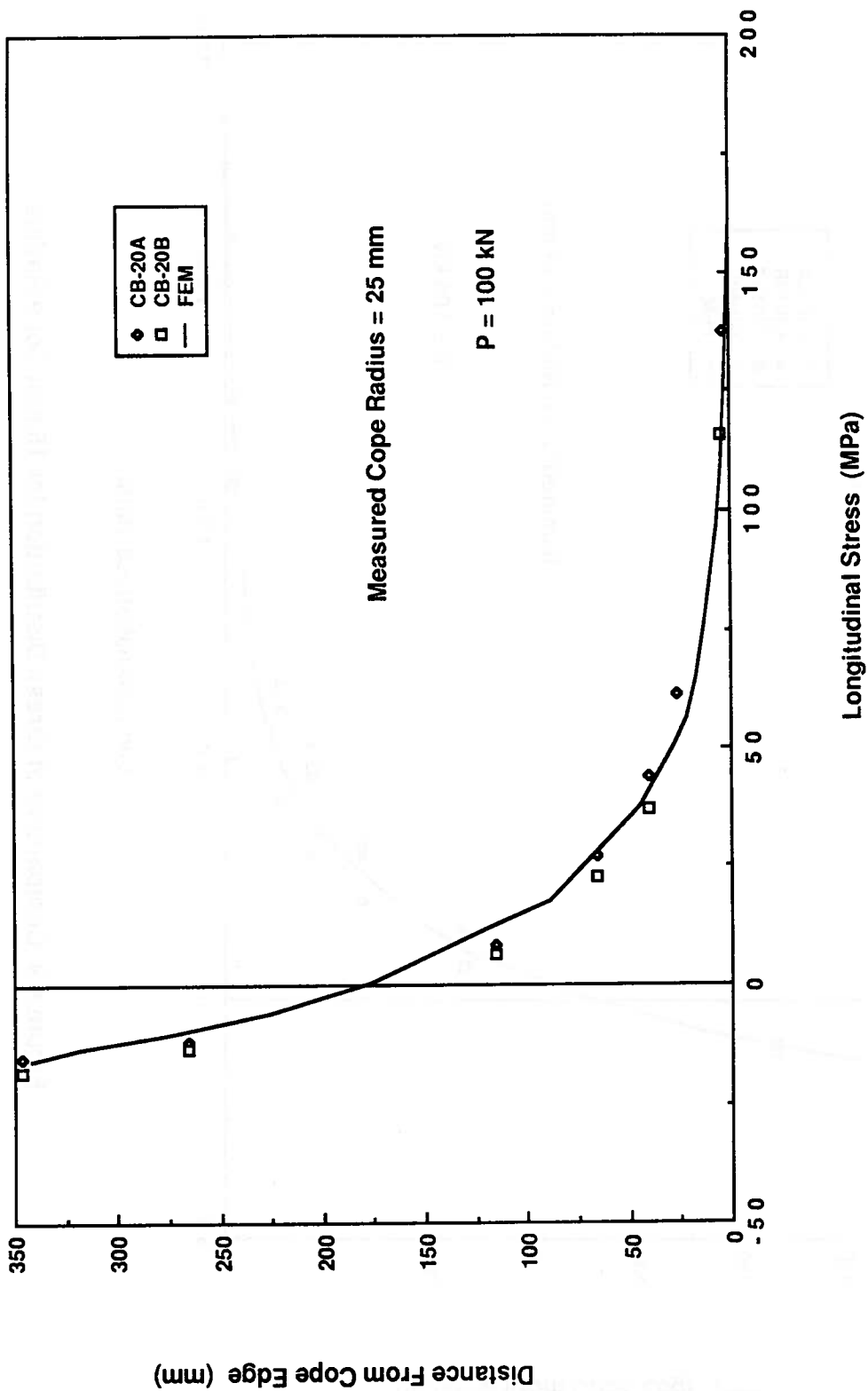
Figure 4.10 Comparison of Stress Distribution for 25 mm Cope Radius
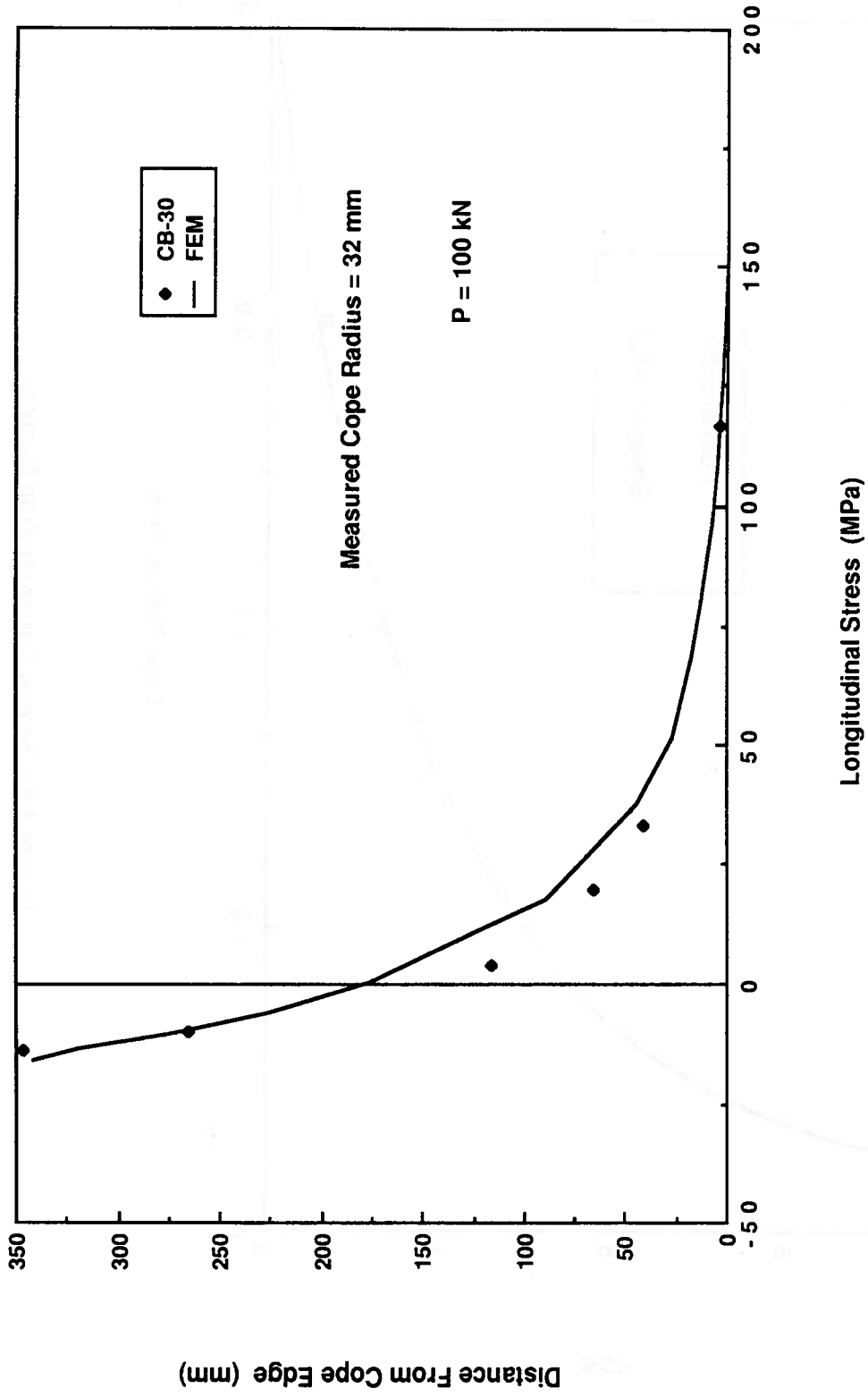
Figure 4.11 Comparison of Stress Distribution for 30 mm Cope Radius
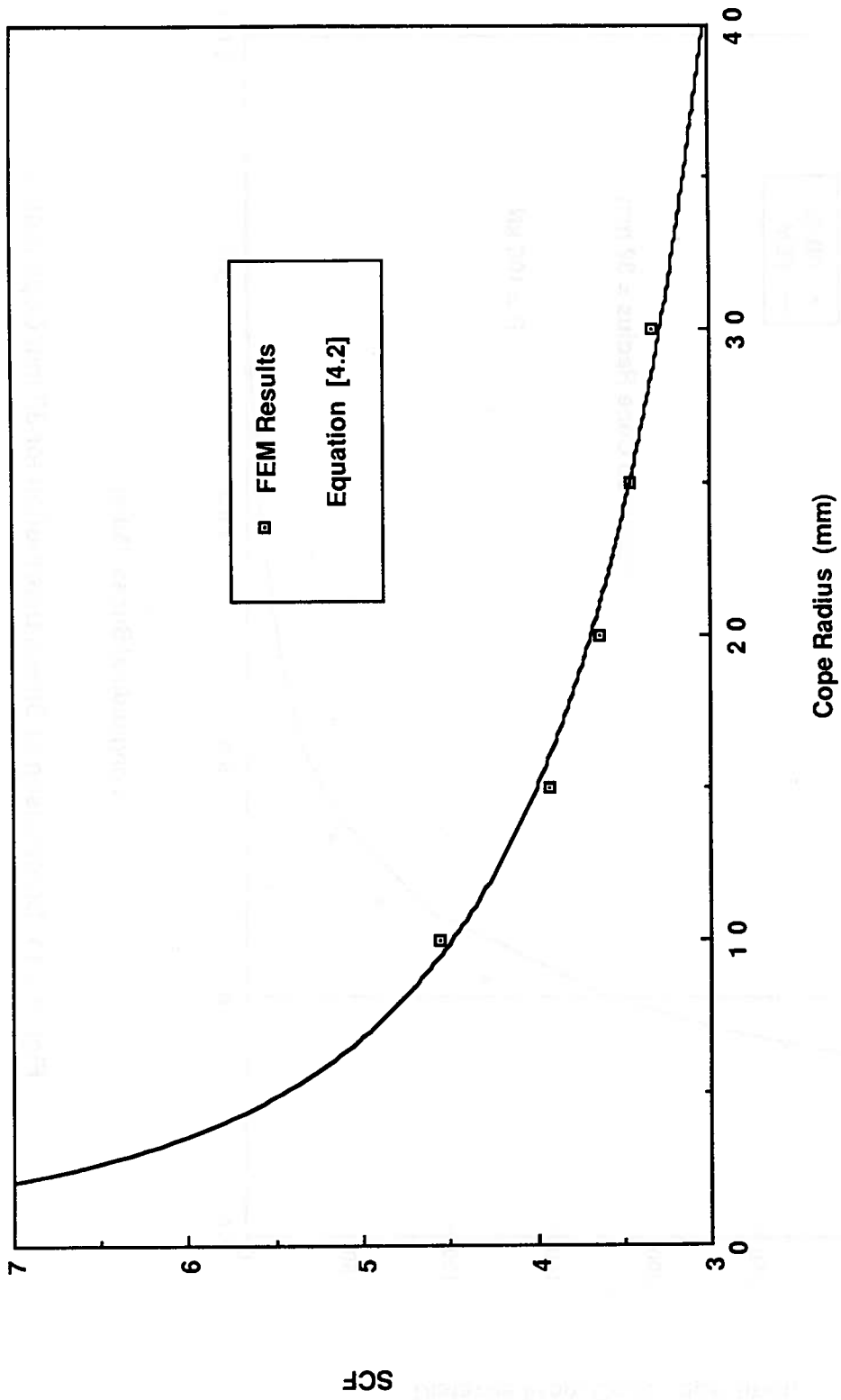
Figure 4.12 Stress Concentration Factors

Figure 4.13 S-N Curve for Experimental Results

5. FRACTURE MECHANICS ANALYSIS OF TEST SPECIMENS

5.1 General Background

The Linear Elastic Fracture Mechanics (LEFM) approach was employed to analyze the fatigue strength of coped beams. This approach is based on the stress intensity factor, K, as a similitude parameter which relates the stress field at the crack tip region to the nominal stress, σ, applied to the structure and the crack or crack-like defect of length a. The factor K can also be physically interpreted as a parameter which reflects the redistribution of stresses in a body due to the presence of a crack. In general, there are three basic mode of crack surface displacements, namely: opening mode (Mode I), shearing mode (Mode II), and tearing mode (Mode III). The stress intensity factor for opening mode, K_I, is the dominant term in the elastic stress field distribution at the crack tip (Irwin 1957). The general equation for K_I is :

$$K_I = F \, \sigma \, \sqrt{\pi a} \qquad\qquad [5.1]$$

where,

F : the crack size dependent correction factor which is a function of specimen geometry, crack size, shape and orientation, and nonuniform opening stresses.

σ : the nominal stress at the location remote from the crack.

a : the crack size.

The value of F will be discussed in the following section.

The fatigue life of a structural component ideally consists of three stages, namely : fatigue crack initiation, fatigue crack propagation, and

66

final fracture. If initial flaws exist in the structure, the only useful fatigue life of the structure will be determined by the fatigue crack propagation stage. The fatigue crack propagation rate is related to the range of stress intensity factor, ΔK, in the form of (Paris 1963) :

$$\frac{da}{dN} = C\ (\Delta K)^n \qquad\qquad [5.2]$$

where C and n are material property constants. The range of stress intensity factor is defined as (Fuchs and Stephens, 1980):

$$\Delta K_I = K_I max - K_I min \qquad\qquad \text{if } K_I min > 0 \qquad [5.3a]$$
$$\Delta K_I = K_I max \qquad\qquad \text{if } K_I min \leq 0 \qquad [5.3b]$$

The number of cycles of loading, N, can be evaluated by rearranging equation [5.2] and integrating from the initial crack size a_i to the final crack size a_f,

$$N = \left[\int_{a_i}^{a_f} \frac{da}{C\left(\dfrac{\Delta K}{\sigma_r}\right)^n} \right] \sigma_r^{-n} \qquad\qquad [5.4]$$

where σ_r is the nominal stress range and N is the elapsed fatigue life in cycle. Equation [5.4] can be further reduced to the following form :

$$N = A\ \sigma_r^{-n} \qquad\qquad [5.5]$$

where A is a geometry dependent parameter which can be determined from experimental studies (Fisher 1970). The current S-N curves in CAN3-S16.1-M84 (1984) are based on equation [5.5] and experimental data expressed using a log-log scale, that is :

$$\log N = \log A - n \log \sigma_r \qquad [5.6]$$

5.2 Analytical Solutions of Crack Size Dependent Correction Factor , F, for Cope Details

The stress intensity factor, K_I, for a central crack of size 2a in an infinite plate subjected to uniform stress is defined as (Irwin 1961) :

$$K_I = \sigma \sqrt{\pi a} \qquad [5.7]$$

To properly account for different crack geometry, loading, and finite dimension details, equation [5.7] is modified by a crack size dependent correction factor F which is defined as :

$$F = F_S F_W F_E F_G \qquad [5.8]$$

where F_S is the free surface correction factor, F_W is the finite width correction factor, F_E is the crack front shape correction factor and F_G is the stress gradient correction factor which adjusts for the stress concentration caused by the detail geometry. It is assumed in equation [5.8] that the correction factors are independent. Thus, they can be superimposed to provide a reasonable estimate of the stress intensity

factor for different situations. A through-thickness crack was assumed for cope details. Therefore F_E was taken as unity in the analysis.

5.2.1 Free Surface Correction Factor, F_S

According to Tada and Irwin (1973), F_S for an edge crack of size a in a semi-infinite plate subjected to uniform stress is defined as :

$$F_S = 1.12 \qquad\qquad [5.9]$$

For a partial through crack, F_S is defined as (Páris and Sih 1965):

$$F_S = 1 + 0.12 \left[1 - \left(\frac{a}{c}\right) \right] \qquad\qquad [5.10]$$

where a and c are the length of the minor and major semi-axes of an elliptical crack, respectively.

Since a through-thickness crack was assumed for cope details, equation [5.9] was used in the following analysis.

5.2.2 Finite Width Correction Factor, F_W

The finite width correction factor, F_W, for a central crack of size 2a in a plate of finite width w is defined as (Irwin 1968) :

$$F_W = \sqrt{\sec \frac{\pi a}{w}} \qquad\qquad [5.11]$$

Another approximation of F_W had also been proposed by Irwin in 1962 :

$$F_W = \frac{w}{\pi a} \sqrt{\tan \frac{\pi a}{w}}$$ [5.12]

Nevertheless, equation [5.11] is known to be more accurate for two-dimensional cases (Albrecht and Yamada 1977). For cope details w was taken as twice the depth of the coped section.

5.2.3 Stress Gradient Correction Factor, F_G

To properly account for the non-uniform loading and the severe stress gradient effect produced by the cope geometry, the Green's function method, proposed by Albrecht and Yamada (1977) was used to develop the value of F_G. This method is based on Bueckner's formulation (1958) which states that the strain energy needed for crack extension in an arbitrary body can be evaluated by imposing the stress field from the uncracked body onto the plane where the crack forms. Hence, in order to use this approach, the crack plane must be known. Since only the stress field from the uncracked body is required, therefore only one stress analysis is needed for each cope geometry. The stress analysis for different cope radii was performed by finite element analysis as presented in chapter 4. F_G developed by the Green's function method is defined as :

$$F_G = \frac{2}{\pi} \int_0^a \frac{K_t}{\sqrt{a^2 - L^2}} \, dL$$ [5.13]

where a is the desired crack length and L is the the distance along the crack path from the edge. K_t, the stress concentration factor at length L, is defined as the ratio of the stress perpendicular to the crack plane obtained from finite element analysis to the nominal longitudinal stress at the cope line. It is important to note that the value of K_t depends on the nominal stress used in equation [5.1].

A numerical solution for equation [5.13] was suggested by Albrecht and Yamada (1977) :

$$F_G = \frac{2}{\pi} \sum_{j=1}^{m} K_{tj} \left[\sin^{-1}\left(\frac{L_{j+1}}{a}\right) - \sin^{-1}\left(\frac{L_j}{a}\right) \right] \qquad [5.14]$$

where K_{tj} is the stress concentration factor in element j of the finite element discretization, L_j and L_{j+1} are the crack lengths defined in Figure 5.1 and m is the number of elements.

A closed form solution is also available for equation [5.13] if K_t can be expressed in terms of a polynomial equation such as :

$$K_t = A + BL + CL^2 + DL^3 + EL^4 \qquad [5.15]$$

where A, B, C, D, and E are dimensionless constants. Using equation [5.15] and integrating equation [5.13] by parts, the closed form solution for F_G is :

$$F_G = A + \frac{2B}{\pi}L + \frac{C}{2}L^2 + \frac{4D}{3\pi}L^3 + \frac{3E}{8}L^4 \qquad [5.16]$$

Equation [5.16] was used to evaluate the F_G for cope details in this studies.

5.2.3.1 Procedure of Evaluating F_G for Cope Details

Based on the stress analysis by the FEM on different measured cope radii in the previous chapter, the following steps were used to develop the F_G curves for the test specimens :

i) Obtain the crack location from the failed specimens.

ii) Evaluate the stresses perpendicular to the crack plane upto the desired crack length from the FEM solutions (figures 5.2 to 5.8).

iii) Fit a polynomial function to the stress distribution normal to the crack plane.

iv) Evaluate F_G based on equations [5.15] and [5.16].

The stress distributions based on the crack locations measured from the failed specimens are shown in figures 5.2 to 5.8. It should be noted that these stress distributions correspond to the nominal stress range applied to the specimen as presented in chapter 2.

The F_G curves of test specimens based on the above procedure are shown in figures 5.9 to 5.15. It can be seen from these curves that the rate of decay of F_G increases with decreasing cope radius. For specimen CB-10E, two third-degree polynomial functions were used to fit the stress distribution along the crack plane because a very high stress gradient existed in the vicinity of the cope edge.

5.3 Prediction of Fatigue Life and Comparison with Test Results

Fatigue life of test specimens can be evaluated by rearranging equation [5.2] and integrating from a_i to a_f:

$$N = \int_{a_i}^{a_f} \frac{da}{C(\Delta K)^n} \qquad [5.17]$$

where

$$\Delta K = 1.12 \sqrt{\sec \frac{\pi a}{w}} \; F_G \, \sigma_r \sqrt{\pi a} \qquad [5.18]$$

The constants C and n in equation [5.17] reported by Barsom (1971) in SI units for ferrite-pearlite steels are 2.179 x 10^{-13} and 3, respectively. This value of C is the upper bound value which provides a conservative estimate of crack growth rate according to equation [5.2]. Hirt and Fisher (1973) suggested the value of 1.24 x 10^{-13} for C. This value was derived from the mean regression analysis of the fatigue test data on welded beams. Nevertheless, C equal 2.179 x 10^{-13} was used in this analysis.

Since step-wise integration was used to evaluate the integral in equation [5.17], the differential crack length da must be small. It was found that the integral was evaluated accurately with da of 0.038 mm.

The predicted fatigue life using equation [5.17] and the measured fatigue life of the test specimens at a final crack size of 30 mm are shown in Table 5.1. Specimen CB-0 was not considered in the fracture mechanics analysis because the theoretical SCF at the sharp cope corner is infinite. Since the test results did not conclusively show the effect of cope fabrication process, therefore the fatigue life of specimen CB-20B was not included in the analysis either. The initial crack size of 0.38 mm, corresponding to the depth of the martensite after flame-cutting as suggested by Fisher (1984), was used in the analysis. For specimen CB-10A, a 1 mm deep notch was found in the cope region where the fatigue

crack initiated; hence, the fatigue life corresponding to an initial crack size of 1 mm was also considered in the analysis, as shown in Table 5.1. As can be seen from the table, the predicted fatigue life of all specimens with initial crack size of 0.38 mm is significantly lower than the measured fatigue life. This may be due to the conservatism of the constant C, the approximation of the cope geometry in the finite element analysis, and the estimation of the initial crack size. The latter is known to have a very significant effect on the fatigue life of a structural member (Rolfe and Barsom 1977). The ratio of the measured fatigue life to the predicted fatigue life for each specimen is shown in column six of Table 5.1. The ratio ranges from 0.37 to 0.79 for the assumed initial crack size of 0.38 mm.

In order to illustrate the effect of initial crack size on predicted fatigue life, various initial crack sizes were used to evaluate the fatigue life for specimen CB-10A. These are shown in Figure 5.16. It can be seen from this figure that the predicted fatigue life for the specimen increases rapidly as the initial crack size decreases from a value of about 0.5 mm. As shown in the figure, for an initial crack size larger than about 1 mm the fatigue life of the specimen predicted by the analysis is not significantly affected by the initial crack size.

The test results and predictions by LEFM are also plotted in Figure 5.17. In plotting these data points, the theoretical stress range, which is the nominal stress range multiplied by the theoretical SCF at the cope edge (eqn. [4.2]), is used in order to observe the effect of stress range on fatigue life. It can be seen from this figure that all experimental data points lie above the mean regression line obtained using the analytical solution. The mean regression line of the experimental results is also plotted on the

figure. Since the analytical procedure requires the location of the crack plane from the failed specimens, the analytical results are therefore semi-empirical. This is illustrated by the fact that the analytical data are scattered as shown in the figure.

The 95% confidence limit for the analytical solution is plotted in Figure 5.18 along with categories A, B, and C from the current CAN-3-S16.1-M84 (1984) specification. It can be seen from this figure that all the data points lie above the 95% confidence limit for the analytical solution which provides conservative estimate of the fatigue strength of coped beams. Based on the available test data, estimating the fatigue strength of coped beams by Category B is believed to provide reasonable predictions. However, because of the limited number of test data, the use of Category C to predict the fatigue strength of coped beams is more desirable.

Predictions of the fatigue strength of test specimens based on equation [1.1] as suggested by Fisher and the theoretical stress range are shown in Table 5.2. Test results and predictions by the Green's function approach are also presented in the table for comparison. As mentioned previously stress concentration produced by cope geometry is very localized. Hence once the crack propagates away from this small region, the stress concentration effect decreases rapidly. Therefore it can be seen that equation [1.1] overestimates the stress intensity factor for this detail because it does not take into account the change in the applied stress range due to the change in stress concentration effect as the crack propagates. This overestimation of the stress intensity factor is reflected in the conservative predictions of the fatigue strength as shown in Table 5.2.

Table 5.1 Comparison of Fatigue Life Predictions with Test Results

Specimen Designation	Nominal Stress Range (MPa)	Initial Crack Size (mm)	Predicted Fatigue Life (N Cycles)	Measured Fatigue Life (N Cycles)	Predicted to Measured Ratio
CB-10A	50	0.38	321 000	405 800	0.79
		1.00	244 800	405 800	0.60
CB-10B	40	0.38	698 900	928 000	0.75
CB-10C	70	0.38	108 300	292 500	0.37
CB-10D	70	0.38	131 700	318 600	0.41
CB-10E	70	0.38	121 900	211 500	0.58
CB-20A	50	0.38	479 000	1 080 000	0.44
CB-30	50	0.38	713 800	1 390 000	0.51

Note : Final crack size = 30 mm

Table 5.2   Comparison of Fatigue Life Predictions by Green's Function Method with Equation [1.1]

Specimen Designation	Theoretical Stress Range (MPa)	Initial Crack Size (mm)	Predicted Fatigue Life by Green's Function (N Cycles)	Predicted Fatigue Life by Eqn. [1.1] (N Cycles)	Measured Fatigue Life (N Cycles)
CB-10A	200	1.00	244 800	125 100	405 800
CB-10B	160	0.38	698 900	422 500	928 000
CB-10C	280	0.38	108 300	78 820	292 500
CB-10D	280	0.38	131 700	78 820	318 600
CB-10E	314	0.38	121 900	55 900	211 500
CB-20A	173	0.38	479 000	334 200	1 080 000
CB-30	164	0.38	713 800	392 300	1 390 000

Note : Final crack size = 30 mm
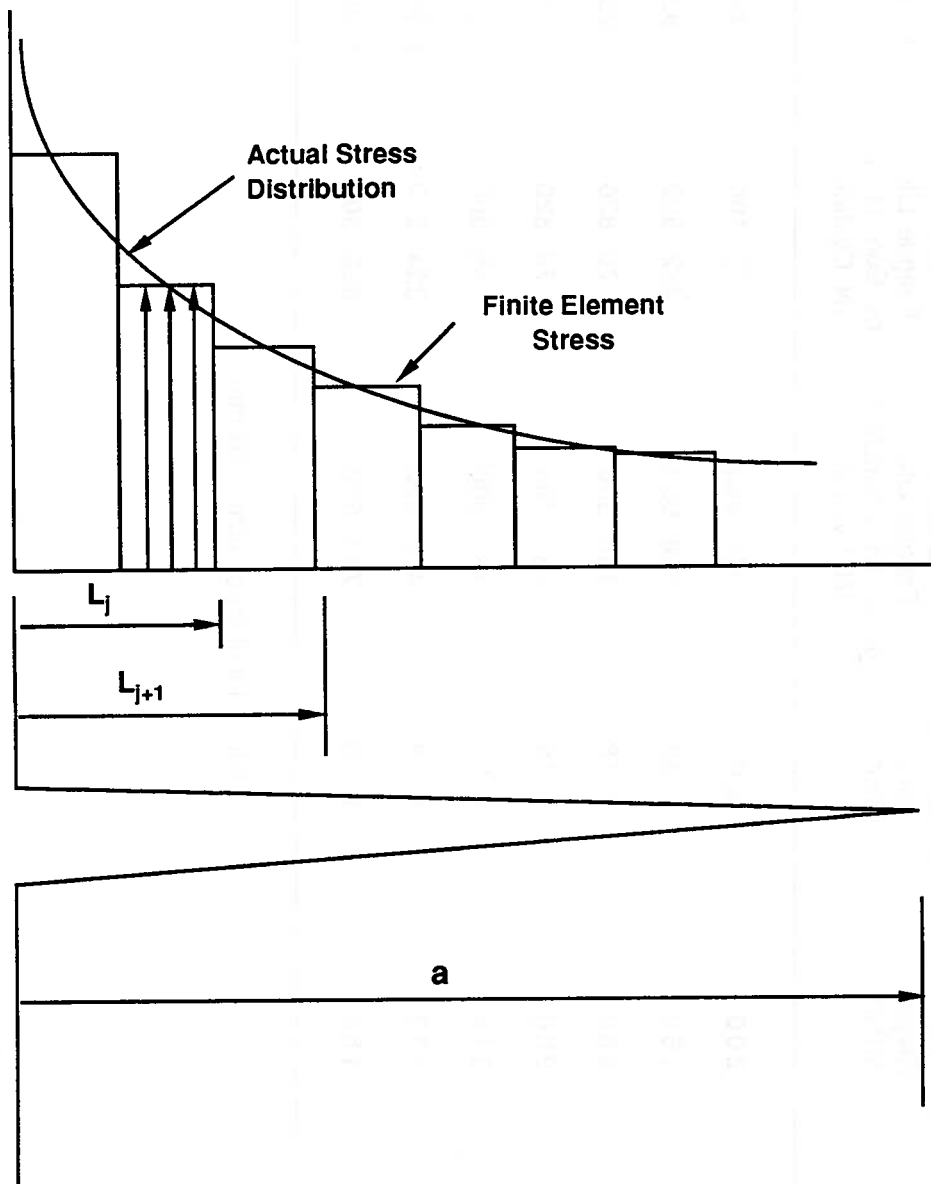
Figure 5.1 Finite Element Discretization for F$_G$
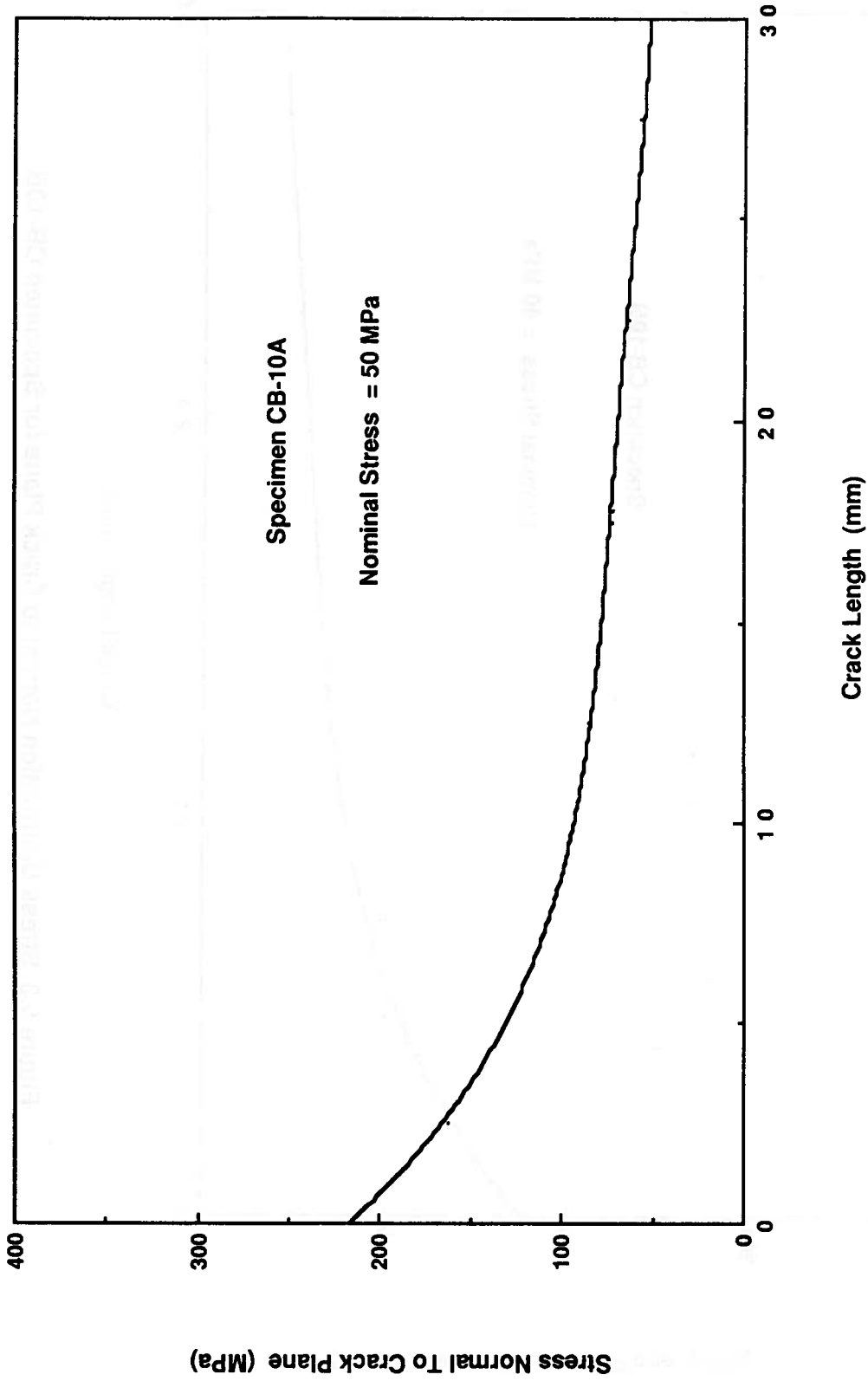
Figure 5.2 Stress Distribution Normal to Crack Plane for Specimen CB-10A
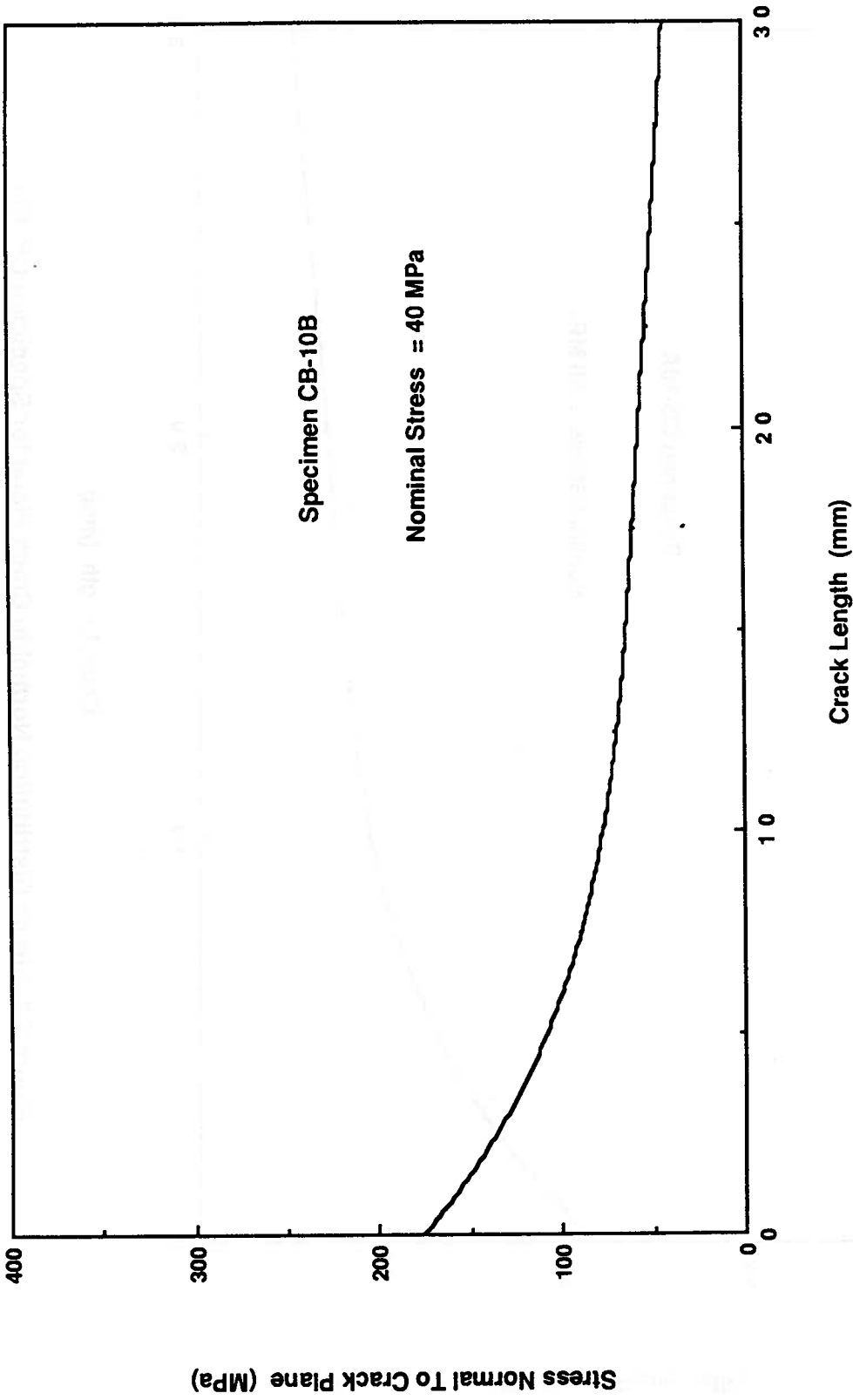
Figure 5.3 Stress Distribution Normal to Crack Plane for Specimen CB-10B
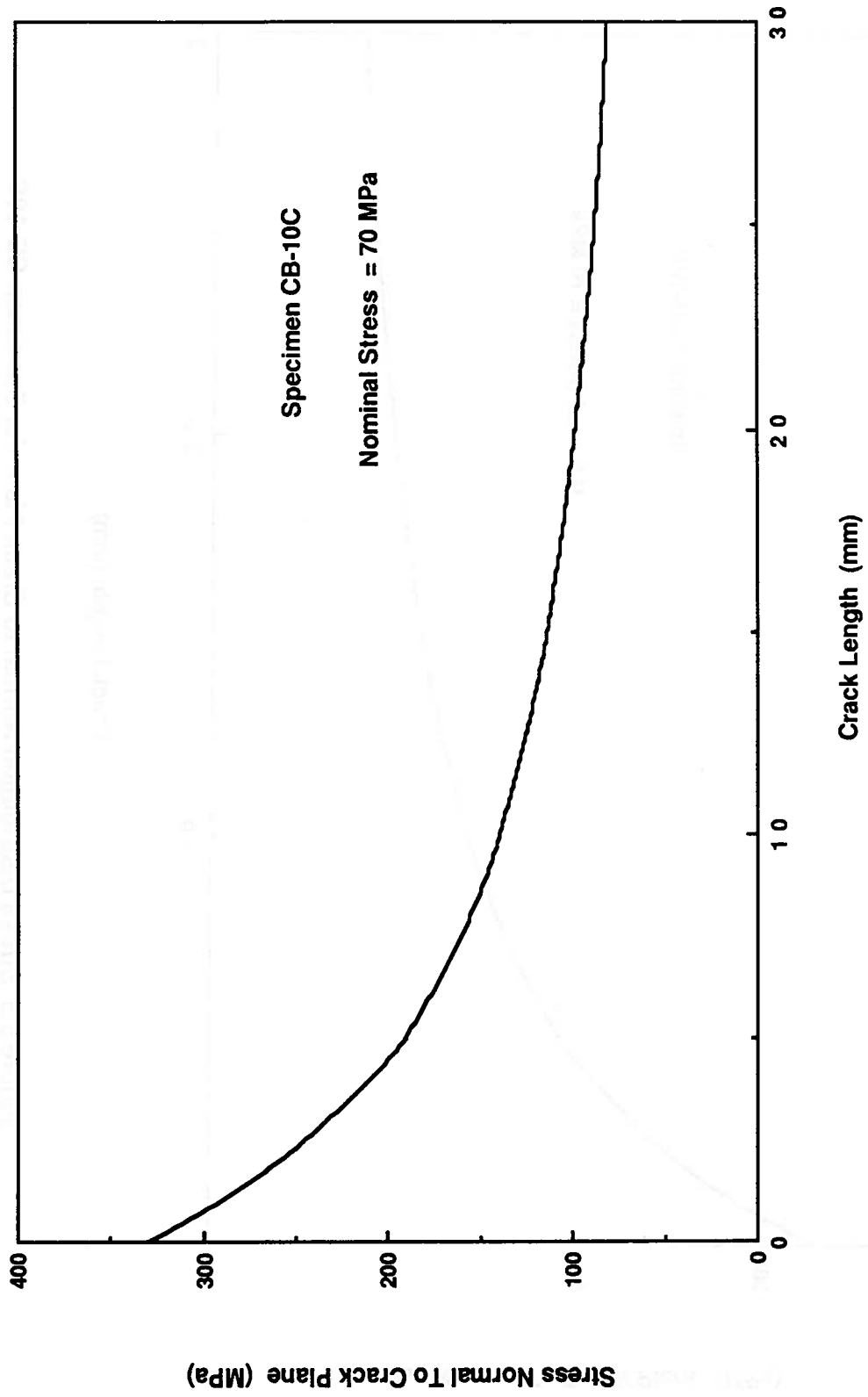
Figure 5.4 Stress Distribution Normal to Crack Plane for Specimen CB-10C
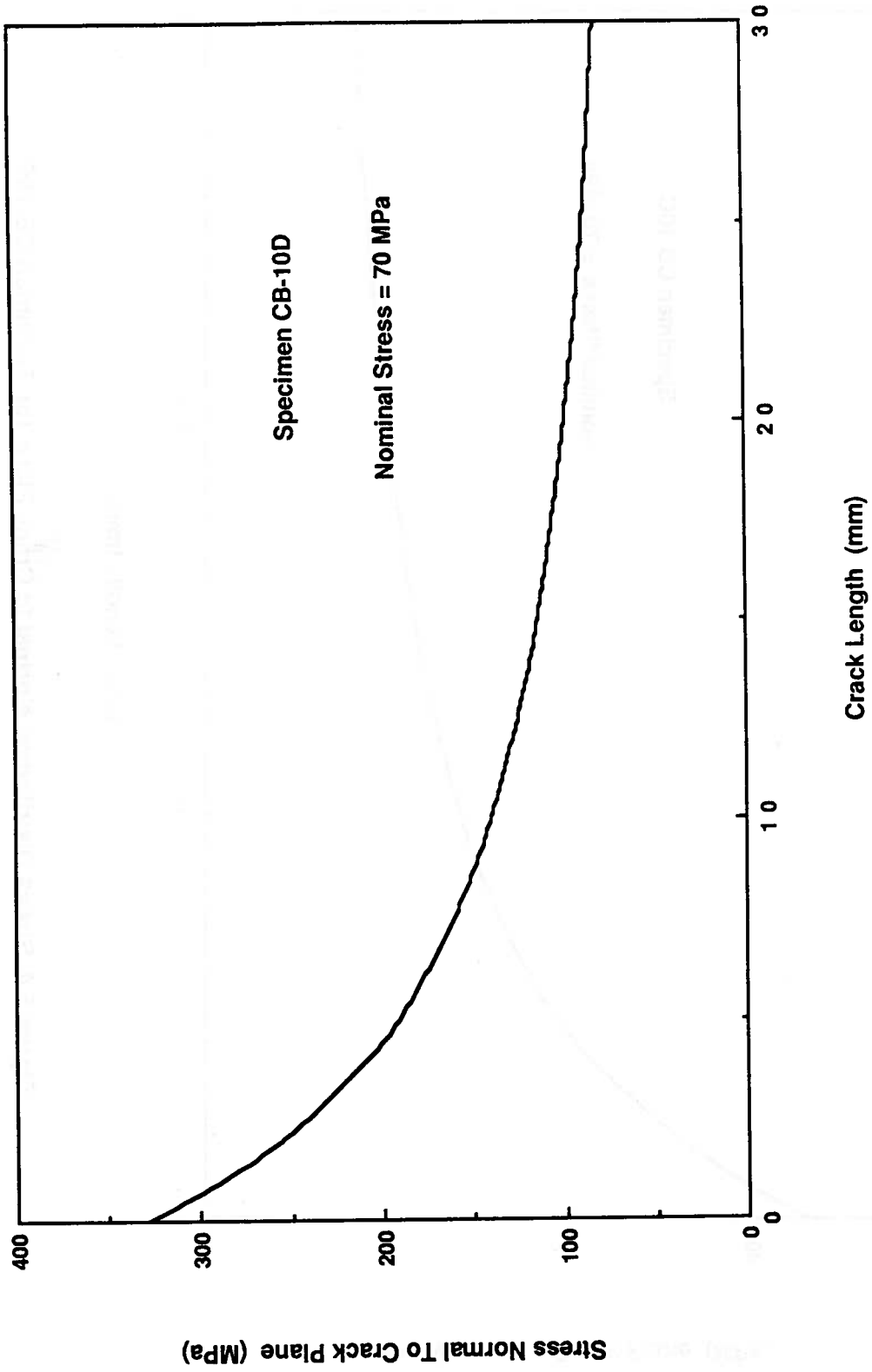
Figure 5.5 Stress Distribution Normal to Crack Plane for Specimen CB-10D
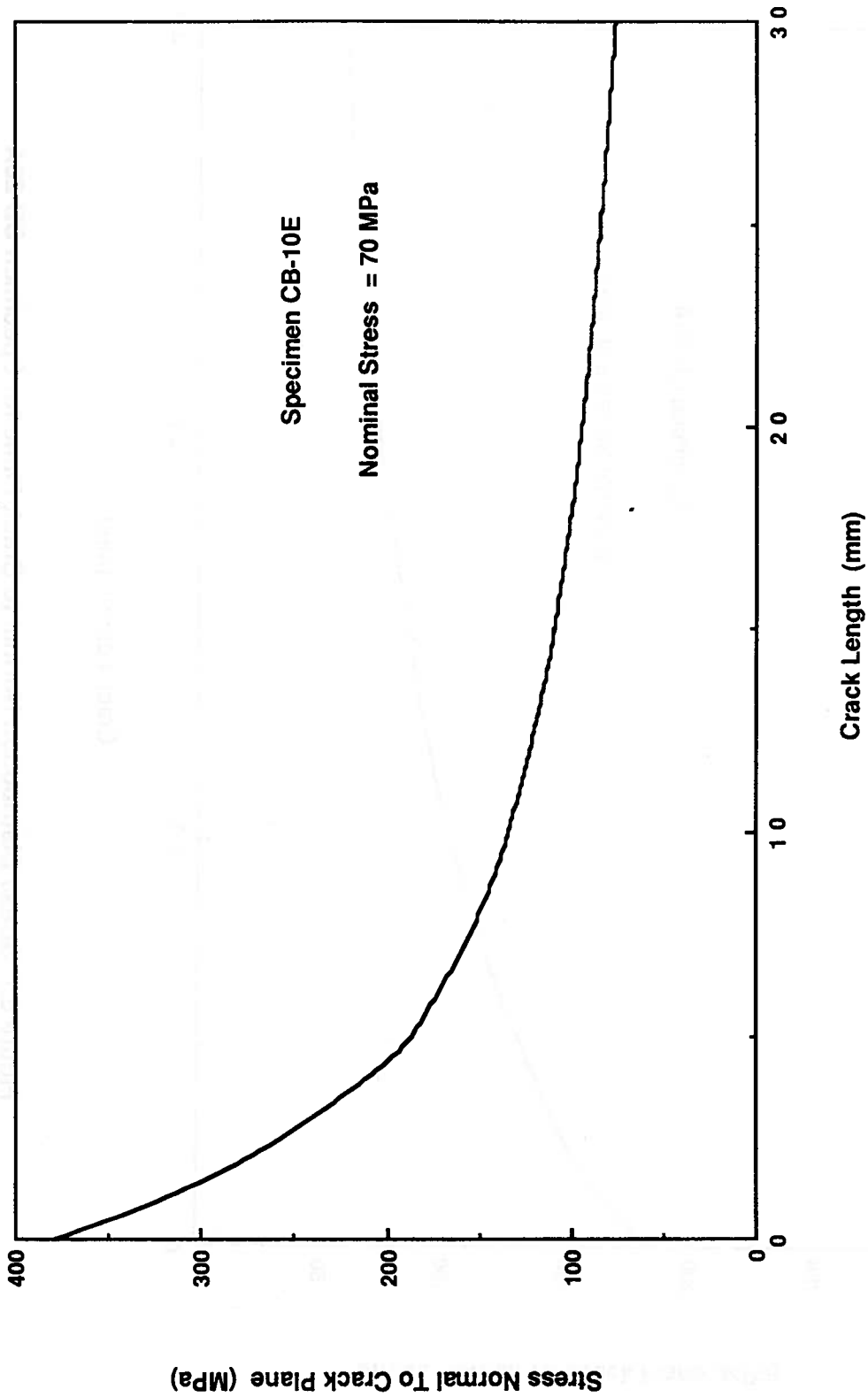
Figure 5.6 Stress Distribution Normal to Crack Plane for Specimen CB-10E
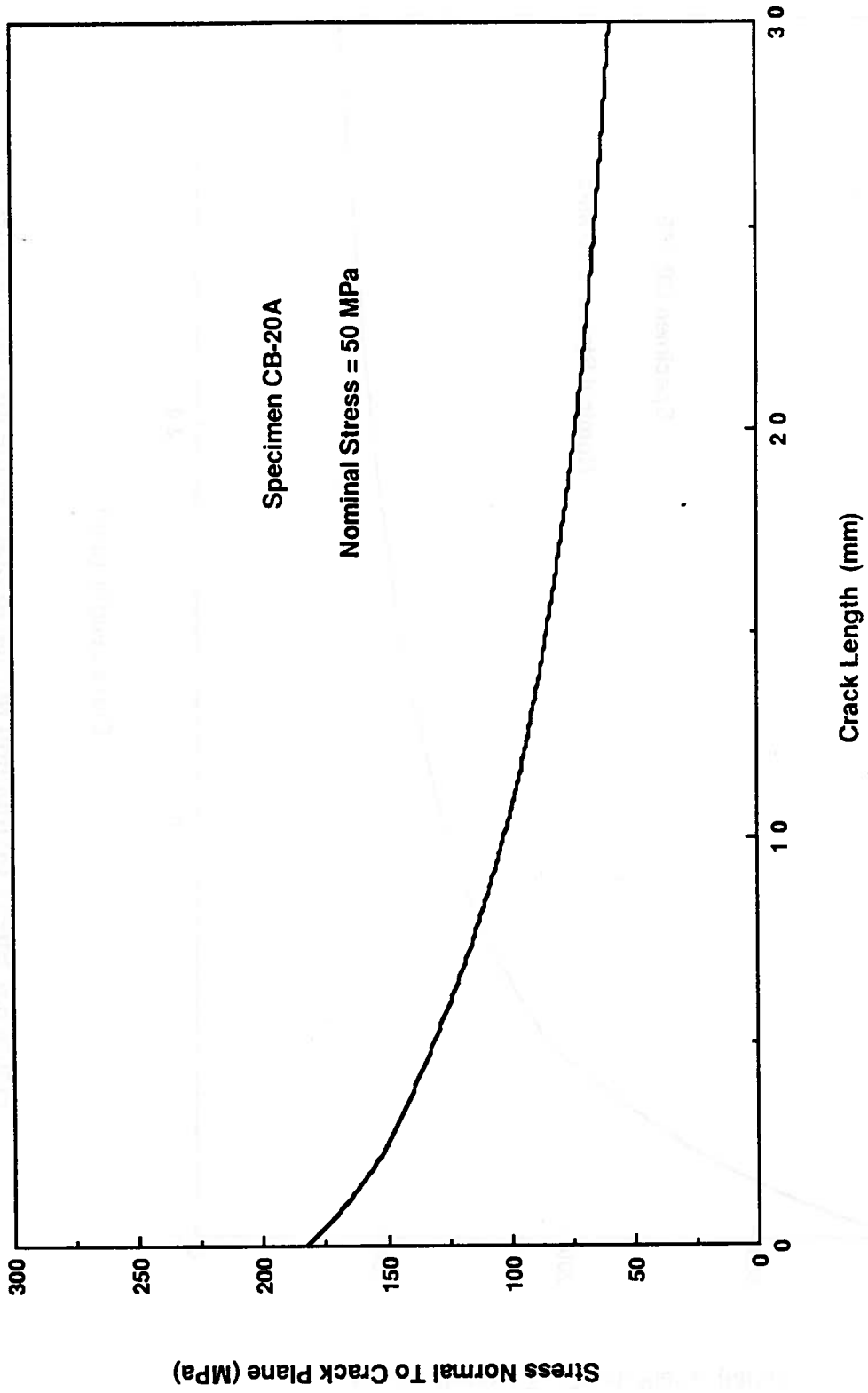
Figure 5.7 Stress Distribution Normal to Crack Plane for Specimen CB-20A

Specimen CB-20A

Nominal Stress = 50 MPa

Crack Length (mm)

Stress Normal To Crack Plane (MPa)
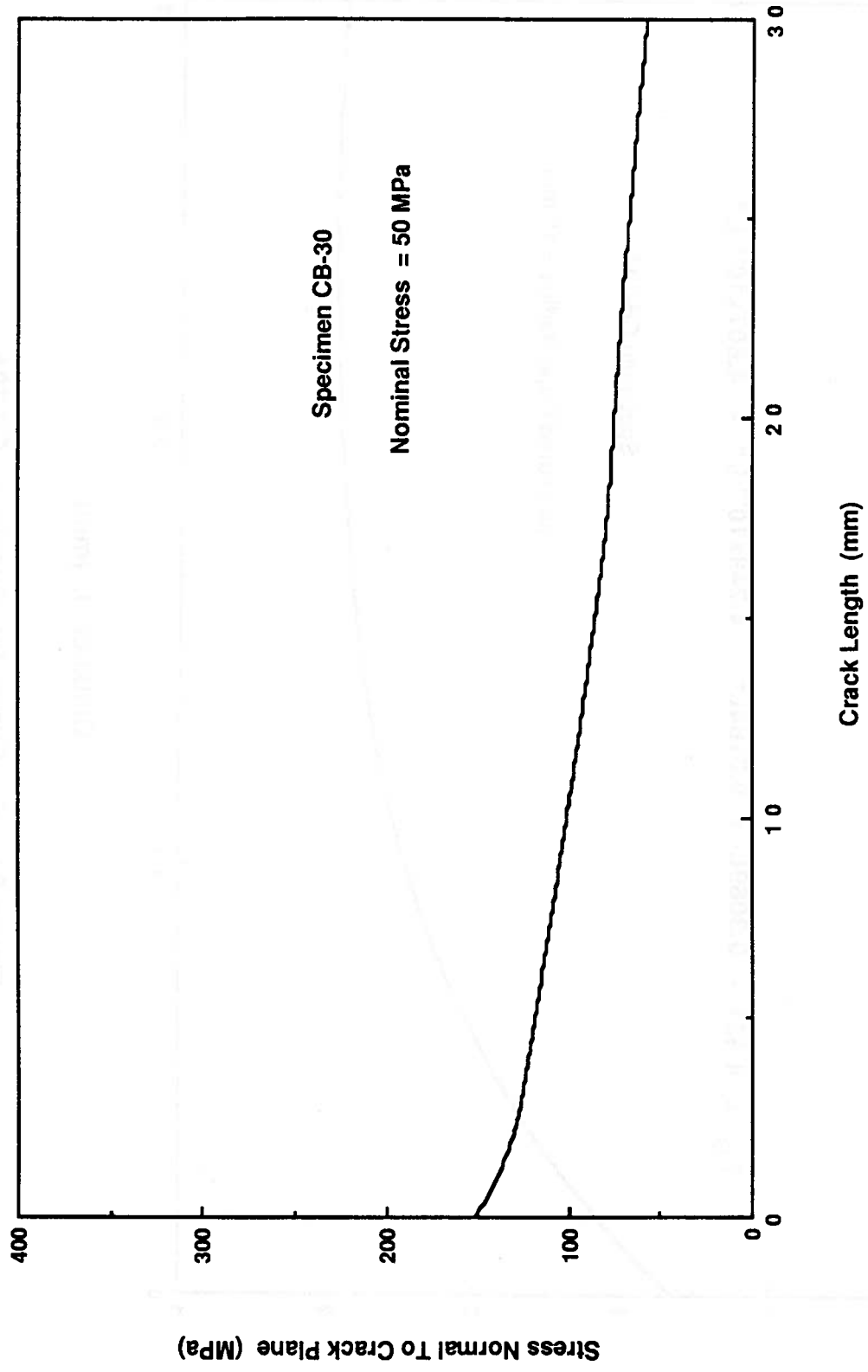
Figure 5.8 Stress Distribution Normal to Crack Plane for Specimen CB-30

$$F_G = 4.431 - 0.3069L + 0.0164L^2 - 4.249 \times 10^{-4} L^3 + 4.607 \times 10^{-6} L^4$$

Specimen CB-10A

Measured Cope Radius = 15 mm

Distance L (mm)
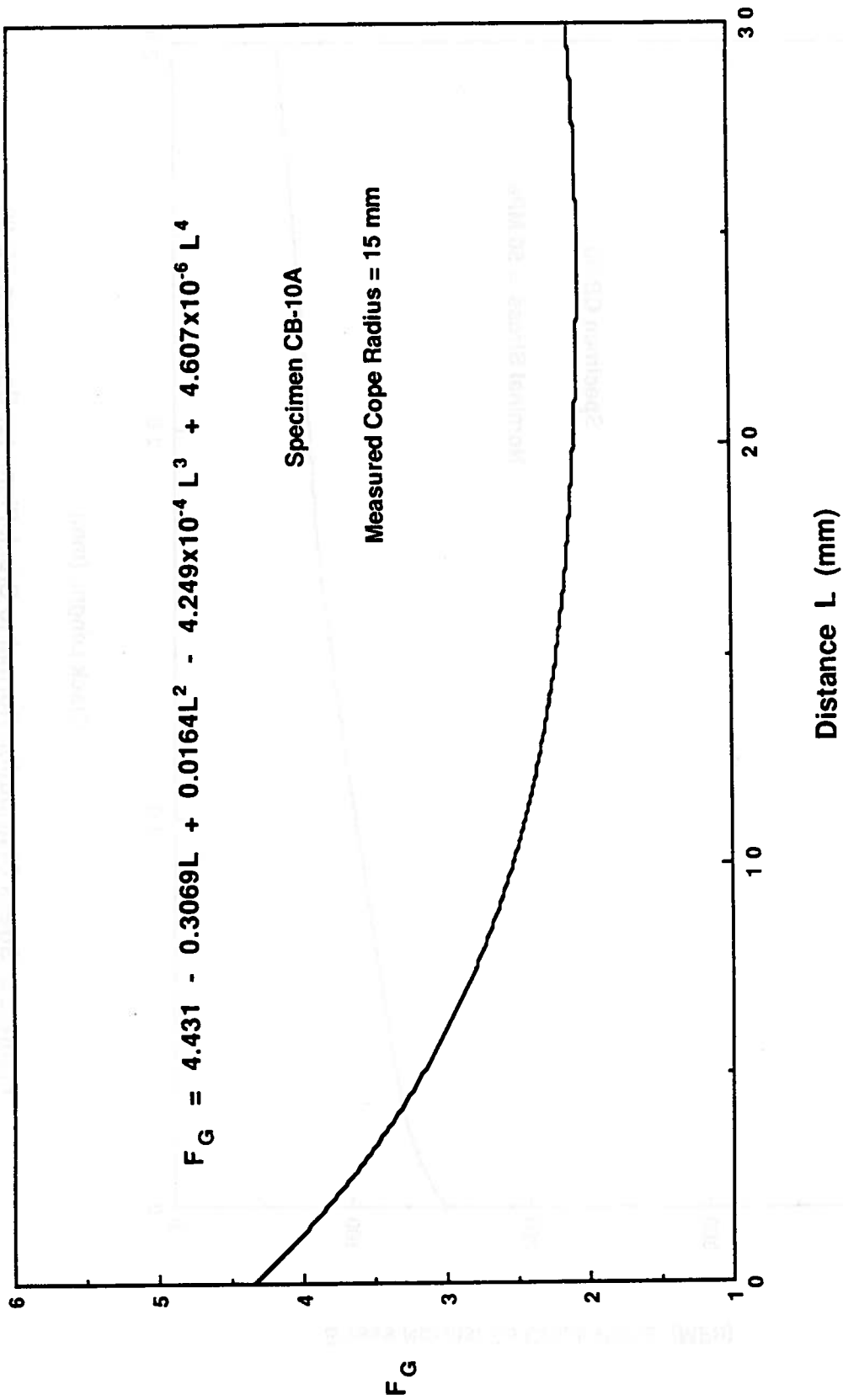
Figure 5.9 F_G Curve for Specimen CB-10A

$$F_G = 4.405 - 0.299L + 0.0154L^2 - 4.079 \times 10^{-4} L^3 + 4.155 \times 10^{-6} L^4$$

Specimen CB-10B

Measured Cope Radius = 15 mm

Distance L (mm)
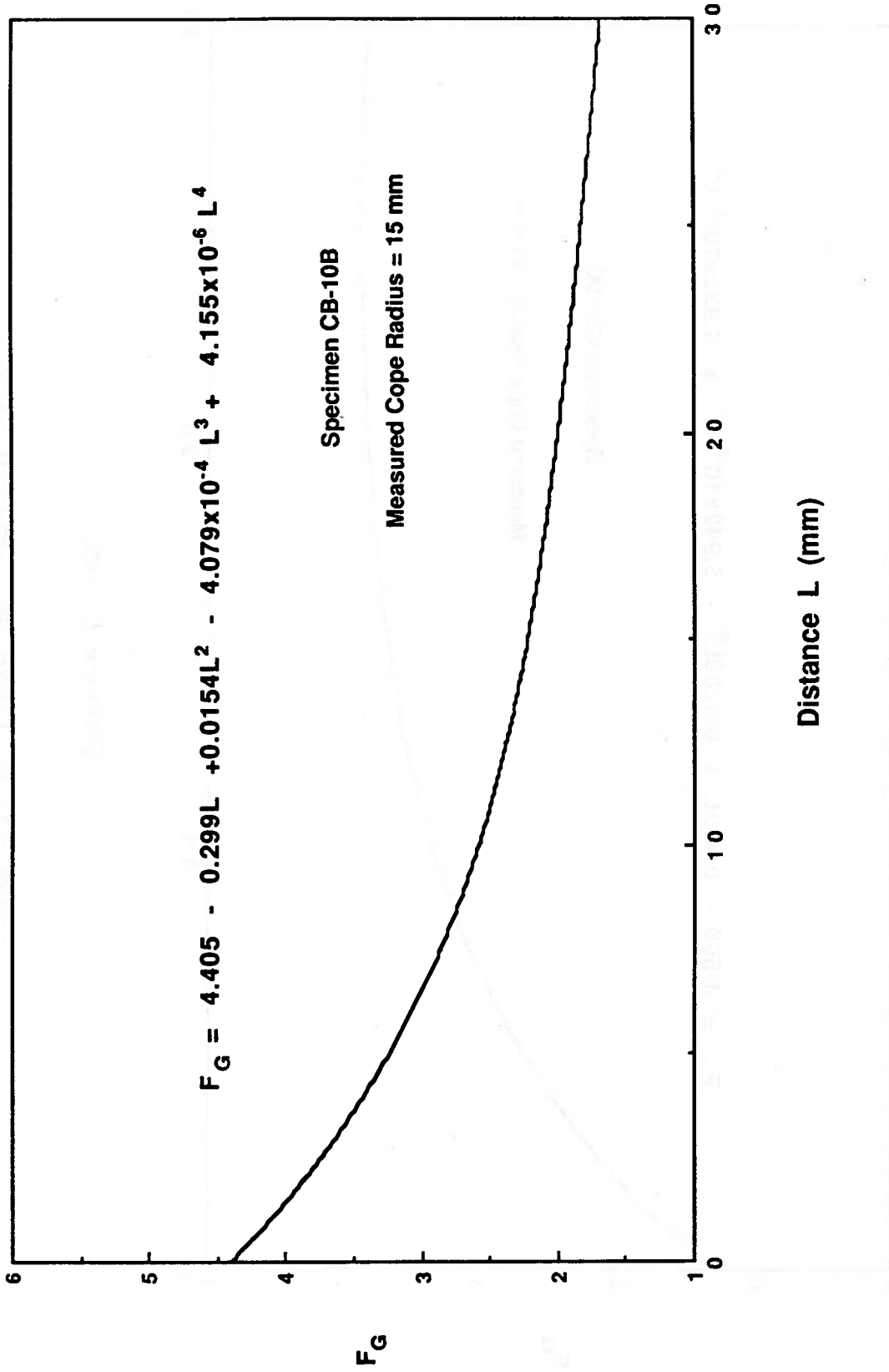
Figure 5.10 F_G Curve for Specimen CB-10B

$$F_G = 4.698 - 0.359L + 0.0208L^2 - 5.942 \times 10^{-4} L^3 + 6.923 \times 10^{-6} L^4$$

Specimen CB-10C

Measured Cope Radius = 15 mm

Distance L (mm)
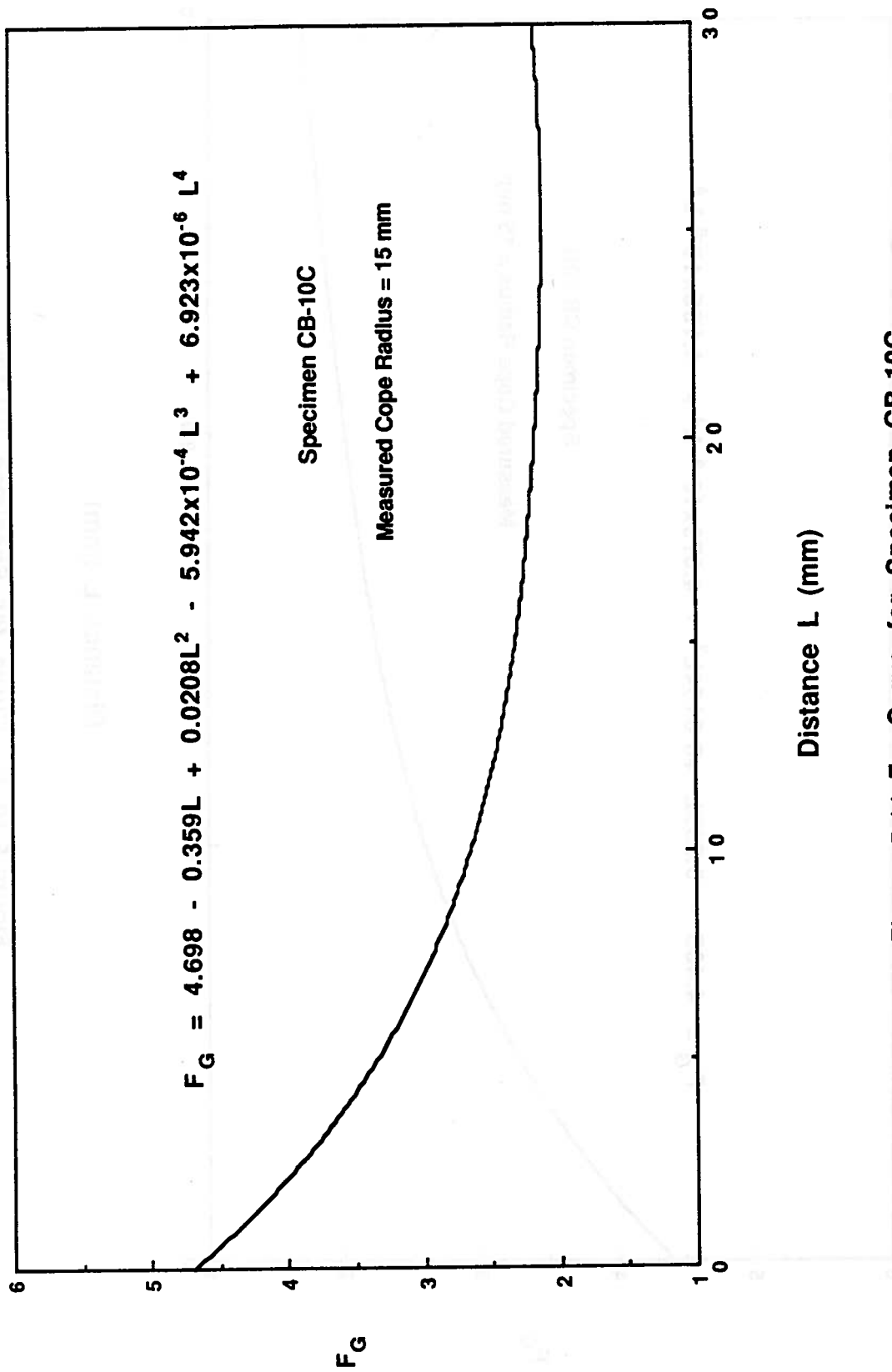
Figure 5.11 F_G Curve for Specimen CB-10C

$$F_G = 4.677 - 0.359L + 0.0209L^2 - 6.366 \times 10^{-4} \ L^3 + 7.129 \times 10^{-6} \ L^4$$

Specimen CB-10D

Measured Cope Radius = 15 mm

Distance L (mm)
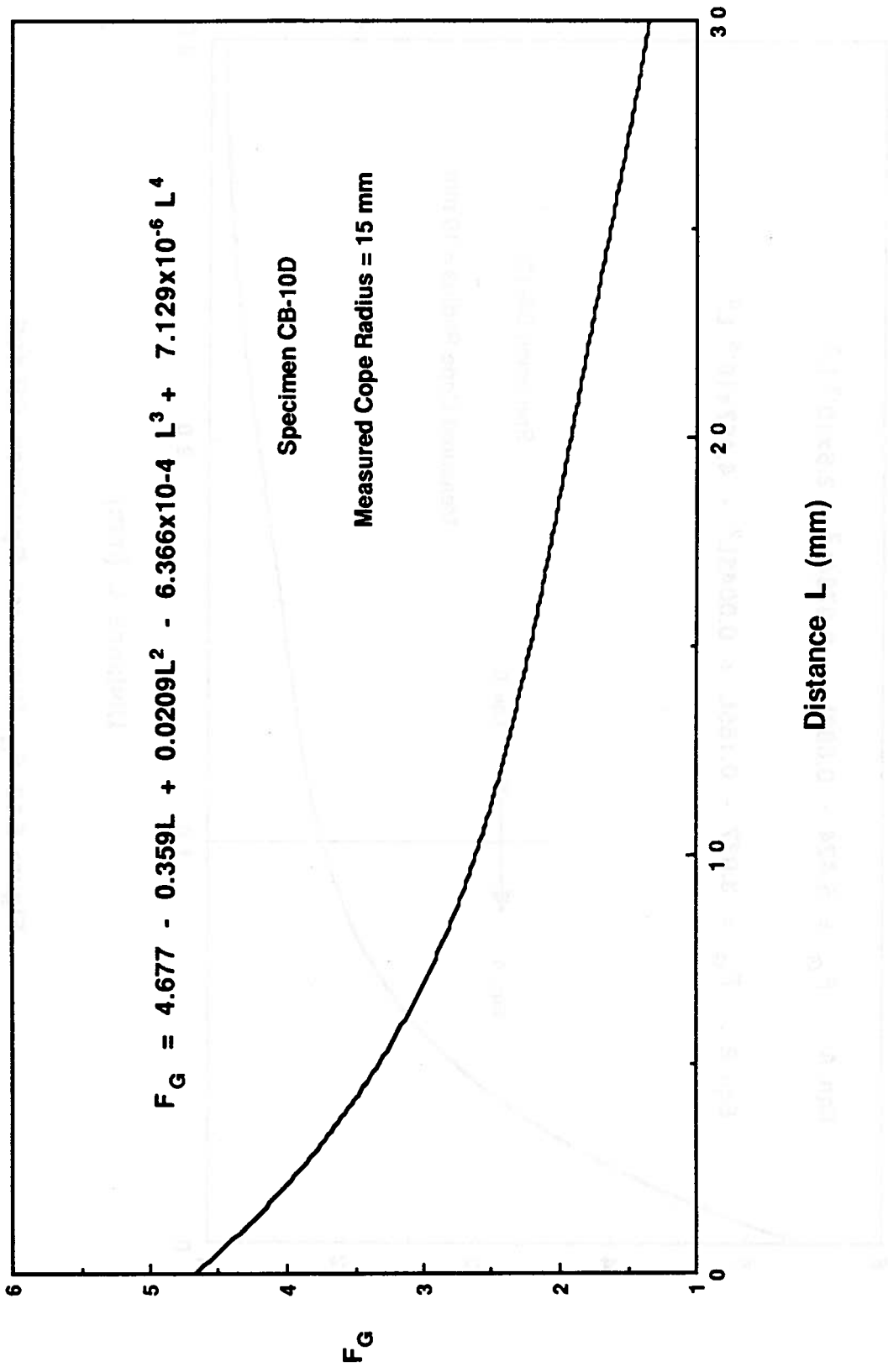
Figure 5.12 F_G Curve for Specimen CB-10D

Eqn. A : $F_G = 5.424 - 0.880L + 0.0784L^2 - 2.6 \times 10^{-3} L^3$

Eqn. B : $F_G = 3.077 - 0.155L + 0.0043L^2 - 4.457 \times 10^{-5} L^3$

Specimen CB-10E

Measured Cope Radius = 10 mm

Eqn. B

Eqn. A

Distance L (mm)
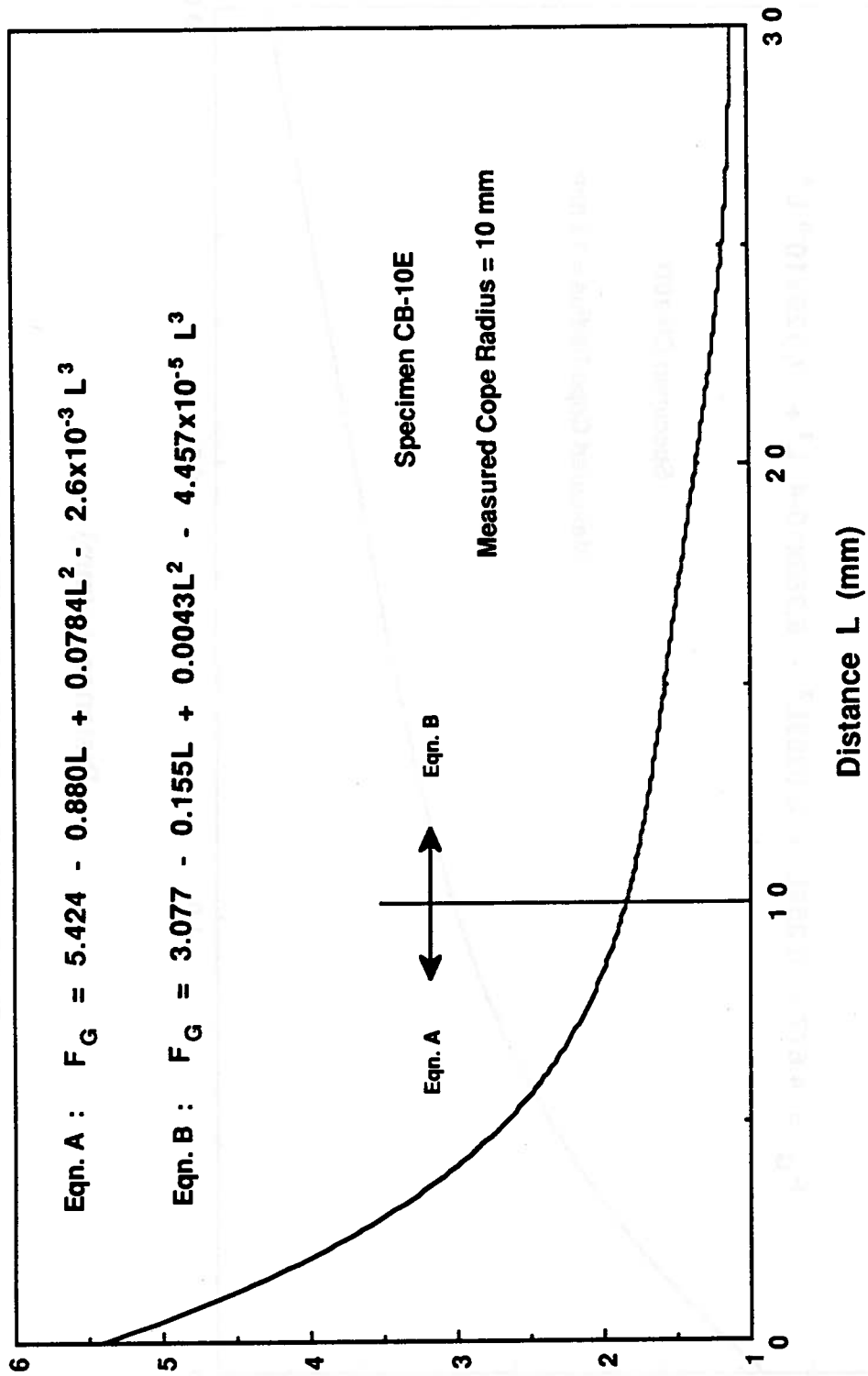
Figure 5.13 F_G Curve for Specimen CB-10E

$$F_G = 3.640 - 0.174L + 0.0077L^2 - 2.010 \times 10^{-4}\, L^3 + 2.160 \times 10^{-6}\, L^4$$

Specimen CB-20A

Measured Cope Radius = 25 mm

Distance L (mm)

F_G
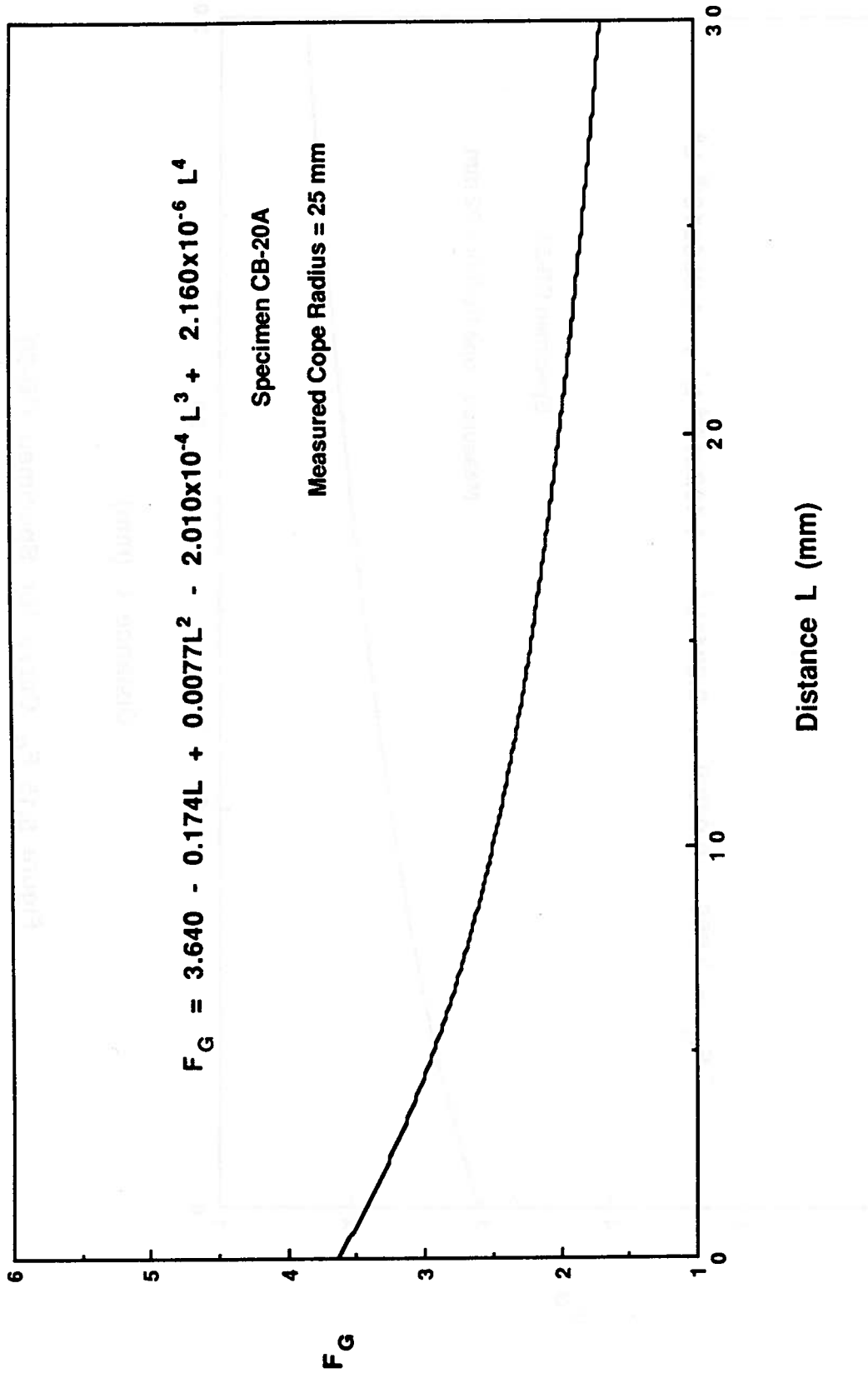
Figure 5.14 F_G Curve for Specimen CB-20A

$$F_G = 2.986 - 0.0982L + 0.0041L^2 - 1.162 \times 10^{-4} \, L^3 + 1.355 \times 10^{-6} \, L^4$$

Specimen CB-30

Measured Cope Radius = 32 mm

Distance L (mm)
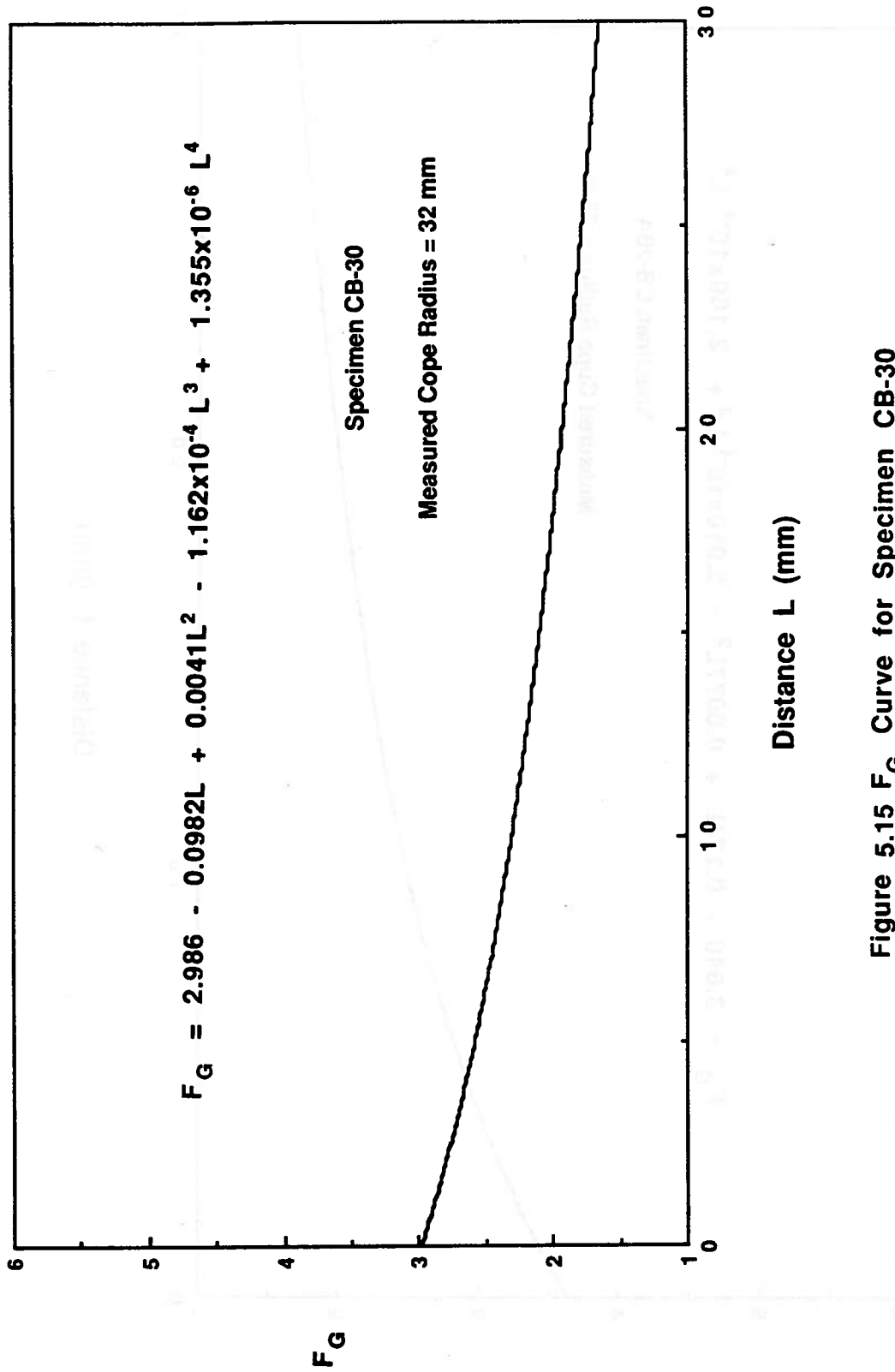
Figure 5.15 F_G Curve for Specimen CB-30
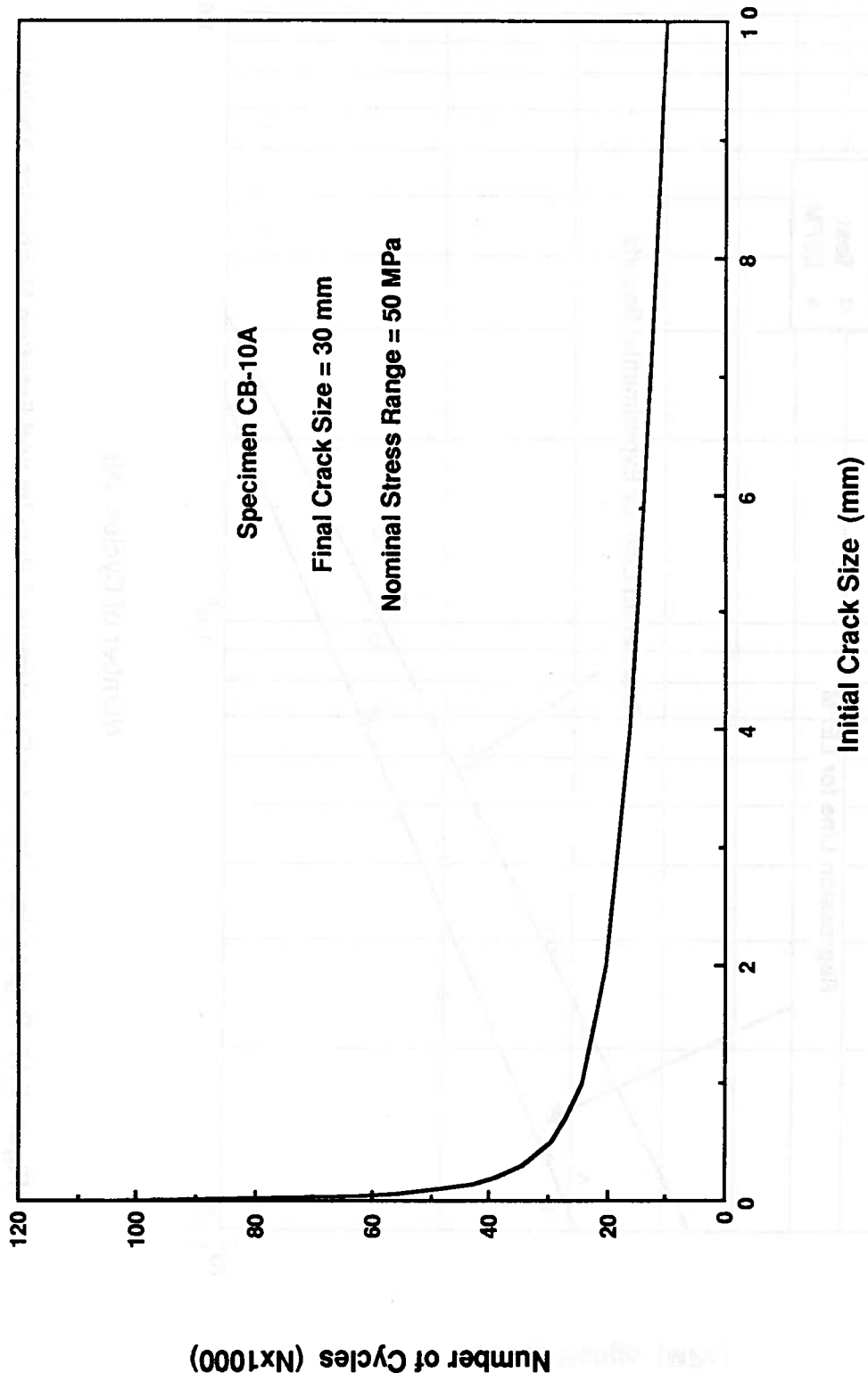
Figure 5.16 Effect of Initial Crack Size on Predicted Fatigue Life for CB-10A

Specimen CB-10A

Final Crack Size = 30 mm

Nominal Stress Range = 50 MPa

Initial Crack Size (mm)

Number of Cycles (Nx1000)
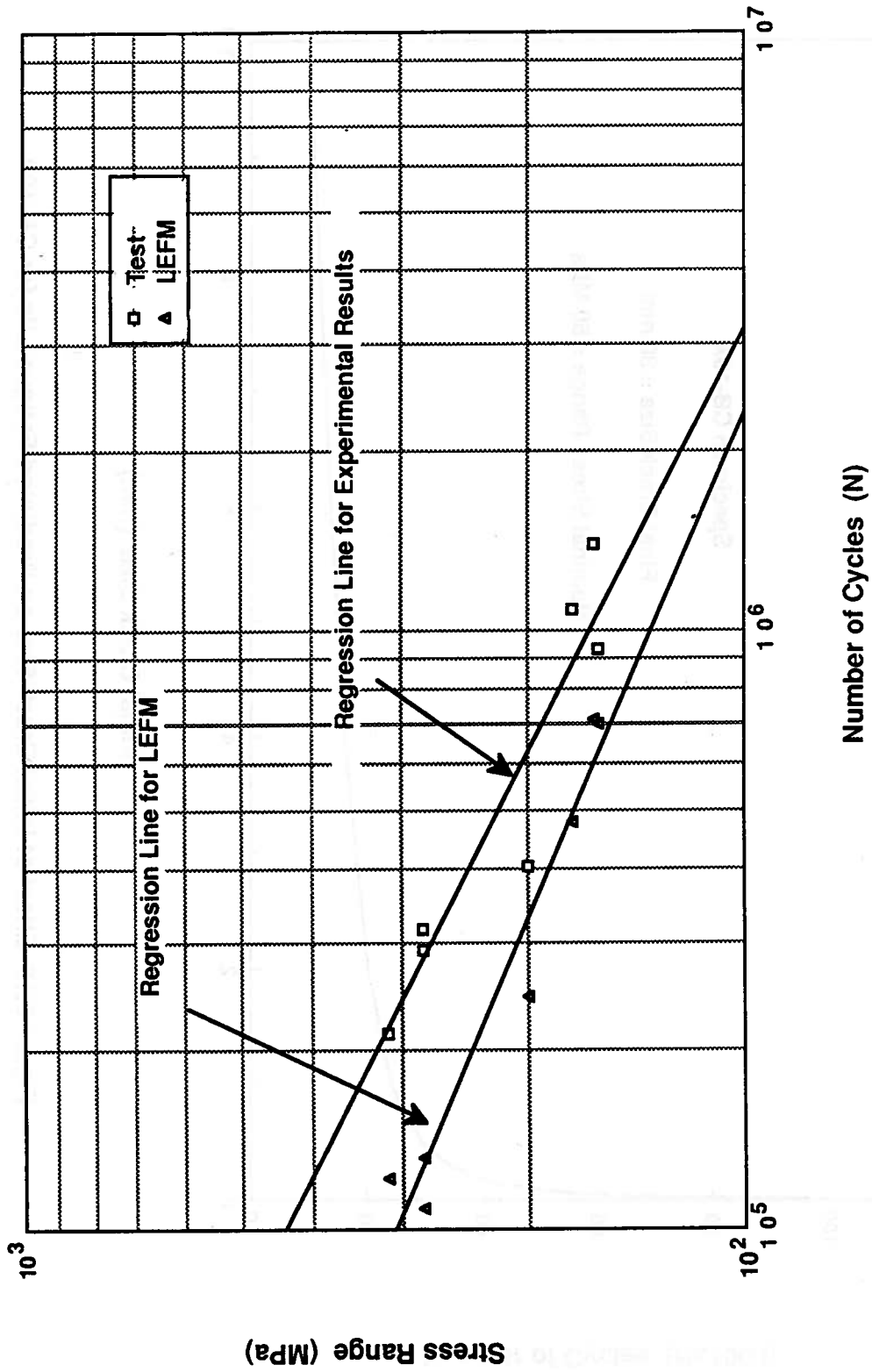
Figure 5.17 Regression Lines for Experimental Results and Fracture Mechanics Analysis
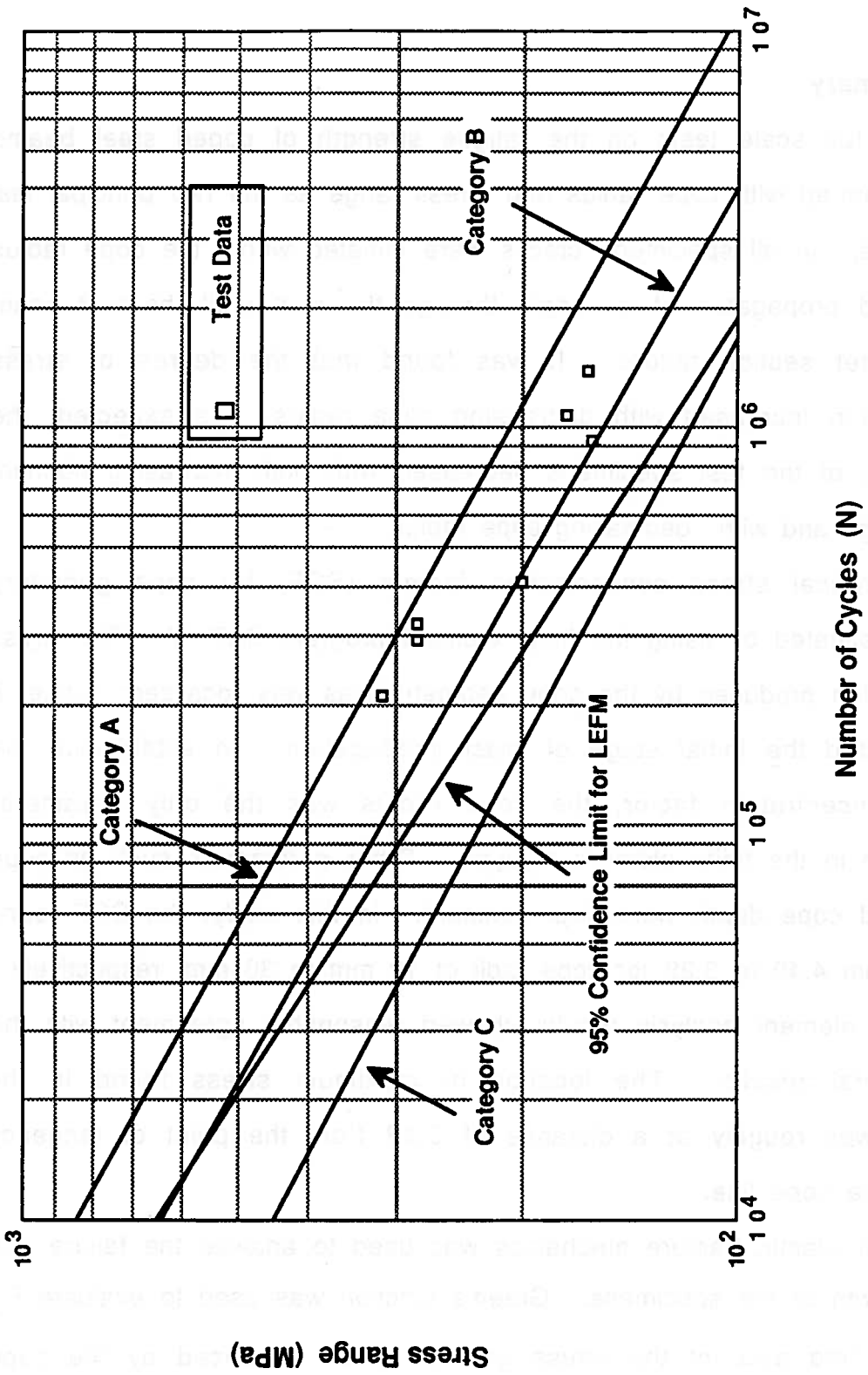
Figure 5.18 Comparison of Experimental and Analytical Results with Existing S-N Curves

6. SUMMARY AND CONCLUSIONS

6.1 Summary

Nine full scale tests on the fatigue strength of coped steel beams were performed with cope radius and stress range as the two principal test parameters. In all specimens cracks were initiated within the cope radius region and propagated at an angle through the web until the test beam reached net section failure. It was found that the degree of stress concentration increased with decreasing cope radius. As expected, the fatigue life of the test specimens decreased with both increasing nominal stress range and with decreasing cope radius.

Theoretical stress concentration factors (SCF) for cope geometry were investigated by using the finite element program SAP IV. The stress concentration produced by the cope geometry was very localized; hence, it only affected the initial stage of crack propagation. In establishinf the stress concentration factor, the cope radius was the only parameter considered in the finite element analysis. Other parameters such as cope length and cope depth were kept constant. In this study, the SCF found ranged from 4.49 to 3.28 for cope radii of 10 mm to 30 mm, respectively . The finite element analysis results showed reasonable agreement with the experimental results. The location of maximum stress found in the analysis was roughly at a distance of 0.3R from the point of tangency towards the cope line.

Linear elastic fracture mechanics was used to analyse the failure and crack growth of the specimens. Green's function was used to evaluate F_G and took into account the stress gradient effect produced by the cope geometry and the non-uniform loading. It was found that the LEFM approach

provided a conservative estimate of the fatigue strength of coped beams. The predictions by LEFM were also compared with the existing S-N curves in CAN3-S16.1-M84(1984). The comparison showed that the S-N curve of category B would provide reasonable estimate of the fatigue strength of coped beams.

As expected, flame cutting induced high tensile residual stresses near the cut edge and also produced significant surface roughness. The effect of the cope fabrication procedure on the fatigue strength of coped beams was not clearly identified by the experimental results.

6.2 Conclusions

Based on the investigation presented herein it can be concluded that coped beams subjected to cyclic loading are very susceptible to fatigue damage. Hence, design guidelines are needed for designing this detail. In order to use the conventional S-N curve approach, that is, using the nominal stress range with the appropriate fatigue strength category, many tests must be done so that cope details can be classified into categories. Therefore, based on the analytical study and limited number of experimental data it is recommended that the actual stress range, which is the nominal stress range multiplied by the appropriate SCF given by equation [4.2], could be used along with Category B from the S-N curves in CAN3-S16.1-M84 (1984) when designing coped beams subjected to fatigue loading. For a more conservative estimate of the fatigue strength of coped beams, Category C should be used in place of Category B.

Although test results did not show conclusively the effect of cope fabrication process, it is recommended that flame-cut edges should always be ground smooth in order to avoid local discontinuities. The cope radius

should always be made as large as possible in order to minimize the effect of stress concentration.

6.3 Recommendations for Future Research

In order to develop a complete design guideline for coped beams subjected to cyclic loading, the following areas should be futher investigated:

1) A parametric study on the SCF for various cope geometry such as cope length, cope depth, and cope radius should be performed in order to verify equation [4.2].

2) More tests should be conducted to investigate the fatigue strength of coped beams at various stress ranges and cope radii and the effect of grinding should be examined

3) The effect of cope fabrication procedure on the fatigue strength should be further investigated.

4) Coped beams subjected to compressive stress range and/or secondary out-of-plane bending stress range should be considered in future testing.

5) The size of the initial crack produced by flame cutting should be examined in future research.

REFERENCES

AASHTO, 1977. Standard Specifications for Highway Bridges. The American Association of State Highway and Transportation Officials, Washington, D.C.

AISC, 1986. Specification for the Design, Fabrication and Erection of Structural Steel for Buildings, Chicago.

Albrecht, P. and Yamada, K. 1977. **Rapid Calculation of Stress Intensity Factors**. Journal of the Structural Division ASCE Vol. 103, No. ST2, February, pp. 377-389.

Barsom, J. M., 1971 **Fatigue Crack Propagation in Steels of Various Yield Strengths**, Transactions, American Society of Mechanical Engineers, Journal of Engineering for Industry, Series B, 93, No. 4.

Bathe, K. J., Wilson, E. L., and Peterson, F.E. 1974. **SAP IV - A Structural Analysis Program for Static and Dynamic Response of Linear Systems**, Earthquake Engineering Research Center Report No. EERC 73-11, University of California, Berkeley, California.

Broek, D. 1986. **Elementary Engineering Fracture Mechanics**. Martinus Nijhoff Publishers, pp. 266-269.

BS 5400: Part 10 1980. Steel, Concrete, and Composite Bridges, Part 10, Code of Practice for Fatigue, British Standards Institute.

Bueckner, H. F. 1958. **The Propagation of Cracks and Energy of Elastic Deformation**, Transactions, American Society of Mechanical Engineers, Vol. 80, p. 1225.

CAN3-S6-M78 1978. Design of Highway Bridges. Canadian Standard Association, Rexdale, Ontario.

CAN3-S16.1-M84 1984. Steel structures for Buildings - Limit States Design. Canadian Standards Association, Rexdale, Ontario.

Cheng, J. J. and Yura, J. A. 1986. **Local Web Buckling of Coped Beams**, Journal of the Structural Engineering, ASCE, Vol. 112, No. 10, October, pp. 2314-2331.

Fisher, J. W. , Frank, K. H., Hirt, M. A. and McNamee, B. M. 1970. **Effect of Weldments on the Fatigue Strength of Steel Beams**, NCHRP Report 102, Highway Research Board, National Research Council, Washington, D.C.

Fisher, J. W. 1977. **Bridge Fatigue Guide - Design and Details**, American Institution of Steel Construction, Chicago.

Fisher, J. W. and Yuceoglu, U. 1981. **A Survey of Localized Cracking in Steel Bridges**, Interim Report, Federal Highway Administration, DOT-FH-11-9506.

Fisher, J. W. 1984. **Fatigue and Fracture in Steel Bridges.** John Wiley & Sons, Inc. pp. 302-310.

Fisher, J. W. 1987. Private Communication.

Fuchs, H. O. and Stephens, R. I. 1980. **Metal Fatigue in Engineering.** John Wiley & Sons, Inc. pp. 82.

Goldberg, F., 1973. **Influence of Thermal Cutting and Its Quality on the Fatigue Strength of Steel**, Welding Journal, Res. Suppl., Vol. 52, No. 9, pp. 392s-404s.

Gurney, T. R. 1979. **Fatigue of Welded Structures.** Cambridge University Press. pp. 377 -389.

Hirt, M. A. and Fisher, J. W. 1973. **Fatigue Crack Growth in Welded Beams**, Engineering Fracture Mechanics, Vol. 5, No. 2.

Irwin,G. R. 1957. **Analysis of Stress and Strains Near the End of a Crack Transversing Plate**, Transactions, American Society of Mechanical Engineers, Journal of Applied Mechanics, Vol. 24.

Irwin, G. R. 1961. **Fracturing and Fracture Mechanics**, Theoretical and Applied Mechanics Reports 202, University of Illinois, Urbana. Illinois.

Irwin, G. R. 1962. **Crack Extension Force for a Part-Through Crack in a Plate**, Transactions, American Society of Mechanical Engineers, Series E, Vol. 29.

Irwin, G. R., Liebowitz, H., and Paris, P. 1968. **A Mystery of Fracture Mechanics**, Engineering Fracture Mechanics, Vol. 1.

Kalousek, J., and Bethune, A. E. 1976. **Stringer Stress Measurements on Bridge Mile 51.5, Windermere Subdivision**, Department of

Research, Canadian Pacific Railroad, Report 5538-76, (limited distribution).

Murakami, Y. (editor) 1986. **Stress Intensity Factors Handbook. Committee on Fracture Mechanics.** The Society of Material Science, Japan, Vol. 1 Pergamon Press.

Nishimura, T. 1978. **Fracture in Welded Bridges.** Journal of Japan Welding Society. 10. (in Japanese).

Paris, P. and Erdogan, F. 1963. **A Critical Analysis of Crack Propagation Laws**, Transaction, American Society of Mechanical Engineers, Journal of Basic Engineering, Series D, 85, No. 3.

Paris, P. and Sih, G. C. 1965. **Stress Analysis of Cracks, Fracture Toughness Testing and its Applications**, ASTM, STP 381.

Peterson, R.E. 1974. **Stress Concentration Factors**. J. Wiley & Sons, New York N.Y.

Richards, J. A. and Mueller, R. A., 1982 **FCCU Structural Failure**, Cities Service Company, Tulsa, Oklahoma.

Rolfe, S. T. and Barsom, J. M. 1977. **Fracture and Fatigue Control in Structures, Applications of Fracture Mechanics**. Prentice-Hall, Englewood Cliffs, New Jersey.

Tada, H., Paris, P. C., and Irwin, G. R. 1973. **The Stress Analysis of Cracks Handbook.** Del Research Corp., Hellertown, Pa..

Zettlemoyer, N. and Fisher, J. W. 1978. **Stress Gradient and Crack Shape Effects on Stress Intensity of Welded Details**. Welding Journal, Vol. 57, No. 8, Research Supplement, pp. 246-250.